FACULTY OF TECHNOLOGY

Production of bricks with fiber-reinforced alkali-activated desulfurization slag concretes containing carbonated BOF aggregates

Khaled Mohammad Shaad

DEGREE PROGRAMME
Master's Degree Programme in Environmental Engineering
January 2019

UNIVERSITY OF OULU

FACULTY OF TECHNOLOGY

Production of bricks with fiber-reinforced alkali-activated desulfurization slag concrete containing carbonated BOF aggregates

Khaled Mohammad Shaad

Supervisor(s): Dr. Mohammad Mastali and Dr. Päivö Kinnunen

DEGREE PROGRAMME
Master's Degree Programme in Environmental Engineering
January 2019

THESIS ABSTRACT

University of Oulu Faculty of Technology

Degree programme (bachelor's thesis, master's thesis)	Research Group
Master's Degree Programme in Environmental Engineering	Fibre and Particle Engineering
Author	**Thesis supervisor**
Khaled Mohammad Shaad	Dr. Mohammad Mastali and Dr. Päivö Kinnunen

Thesis title
Production of bricks with fiber reinforced alkali activated desulfurization slag concretes containing carbonated BOF aggregates

Major subject	Thesis type	Submission date	Number of pages
Environmental Engineering/ Energy systems	Master's thesis	January, 2019	102+4 chapters

Abstract

This thesis investigates the efficiency of using carbonated Basic Oxygen Furnace (BOF) aggregates in different alkali-activated binders such as ladle slag and ground granulated blast furnace slag (GGBFS), and desulfurization (DS) slag. Sodium silicate and different molarities of sodium hydroxide were also used as alkali solution. BOF slag has high free CaO content, which leads to volume expansion problem under normal atmospheric condition. Additionally, free CaO and MgO are the reasons of volume expansion problem in desulfurization (DS) slag. To minimize and control this problem, BOF slags are exposed to CO_2 gas, which improves the volume stability.

The aim of the first chapter is to investigate using of carbonated BOF aggregates instead of normal aggregates with GGBFS and ladle slag precursors which activated by alkaline solution. The effects of using different precursor types and contents, aggregate types and contents, and different sodium hydroxide molarities (6M, 8M, and 10M) were determined by assessing the mechanical and mineralogical test.

After investigating the efficiency of carbonated BOF aggregates, the goal of the second chapter is to use carbonated BOF aggregate with different precursors types and content such as carbonated and non-carbonated desulfurization (DS) slag and different sodium hydroxide molarities (6M, 8M, 10M, and 12M). The effects of different parameters were carried out by evaluating mechanical, efflorescence, and pH experiments. Based on the results, mixture containing non-carbonated desulfurization (DS) slag with carbonated BOF aggregates and 8M NaOH provided excellent compressive strength compared to using carbonated DS. However, to minimize the efflorescence rate fiber reinforcement was introduced in the next chapter.

In the third chapter, the objective is to introduce fiber reinforcement to the selected mix composition, which containing alkali activated desulfurization slag with carbonated BOF aggregates and sodium hydroxide (8 M) to develop strength properties and limits the efflorescence rates. In the mix composition 4% fiber (in mass) was added. The selected four different fibers are basalt, PVA (8mm), Cellulose and Polypropylene (PP). Moreover, 4% and 8% combined PVA and basalt fibers are used. According to the results, it was noticed that basalt and cellulose fibers increased 15% (9 MPa) of the compressive strength compared to reference mixture and reduced the efflorescence compared to other used fibers.

In the last chapter, the main aim is to produce the bricks based on the mix compositions using carbonated BOF, desulfurization (DS) slag, and sodium hydroxide (8 M) with basalt and cellulose fibers. The effects of using selected fibers (basalt, cellulose) on the control mixture were conducted by mechanical strength, effects of carbonation, water absorption by capillarity, water absorption by immersion, efflorescence, ultrasonic pulse velocity, drying shrinkage, high temperature, and freeze-thaw test.

Library location: University of Oulu, Science and technology library Tellus

FOREWORD

The purpose of this thesis was to investigate alkali-activated desulfurization (DS) slag binder with recycled carbonated BOF aggregate to produce environmentally friendly construction material. This work was done at the University of Oulu, Fibre and particle engineering laboratory.

All praises are to the Almighty Allah to allow me carrying out this research work and preparing this thesis. I want to express my gratitude to researcher Dr. Päivö Kinnunen for offering me the chance to write this thesis. My sincere gratitude goes to my supervisor, Dr. Mohammad Mastali for his patient guidance, intense supervision, untiring assistance, constant encouragement, valuable suggestions, constructive criticism and inestimable help during every phase of this research work and preparation of thesis.

Special thanks are also to the laboratory staff (Jarno, Elisa and Jani) for their remarkable help with everything and Tun Tun Nyo for help with strength analysis. Also, my sincere appreciation goes to Adesanya Damilola Elijah, Hoang Nguyen, Hugo Kerbrat and Ahmad Alzaza during my thesis work.

Finally, I appreciate the love and prayer from my beloved parents (Shamshad and Nahid), and my relatives for their moral support.

Table of Contents

CHAPTER 1

The performance of carbonated BOF aggregates in alkali activated concretes

1.1 Introduction

In 2016, it was estimated that totally 8% CO_2 emissions are released to ordinary Portland cement (OPC) production (Andrew, 2018). Alkali-activated materials (AAM) have been proposed as potential alternatives to ordinary Portland cement (OPC), which leads to reducing CO_2 emissions as well as advantageous to use wastes in productions of construction materials. In the production of alkali-activated binders, different precursors are activated by using different alkaline solutions. Different precursors are coming from industrial by-products such as fly ash, metakaolin, blast furnace slag, kaolinitic clay, rice husk, and red mud (Aydın & Baradan, 2012) (Davidovits, 1991) (Shi, et al., 2003).

Recently, efforts have been made to maximize the use of recycled materials in alkali-activated binders. One of these efforts is using different recycled aggregates. Steel slag aggregates have also been studied as a potential replacement material for natural and lime aggregates, and concrete with steel slag aggregate showed better compressive and flexural strengths, denser structure, and better chemical resistance than natural or crushed lime aggregate concrete (Maslehuddin, et al., 2003) (Wang, et al., 2011) (Palankar, et al., 2016).

In this chapter, utilize ground granulated blast furnace slag (GGBFS) and ladle slag were utilized as precursors and activated by an alkaline solution. Moreover, carbonated basic oxygen furnace (BOF) used as aggregates in the mixtures. In the first stage of this chapter, the effects of using carbonated BOF aggregates instead of normal aggregates will be investigated.

1.1.1 Ground granulated blast furnace slag (GGBFS)

Ground granulated blast furnace slag (GGBFS) is produced from industrial shock chilling process at high-temperature furnaces as a byproduct Pozzolanic reaction of GGBFS can be activated, if there is an adequate amount of alkaline salts (alkali catalysts) available (Kuo, et al., 2014). Blast furnace slag is a combination of limestone flux and an earthly component of iron ore. Granulated slag is formed when water is quickly mixed with molten slag, or molten slag is cooled with powerful water jets (S.C Pal, 2003). It looks like a noncrystalline glassy form, and when it is finely ground and combined with Portland Cement (PC), it has been given good cementitious properties (Hwang & Lin, 1986).

Alkali-activated slag binders have high compressive strength at an early stage, durability performance is better when acid and sulfate attack, short setting time and rapid hardening (Collins & Sanjayan, 2001). From the chemical compositions of GBFS, it shows that it has calcium oxide

(CaO), higher content of silicon dioxide (SiO_2), and aluminum oxide (Al_2O_3). Increasing the amount of GBFS in the mixtures has a key role in fresh and hardened state properties.

On the other hand, alkali-activated GGBFS binders have some disadvantages; for example, it has a high rate of drying shrinkage. The shrinkage can be the reason of cracks in the mixture surface, which have a negative influence on mechanical and durability properties.

1.1.2 Ladle slag

Ladle slag is a by-product of the steelmaking process which has significant benefits to use as a cementitious material in construction (Adesanya, et al., 2018). Ladle slag is presently utilized crystalline metallurgical residue and uses as a precursor for alkali activation. It is commonly considered as reaction with alkalis, as a result, it has mixed with metakaolin precursors. (Adesanya, et al., 2017).

However, based on (Adesanya, et al., 2017), ladle slag is found a potential sole precursor for alkali-activated binders. The main minerals of ladle slag are γ-dicalcium silicate and mayenite which have found by X-ray diffractometry analysis. Development of compressive strength depends on the different compositional ratio of activating solution which consists of sodium silicate and potassium hydroxide. (Adesanya, et al., 2017)

Moreover, it has observed that ladle slag fine has significant effects on the cementitious property when reaction with alkaline activator. (Shi, 2002).

1.1.3 Basic oxygen furnace (BOF)

Basic oxygen furnace (BOF) slag is produced from the processing of pig iron steel. (Proctor, et al., 2000) (Shi, 2002) (Tossavainen, et al., 2007) found that BOF slag contains calcium, silicon and iron compound and it has high mechanical strength, abrasion resistance, and specific gravity properties. It indicates similar component which presents in the Portland cement, but high iron oxide in BOF slag leads to reduce binding potential (Belhadj, et al., 2014) (Shi & Qian, 2000) (Tsakiridis, et al., 2008) (Shi, et al., 2015).

BOF slag has several recycled applications such as production of cement (Tsakiridis, et al., 2008) (Xue, et al., 2016), construction of a road (Poulikakos, et al., 2017); (Anastasiou, et al., 2015); (Andreas, et al., 2014), preparation of slag glass ceramic (He, et al., 2012).

However, (Shi, 2002) and (Motz & Geiseler, 2001) found that high free CaO content in BOF can create volume expansion problems, which make lower opportunity for construction purpose.

1.1.4 Problems and propose solutions

Carbon dioxide (CO_2) emissions are one of the major problems in the environment. It will be a serious issue to reduce the amount of CO_2 from the environment. Sequester of CO_2 in lime or cement-based products can be a beneficial process to reduce CO_2 from the environment, and the process of CO_2 sequestration in lime or cement-based products is known as carbonation process. CO_2 helps to react with both hydrated products include C-S-H gel and $Ca(OH)_2$ and unhydrated cement compounds (C_3S and C_2S), these reactions create CO_2 gas into stable C-S-H gel or calcium carbonate (Rostami, et al., 2011).

Longtime carbonation process will change the durability of concrete. Mainly, carbonation process depends on several indicators, such as- pore structure of concrete, relative humidity (RH), temperature, and concentration of CO_2 in the environment, availability of $Ca(OH)_2$ and water, and use mineral additives instead of cement (Lea, 1971).

CO_2 sequestration technology will minimize the presence of CO_2 in the atmosphere and will increase curing and strength properties of cementitious construction materials (Bertos, et al., 2004) (Jang, et al., 2016). The carbonation process of alkali-activated materials which is controlled by two ways of a chemical process: (a) carbonation process help to decrease pH values and Na-rich carbonates and (b) decalcification of Ca-rich components (Bernal, 2015). Other authors (Mastali, et al., 2018) found that curing specimens which are going through carbonation increases the compressive strength two and three times compared to curing at the ambient conditions.

Previously mentioned that volume expansion problem in BOF slag caused by high content of CaO, authors (Santos, et al., 2012) found that hot-stage carbonation process can minimize the free CaO content and stabilize slag volume. BOF slag contains calcium compound which is very potential for carbonation. (Ko, et al., 2015) found that the pH values of BOF slag have decreased after the carbonation process which leads to change CaO to $CaCO_3$. They reported that the carbonation process increased the mechanical properties of BOF, and carbonation of BOF slag can capture CO_2 as well as influence on mechanical performance.

1.2 Experimental plan

1.2.1 Mix design and designations

The mortars were comprised of ladle slag, ground granulated blast furnace slag (GGBFS), carbonated basic oxygen furnace (BOF) and normal sand. The chemical compositions of ladle slag, GGBFS, and BOF slag (carbonated and non-carbonated) shown in Table 1.1. The alkali solution was combined by liquid sodium silicate ($\frac{SiO_2}{Na_2O} \approx 2.5$) and sodium hydroxide (with molarities of 6M, 8M, and 10M). Different molar concentrations of sodium hydroxide were prepared by dissolving Na(OH) pellets in water, later the solution cooled at room temperature (with the average temperature of 23 ^{0}C). Thirty-six mix compositions were tested in this chapter. Mix compositions and different mix proportions are listed in Table 2.1.

Table 1.1. The chemical compositions of LS, BOF slag (carbonated and un-carbonated), and GGBFS measured by XRF

Material	Element / Oxides (%, w/w)					
	CaO	**MgO**	**Al_2O_3**	**SiO_2**	**SO_3**	**Fe_2O_3**
LS	50.96	6.31	27.87	8.27	0.8	1.13
GGBFS	38.51	10.24	9.58	32.33	4.00	1.23
Carbonated BOF	54.59	1.86	1.15	12.99	0.18	21.35
Non-carbonated BOF	49.48	2.21	1.67	14.11	0.16	24.81

Table 2.1. Mix compositions

Specimen designation	LD	GGBFS	Aggregate/binder	Alkali/binder	SS/SH	Sodium hydroxide (M)
G1-6M	0	1	3 or 5	1	2.5	6
G1-8M	0	1				8
G1-10M	0	1				10
L1-6M	1	0				6
L1-8M	1	0				8
L1-10M	1	0				10
G0.5L0.5-6M	0.5	0.5				6
G0.5L0.5-8M	0.5	0.5				8
G0.5L0.5-10M	0.5	0.5				10

1.2.2 Carbonation of BOF

In this study, BOF slags used as recycled aggregates, therefore, they were initially sieved to obtain the grain size distribution larger than 0.5 mm. Then, recycled BOF aggregates were treated using carbon dioxide sequestration for 48 hours exposed to CO_2 gas with a pressure of 5%, temperature of 23 ^{0}C, and the relative humidity of 67% (see Fig 1.1). To show the efficiency of the proposed approach to minimize the expansion problems of BOF aggregates, natural aggregates were also used. Since there was a possibility to have some expansion in BOF aggregates, the porosity of mix

compositions was increased. In order to increase the porosity of the mix composition, the aggregate to binder ratio was varied from 3 to 5.

a)

b)

Fig 1.1. a) Carbonation chamber; b) BOF aggregates

1.2.3 Casting and Curing

In the preparation of the mixtures, dry ingredients consisting LS, GGBFS, and carbonated BOF aggregates were mixed for 1 min, then alkali solutions (sodium silicate and sodium hydroxide) added to dry mixture and resultant composition was stirred for 4 min. Fresh mortars were cast within the prismatic molds with dimension (20×20×80 mm) (see Fig 2.1.a). After filled up the molds, machine vertical shaker was used for 60 seconds to vibrate the specimens. Then, the molds were covered with plastic for 24 hours (see Fig 2.1.b). After 24 hours, it was demolded and again cover with plastic (see Fig 2.1.d) and stored in the ambient temperature of lab (averagely 25 ^{0}C and 40% RH). The specimens were until the test day (28 days).

a)

b)

c)

d)

Fig 2.1. a) Casting; b) wrapping with plastic; c) demolding; d) wrapping with plastic

1.3 Test procedures

1.3.1 Flexural strength

Regarding the proposed mix compositions in Table 1.1, totally one hundred and eight prismatic beams were tested to assess the flexural strength under three-point bending (TPB) test. Obtaining

the flexural strength of each mix composition is done by averaging of three prismatic specimens. The test was executed with a load cell of 100 kN capacity and a flexural load with displacement control rate of 0.6 mm/min was imposed to the beams. Equation 1.1 was used to calculate the flexural strength of specimens:

$$\sigma_f = \frac{3FL}{2bh^2} \qquad (1.1)$$

where, σ_f refers the flexural strength in (MPa), L is the length of span (mm), b and h are width (mm) and height (mm) of the prismatic beams.

1.3.2 Compressive strength

The compressive strength test was assessed by using the broken portion of prismatic specimens from the flexural tests. When the test was executed load, a compressive load with displacement control and speed of 1.8 mm/min submitted to the specimens. Obtaining the compressive strength of each mix composition is done by averaging of six portions of prismatic specimens. Equation 2.1 is used for calculating the compressive strength:

$$\sigma_c = \frac{F}{A} \qquad (2.1)$$

where, σ_c indicates the compressive strength in (MPa), F is the compressive load in (N), and A is the loaded area (mm^2).

1.3.3 Mineralogical test

1.3.3.1 SEM/EDS

Zeiss Ultra Plus field emission scanning electron microscope (FESEM) equipped with Oxford energy-dispersive X-ray spectroscopy (EDS) was used to analyze the microstructure and elemental distribution of the samples. The element mapping was collected and quantify using Aztec-Software. To testing electronic microscopy-energy dispersive spectroscopy (SEM/EDS) analysis, samples were prepared in small pieces with 1 cm diameter and 1 cm height. Standard SEM/EDS microscopy used for microstructural analysis of different mix compositions. Chemical compositions and Micrographs were gathered at an accelerated voltage of 15 and 10 kV, individually, and keep a variable distance from 6 to 8mm. Before the execution of SEM/EDS examination, all specimens in the tiny cylinder were coated with a 30-nm thick layer of platinum alloy (Mastali, et al., 2018).

1.3.3.2 X-ray diffraction (XRD) analysis

XRD analysis was performed to find the influence of carbonated BOF and normal aggregate on crystalline phase. XRD data were analyzed by using a Bruker D8 Advance X-ray diffractometer with Ni-filtered Cu radiation (1.54 Å) at 40 mA and 40 kV. Every sample was scanned from 5^0 to 80^0 at a scan rate of 0.5 seconds per step. Phase identification was conducted by using the ICDD PDF4 database from the International Center for Diffraction Data and the Jade 7 software (version 5.1.2600) from Materials Data Inc. (Mastali, et al., 2019)

1.3.3.3 Thermogravimetric analysis (TGA) and differential thermogravimetry (DTG) analysis

To study the reaction products and the conversion processes, a thermogravimetric analysis (TGA) and differential thermogravimetry (DTG) were carried out on the 28 d samples using the Precisa Gravimetrics AG. The samples were crushed, powdered, and heated up to 1000 ºC at 10 ºC / min in a nitrogen atmosphere.

1.4 Results and discussion

1.4.1 Flexural Strength

Fig 3.1 shows the impacts of using different parameters on the flexural strengths such as using different aggregate contents and types, precursor types and contents, and sodium hydroxide molarities. According to the results, using carbonated BOF aggregates commonly improved the flexural strength compared to normal aggregates, which this enhancement was higher in the mixtures containing higher contents of aggregates (aggregate/binder: 5). The maximum improvement was recorded around 3 times in L1-6M.

Interestingly, it was noticed that the maximum flexural strength in the mixtures containing carbonated BOF aggregates was recorded in the ones used a combination precursor consists of GGBFS and ladle slag, regardless of the sodium hydroxide molarities and aggregate contents. Since the maximum flexural strength in the mixtures used natural aggregates was governed by the precursor's types, sodium hydroxide molarities and aggregate content. Regarding the results, the maximum flexural strength was measured around 14 MPa in the mixtures of G0.5L0.5-10M and G0.5L0.5-8M containing carbonated BOF aggregate to binder ratio of 3, while the minimum flexural strength was obtained around 3 MPa in the mixture of L1-6M with natural aggregates to binder ratio of 5.

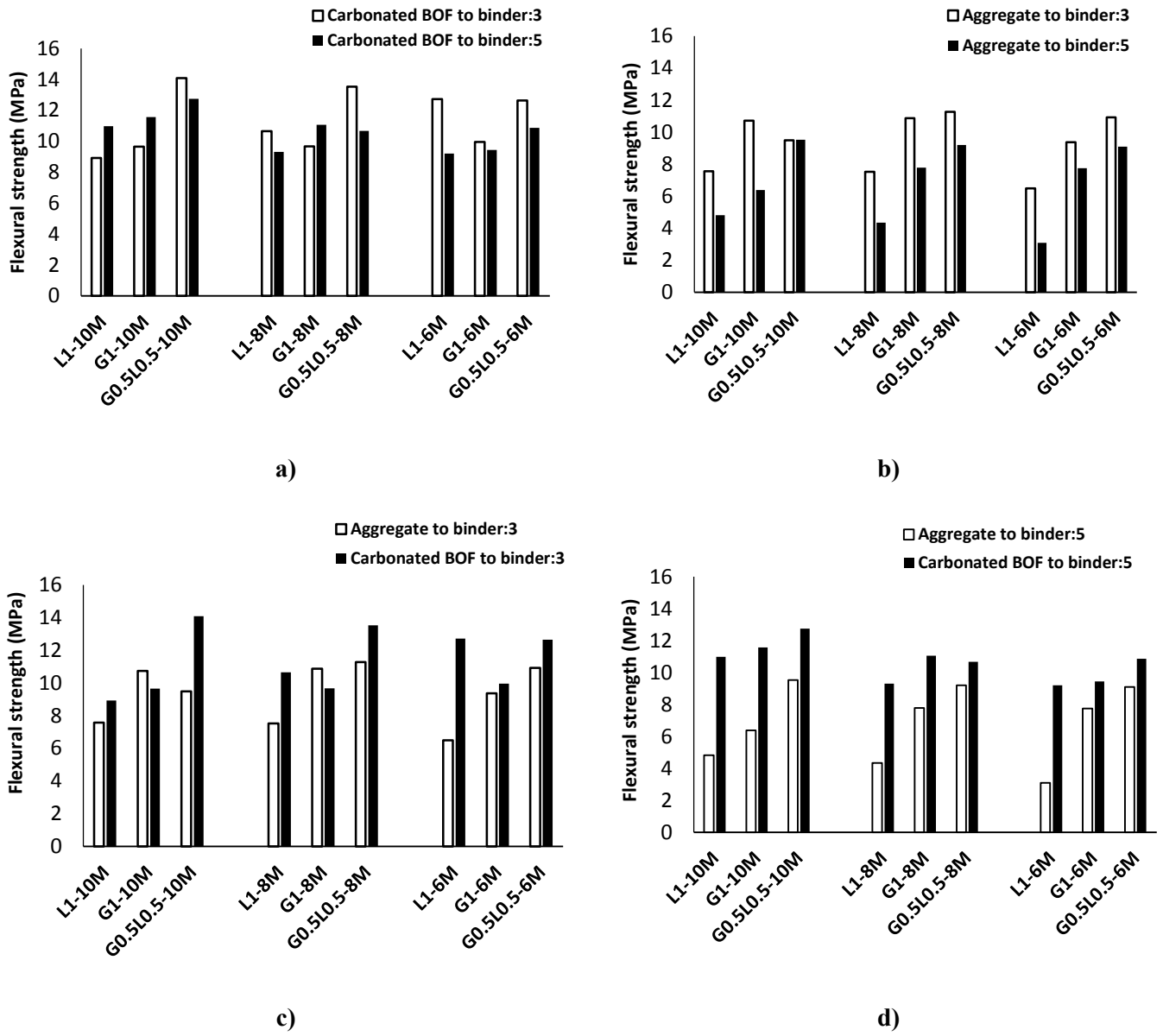

Fig 3.1. a) Effects of using different contents of carbonated BOF on the flexural strength; b) Effects of using different contents of normal aggregate on the flexural strength; c) comparative effects of normal aggregates and carbonated BOF with ratio of 3 on the flexural strength; d) comparative effects of normal aggregates and carbonated BOF with ratio of 5 on the flexural strength.

1.4.2 Compressive Strength

The effects of using different variables on the compressive strengths such as using different aggregate content and types, precursor types and contents, and sodium hydroxide molarities are shown in Fig 4.1. According to the figures, using carbonated BOF aggregates instead of natural aggregates commonly enhanced the compressive strength, which this improvement was due to higher in the specimens including a higher amount of aggregate (aggregate/binder: 5). The

maximum enhancement resulted in the mixture L1-6M with carbonated BOF aggregate to binder ratio of 5 which is around 3 times compared to using natural aggregate to same binder ratio.

Similar to the flexural strength, regardless of the sodium hydroxide molarities, the highest compressive strength was obtained in the mix compositions consisting carbonated BOF aggregates when a combination of ladle slag and GGBFS were used as precursors. Since the maximum compressive strength was affected by the precursor's types, sodium hydroxide molarities and aggregate content in the mixtures used natural aggregates. According to the result, the maximum compressive strength was achieved around 52 MPa and 54 MPa in the mixtures of G0.5L0.5-10M and G0.5L0.5-8M with carbonated BOF aggregate to binder ratio of 3, respectively, while the minimum compressive strength was recorded at specimen L1-6M with natural aggregates to binder ratio of 5 around 11 MPa.

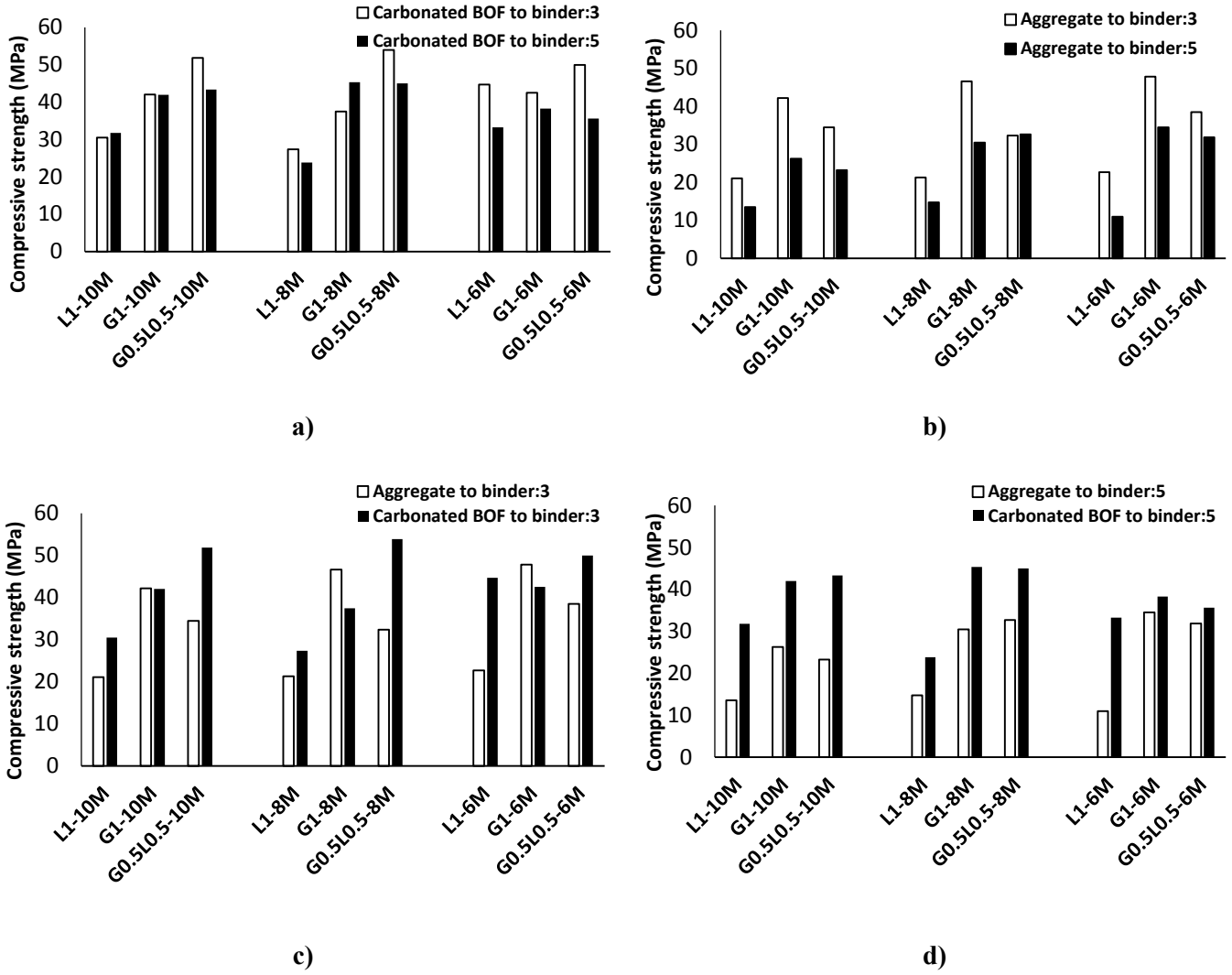

Fig 4.1. a) Effects of using different contents of carbonated BOF on the compressive strength; b) Effects of using different contents of normal aggregate on the compressive strength; c) comparative effects of normal

aggregates and carbonated BOF with ratio of 3 on the compressive strength; d) comparative effects of normal aggregates and carbonated BOF with ratio of 5 on the compressive strength.

1.4.3 Microscopic Analysis

1.4.3.1 SEM analysis

From fig 5.1 to 20.1, shows the morphology of the mixtures using SEM images. The morphologies and elemental maps of the mixtures containing carbonated BOF aggregates and normal aggregates are shown in Fig from 5.1 to 20.1. According to the SEM/EDS analysis, the aggregates affected the SiO_2 and CaO contents in the mixtures. Using carbonated BOF aggregates increased the calcium content and provided denser matrix, while normal aggregates increased the content of SiO_2. Higher CaO/SiO_2 ratio justifies higher strength in the mixtures containing carbonated BOF aggregates than normal aggregates (Quartz based sand). Additionally, it was observed that some cracks formed at interfacial transition zone (ITZ) between normal aggregates and matrix, which could degrade mechanical strengths. Later, it will be discussed that these micro-cracks are due to lack of enough space for the formed crystalline.

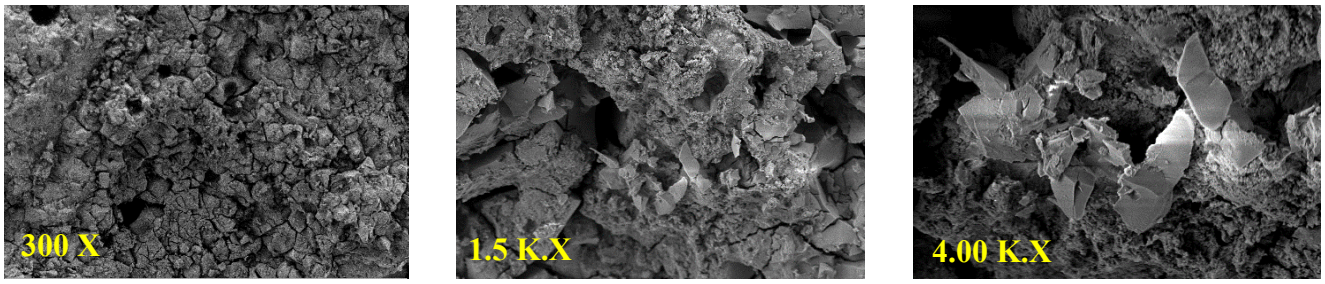

a) Fc: 30.47 MPa

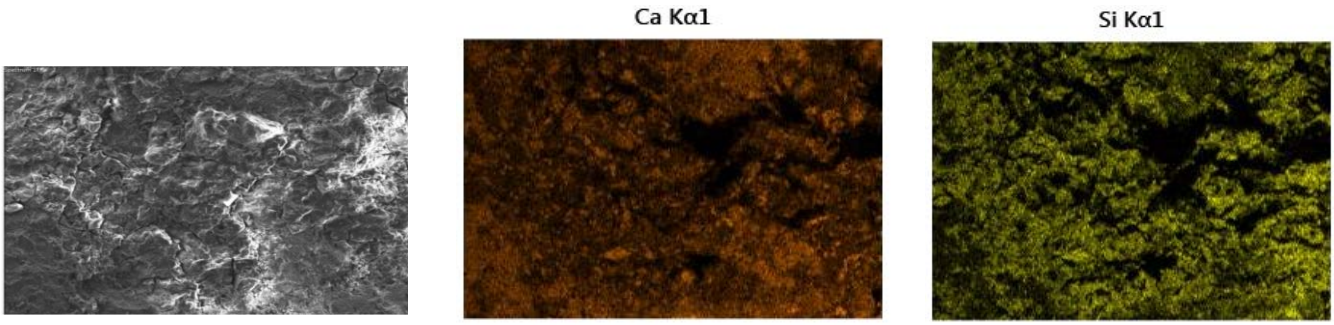

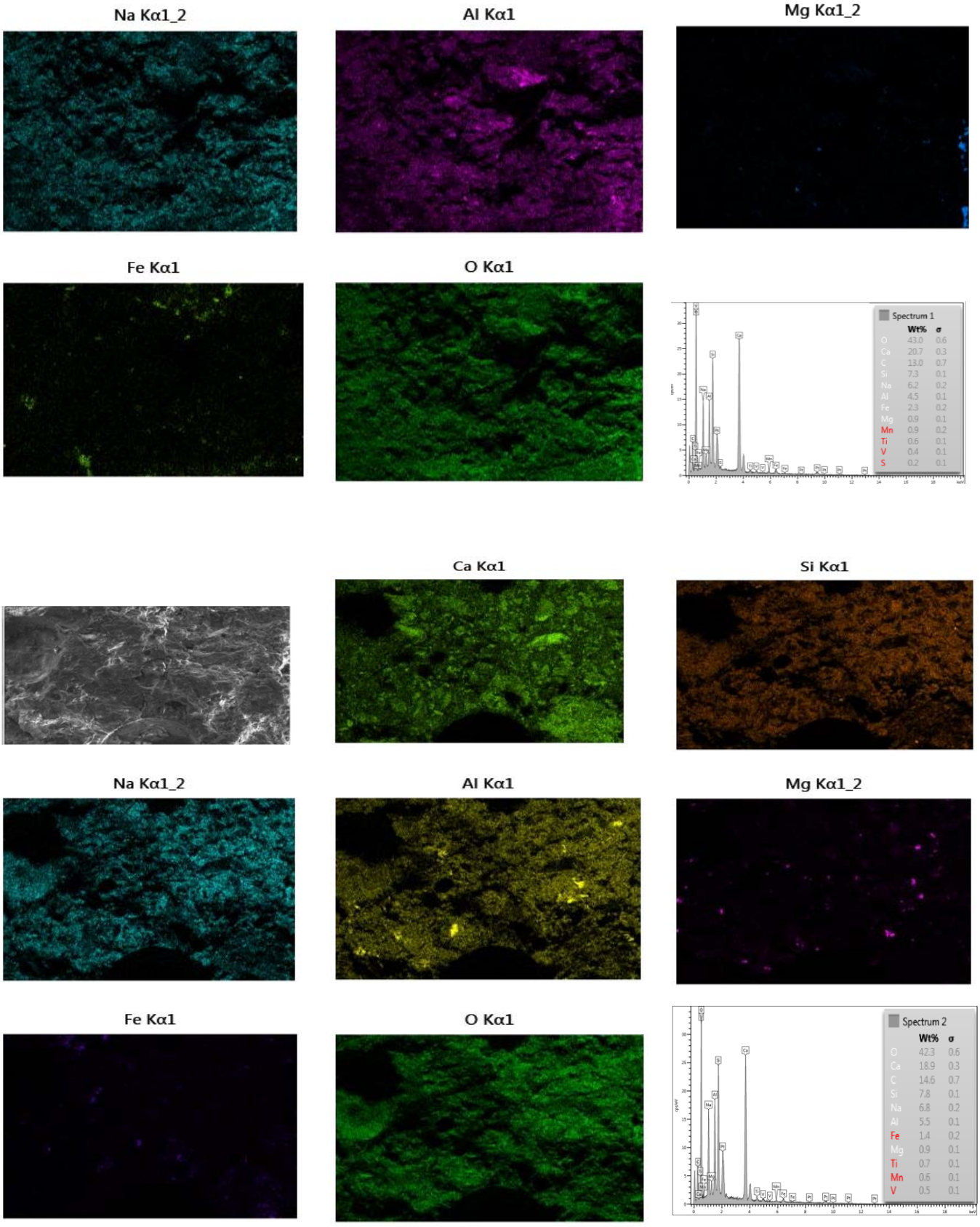

b)

Fig 5.1. The morphology of the mixture L1-10M: a) Carbonated BOF aggregates to binder 3; b) Element map of mixture containing carbonated BOF aggregates to binder 3


300 X

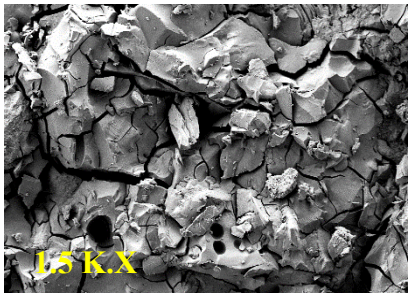
1.5 K.X

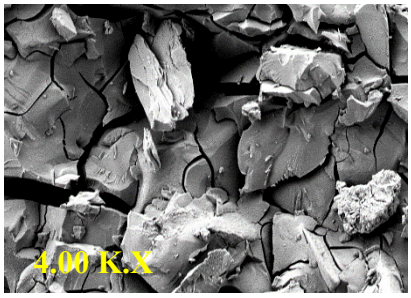
4.00 K.X

a) Fc: 42.04MPa

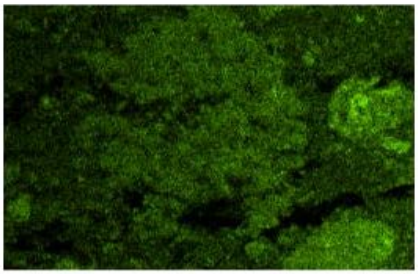
Ca Kα1


Si Kα1


Na Kα1_2


Al Kα1

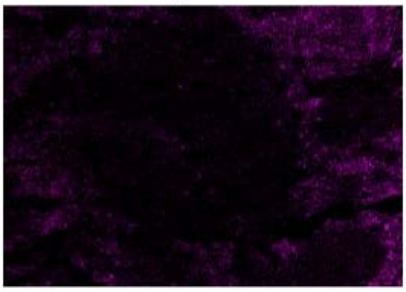
Mg Kα1_2

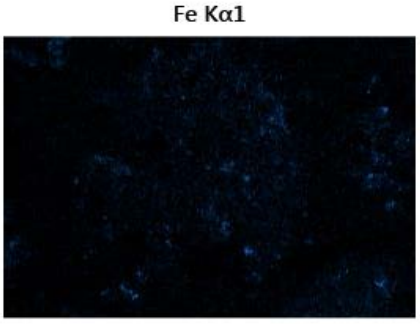
Fe Kα1


O Kα1

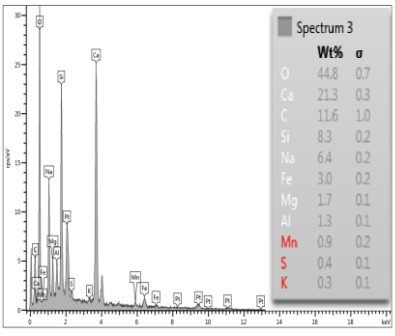
Spectrum 3
Wt% σ
O 44.8 0.7
Ca 21.3 0.3
C 11.6 1.0
Si 8.3 0.2
Na 6.4 0.2
Fe 3.0 0.2
Mg 1.7 0.1
Al 1.3 0.1
Mn 0.9 0.2
S 0.4 0.1
K 0.3 0.1

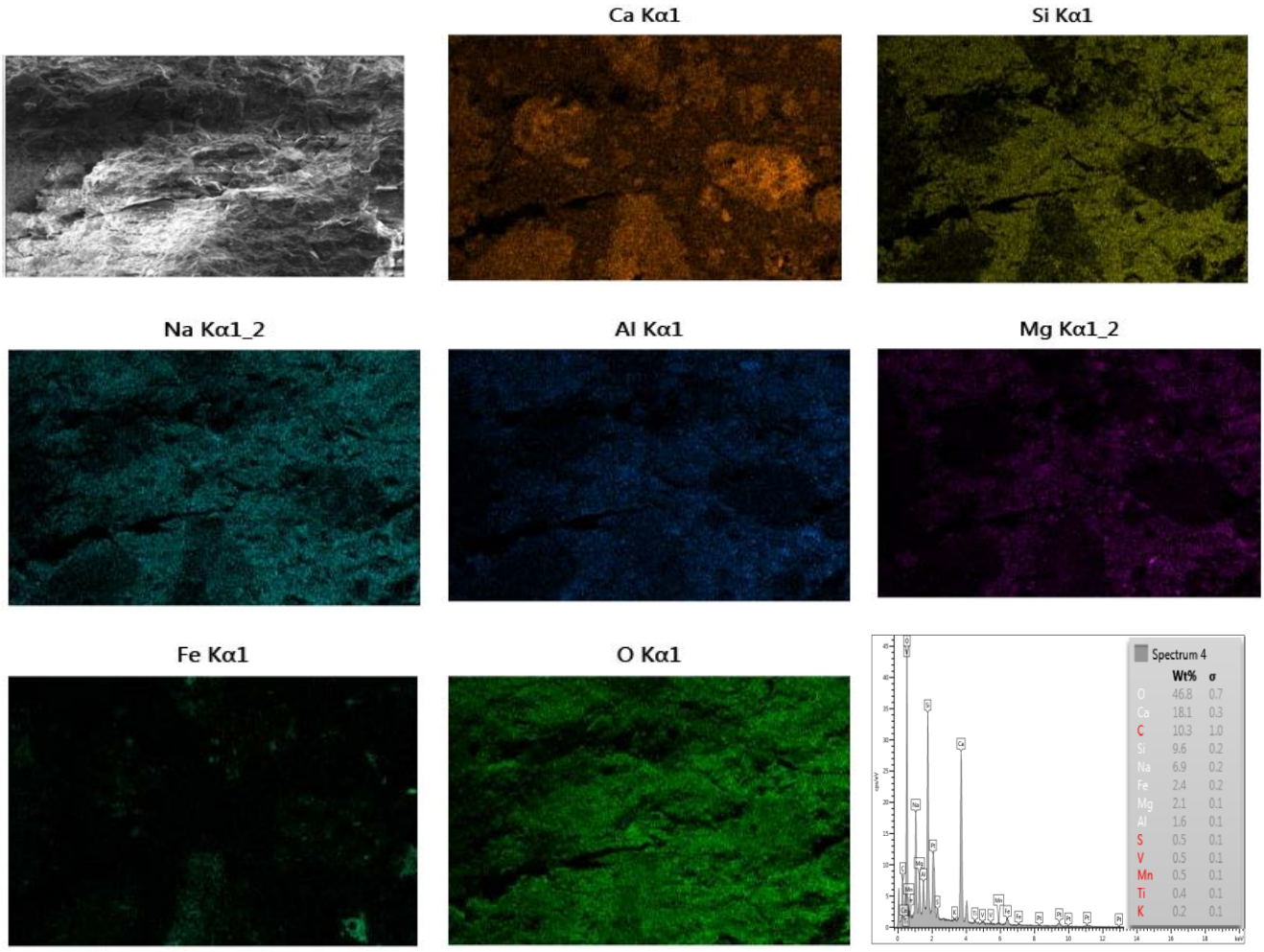

b)

Fig 6.1. The morphology of the mixture G1-10M: a) Carbonated BOF aggregates to binder 3; b) Element map of mixture containing carbonated BOF aggregates to binder 3

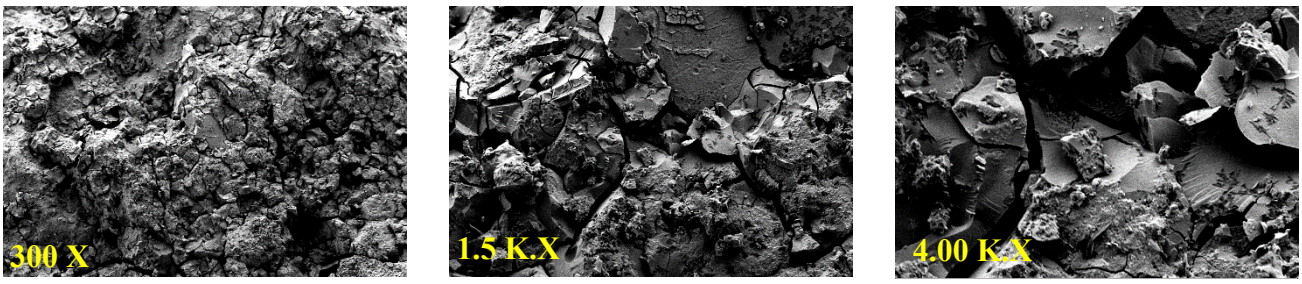

a) Fc: 51.84 MPa

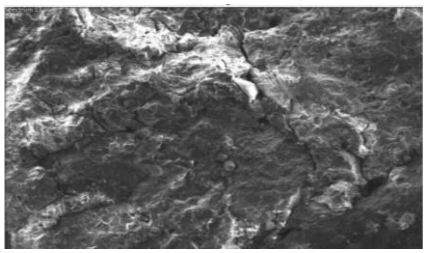

Ca Kα1

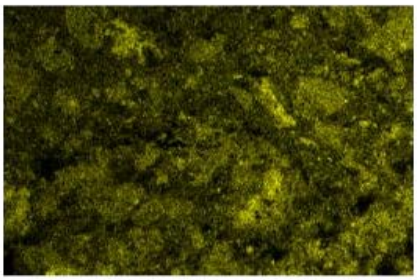

Si Kα1

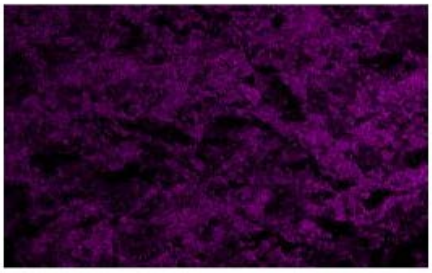

Na Kα1_2

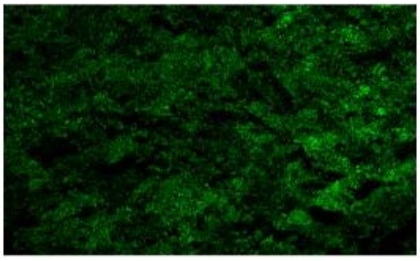

Al Kα1

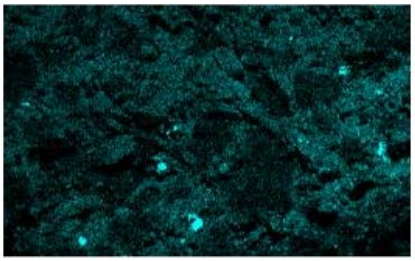

Mg Kα1_2

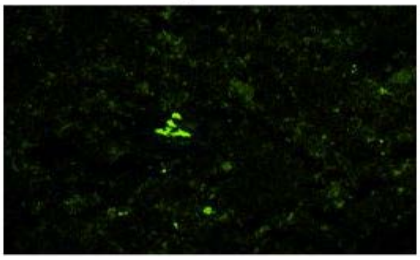

Fe Kα1

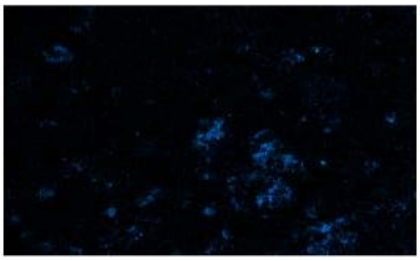

O Kα1

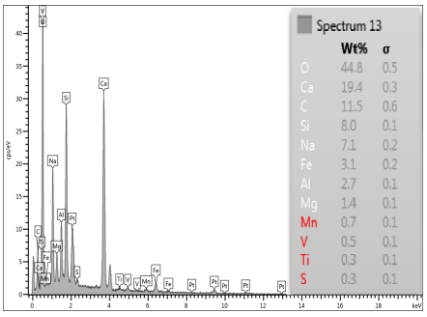

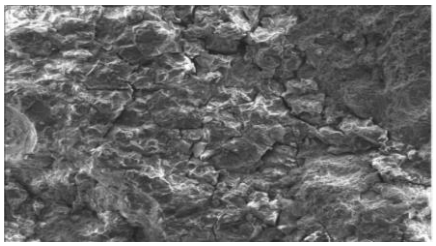

Ca Kα1

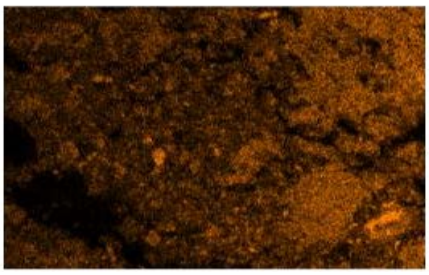

Si Kα1

Na Kα1_2

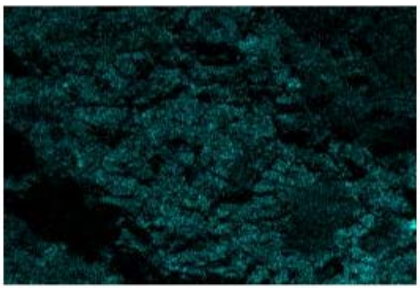

Al Kα1

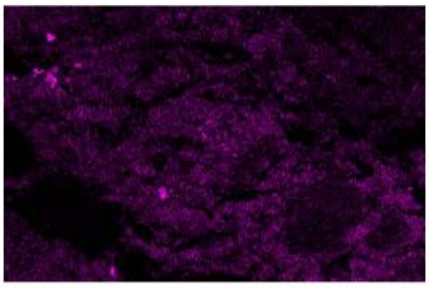

Mg Kα1_2

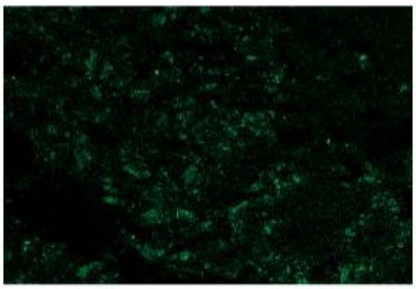

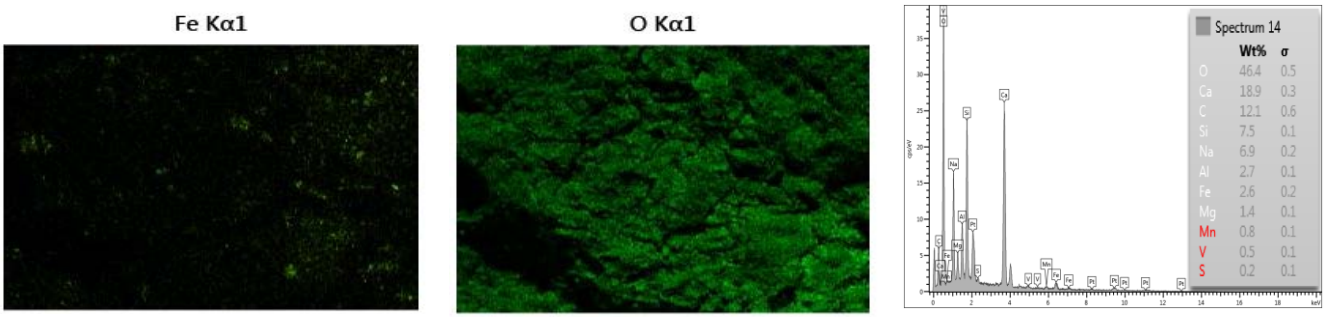

b)

Fig 7.1. The morphology of the mixture G0.5L0.5-10M: a) Carbonated BOF aggregates to binder 3; b) Element map of mixture containing carbonated BOF aggregates to binder 3

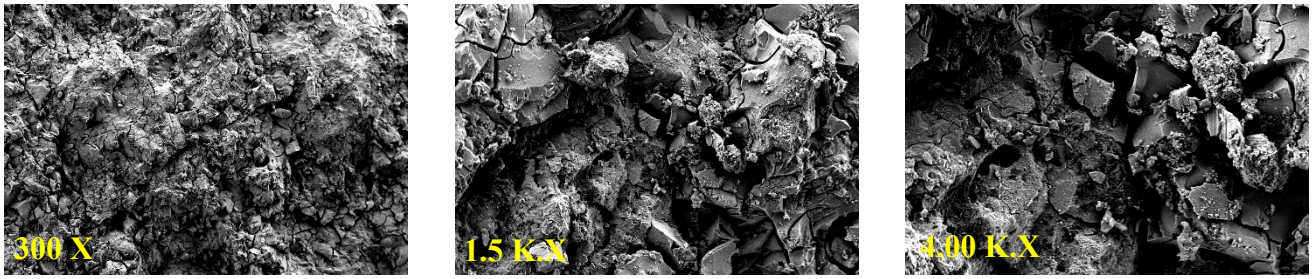

a) Fc: 27.34 MPa

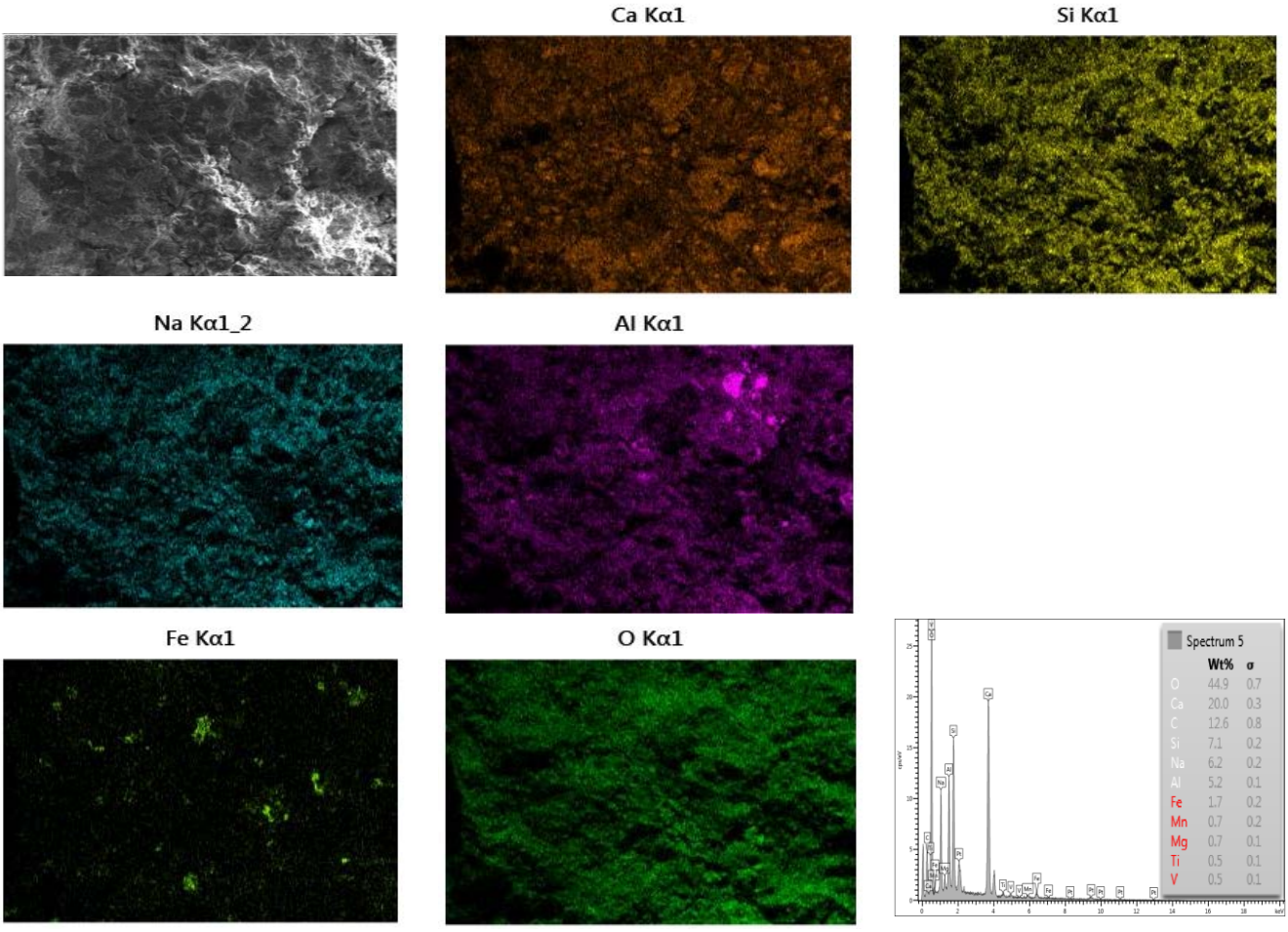

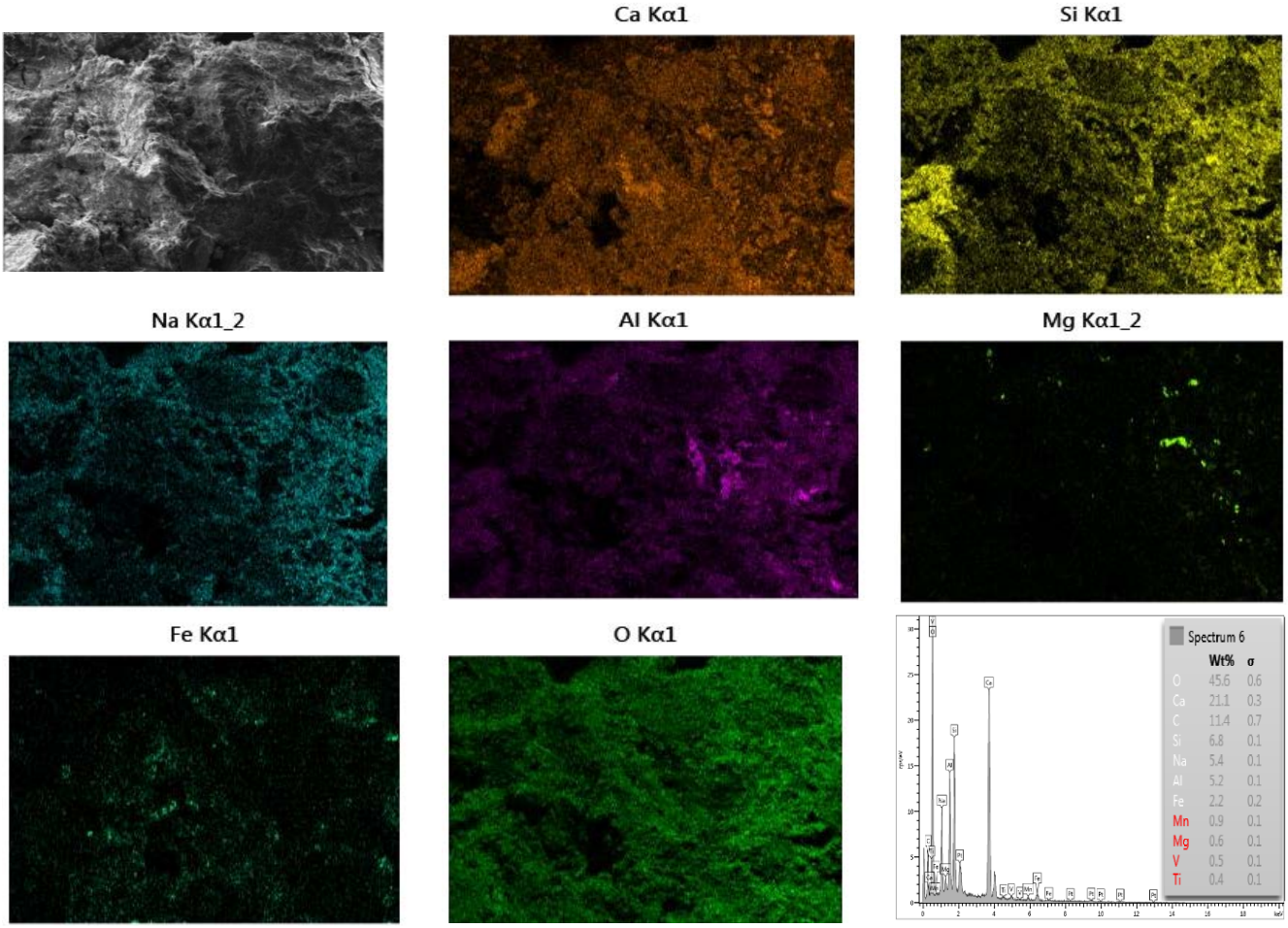

b)

Fig 8.1. The morphology of the mixture L1-8M: a) Carbonated BOF aggregates to binder 3; b) Element map of mixture containing carbonated BOF aggregates to binder 3

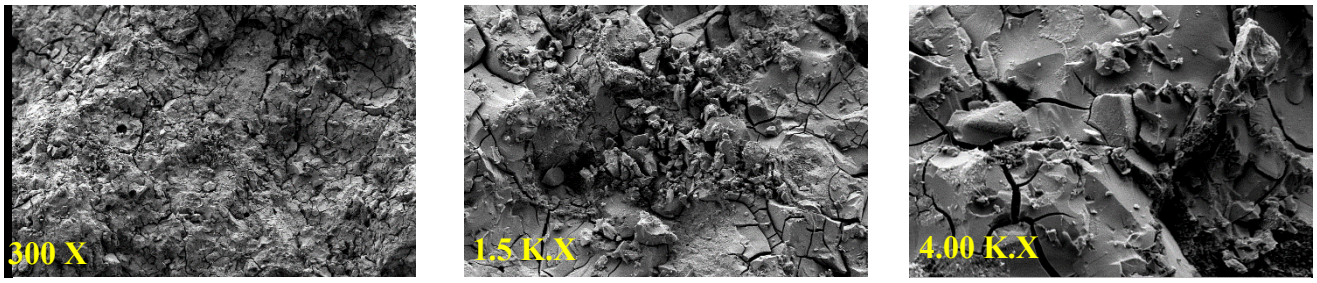

a) Fc: 53.89MPa

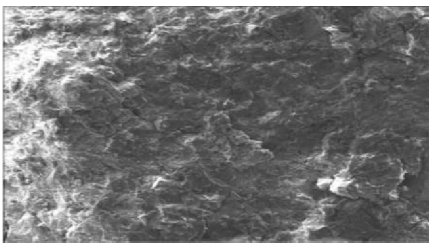

Ca Kα1

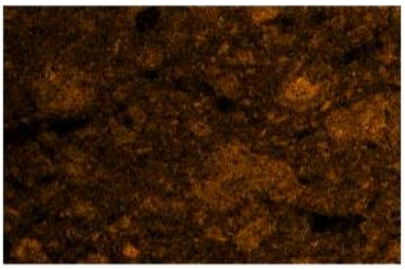

Si Kα1

Na Kα1_2

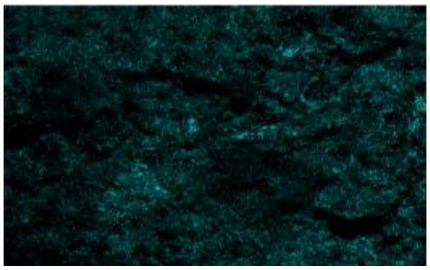

Al Kα1

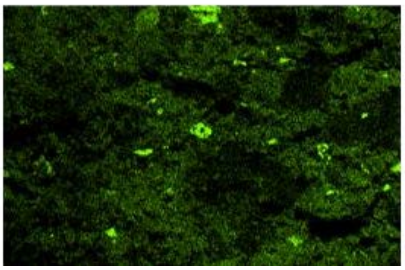

Mg Kα1_2

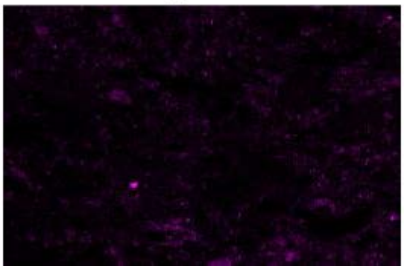

Fe Kα1

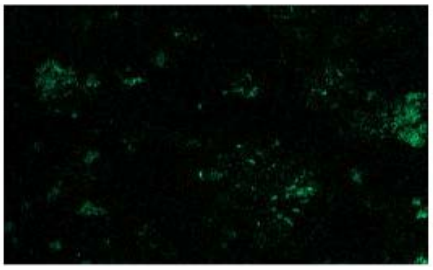

O Kα1

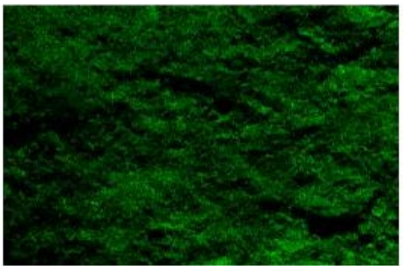

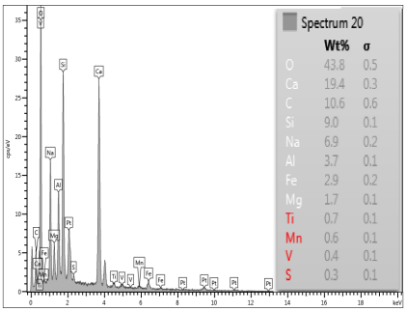

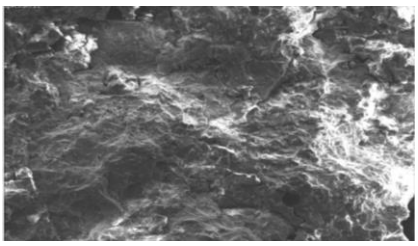

Ca Kα1

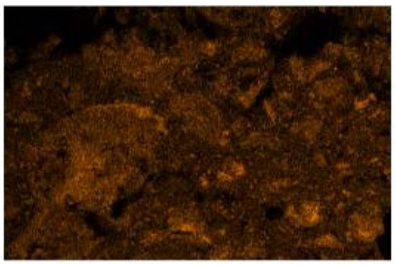

Si Kα1

Na Kα1_2

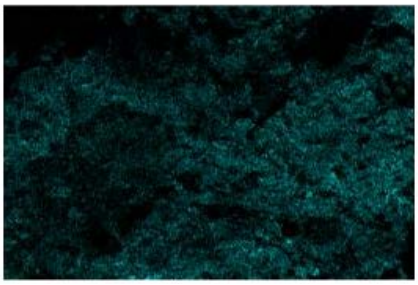

Al Kα1

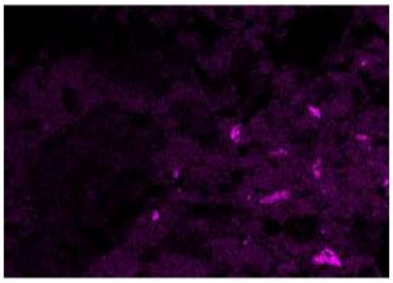

Mg Kα1_2

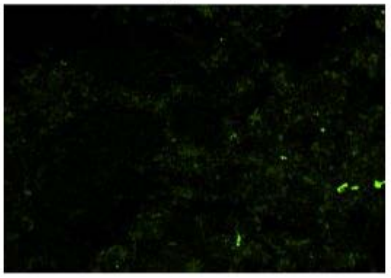

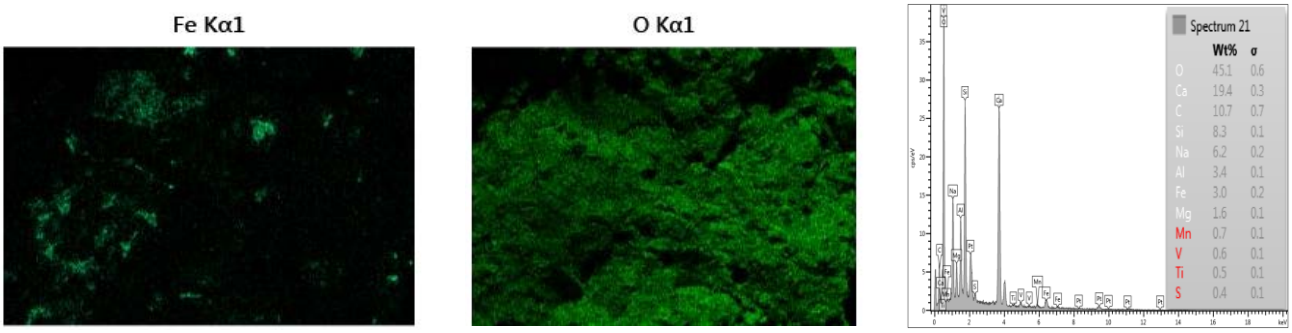

b)

Fig 9.1. The morphology of the mixture G0.5L0.5-8M: a) Carbonated BOF aggregates to binder 3; b) Element map of mixture containing carbonated BOF aggregates to binder 3

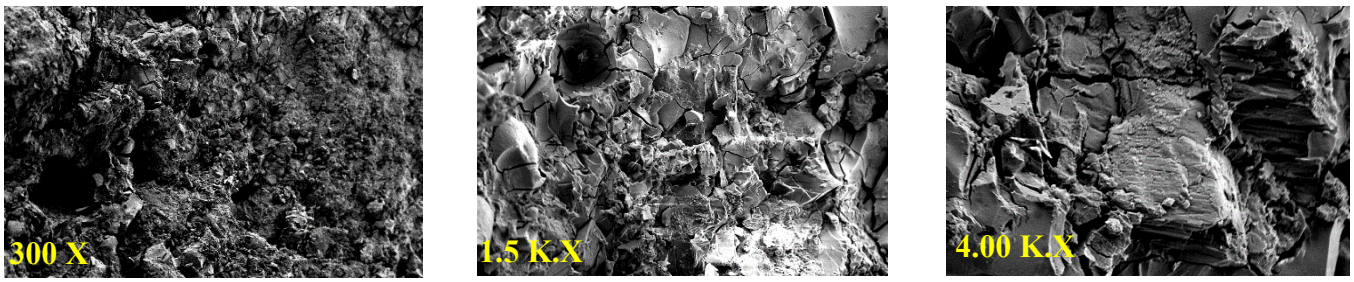

a) Fc: 44.66 MPa

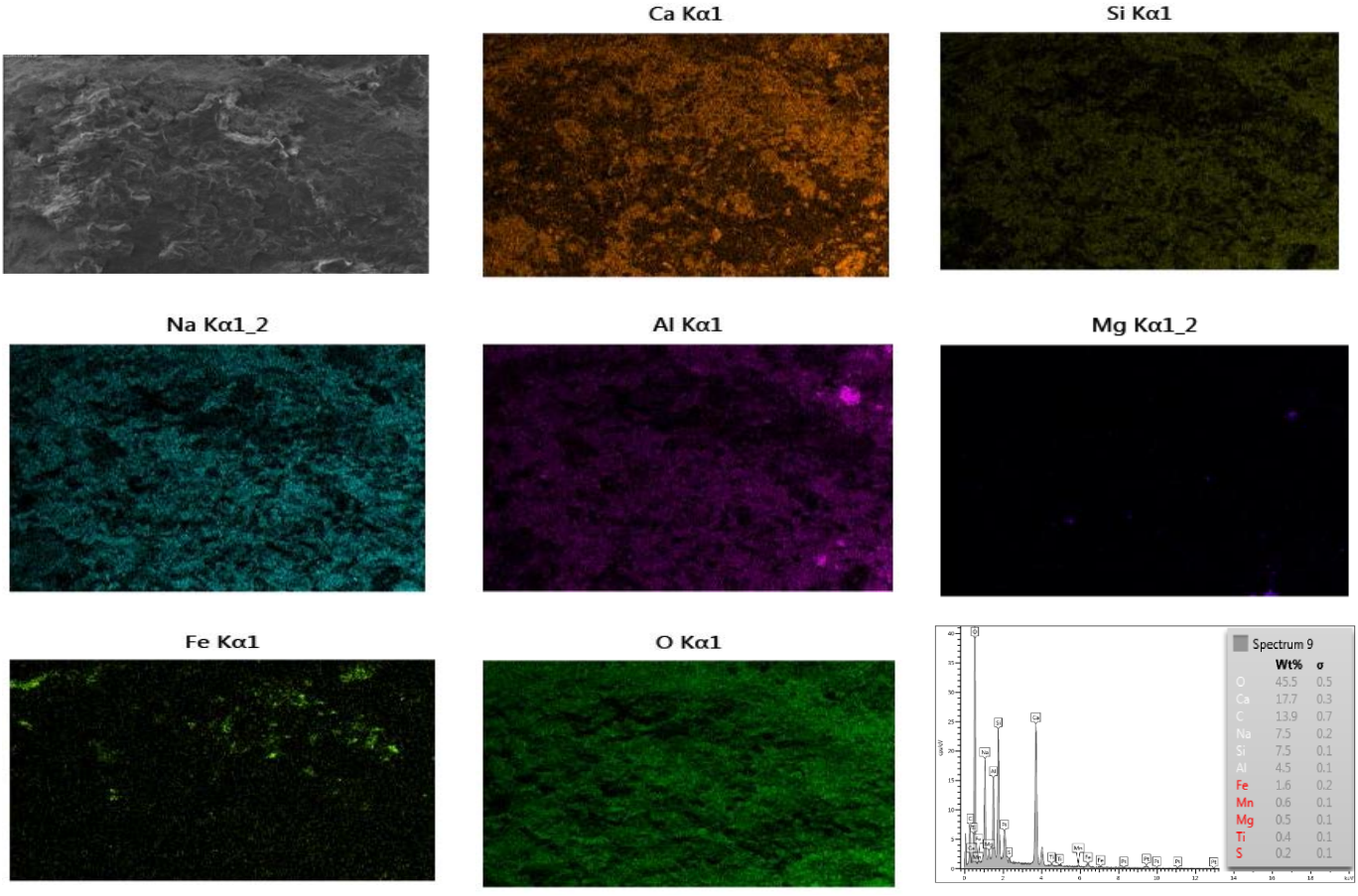

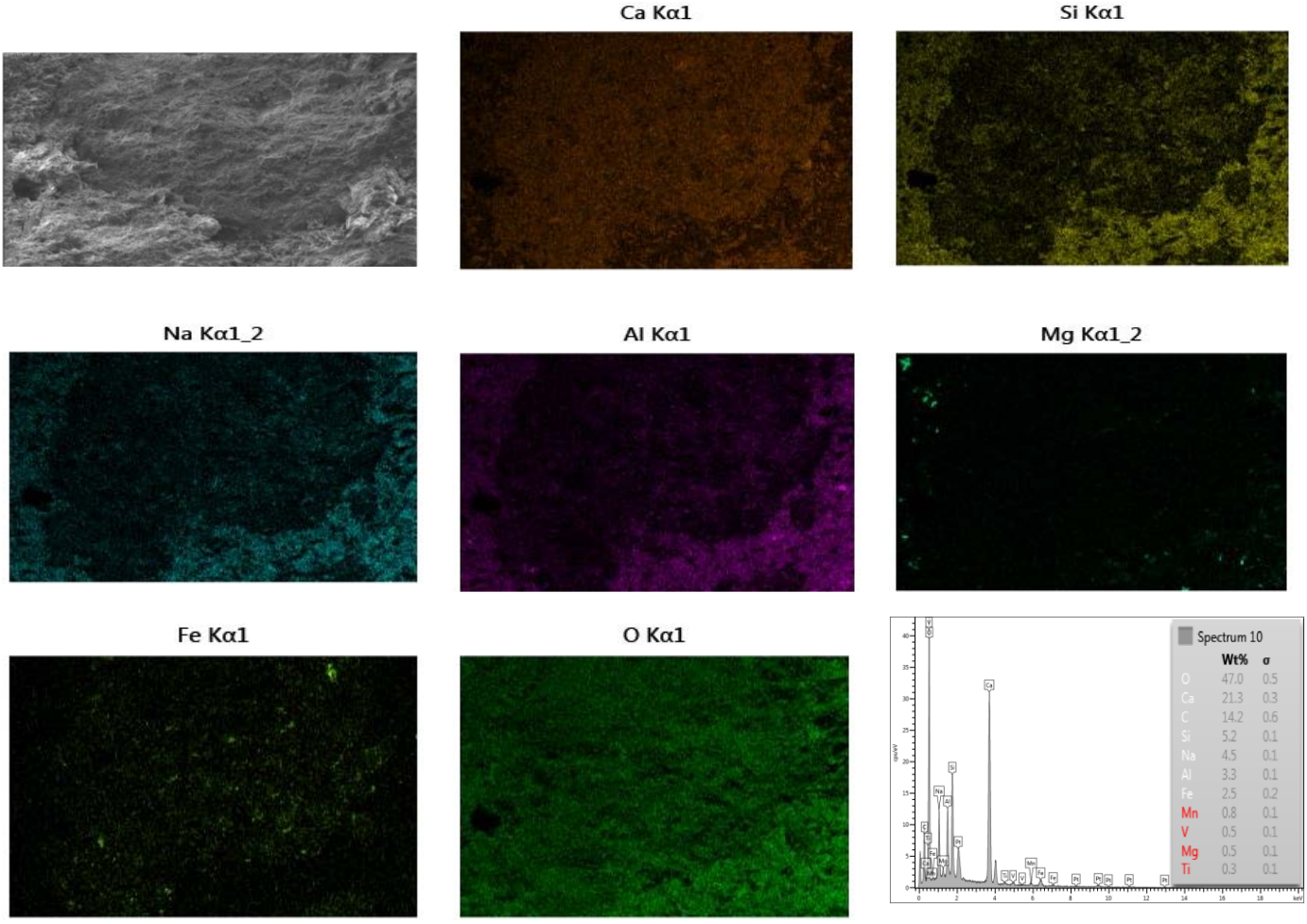

b)

Fig 10.1. The morphology of the mixture L1-6M: a) Carbonated BOF aggregates to binder 3; b) Element map of mixture containing carbonated BOF aggregates to binder 3

a) Fc: 42.51 MPa

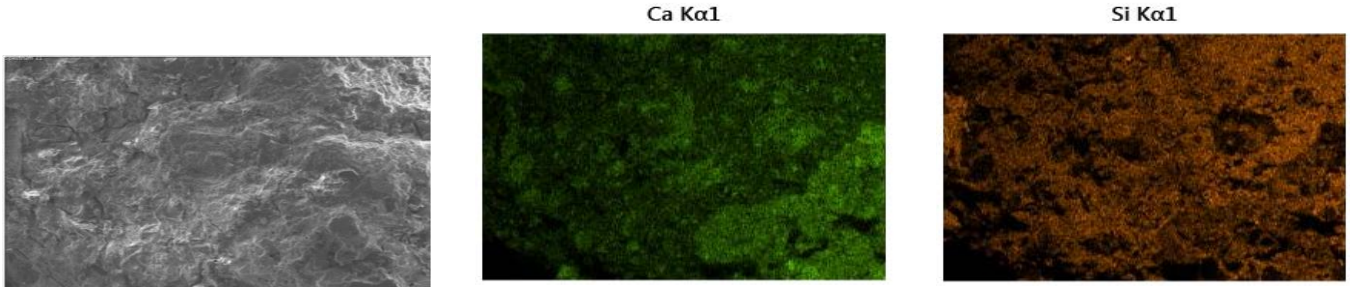

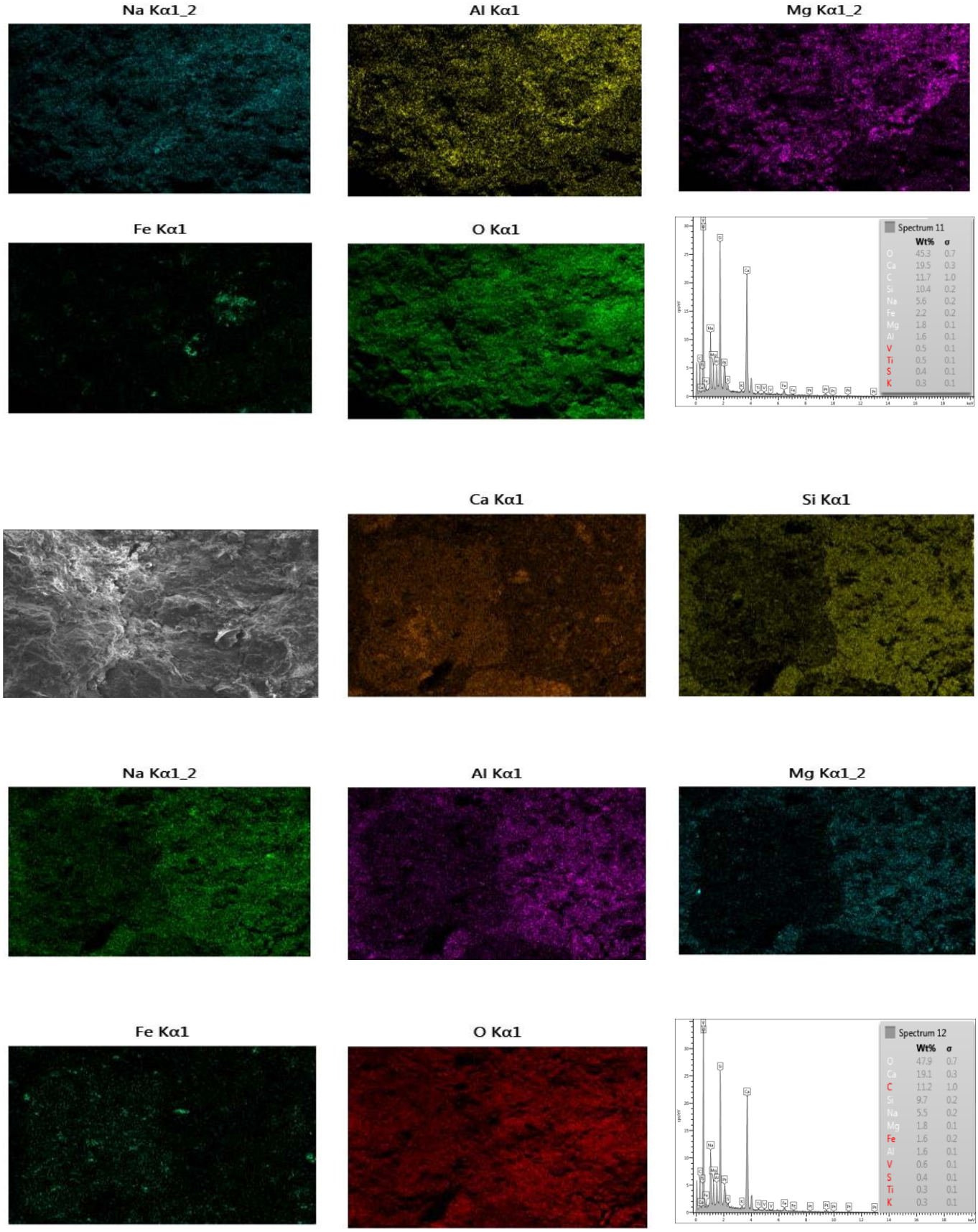

b)

Fig 11.1. The morphology of the mixture G1-6M: a) Carbonated BOF aggregates to binder 3; b) Element map of mixture containing carbonated BOF aggregates to binder 3

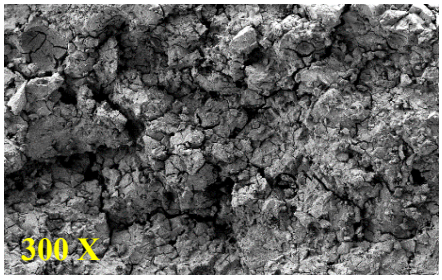

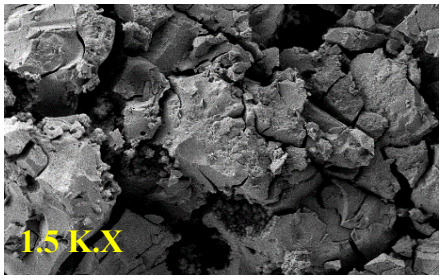

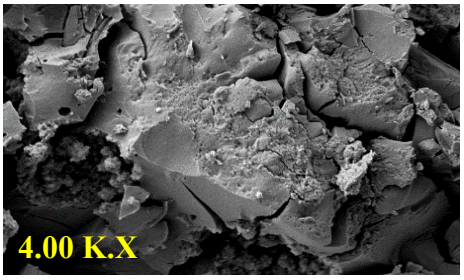

a) Fc: 49.94 MPa

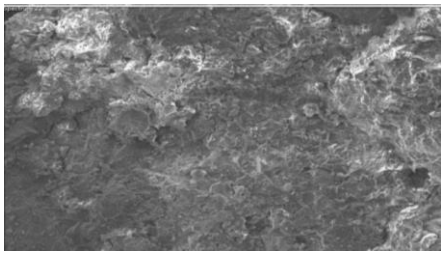

Ca Kα1

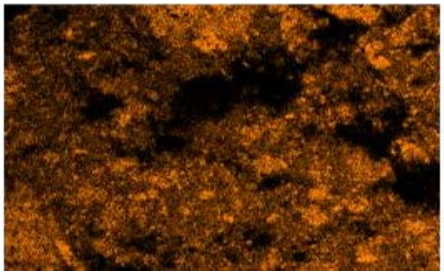

Si Kα1

Na Kα1_2

Al Kα1

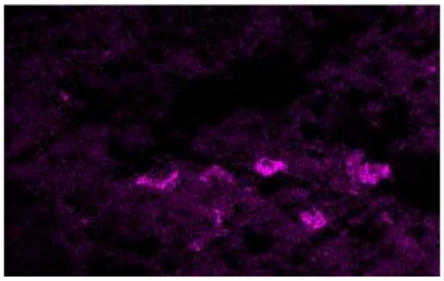

Mg Kα1_2

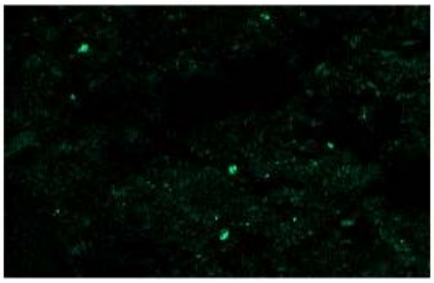

Fe Kα1

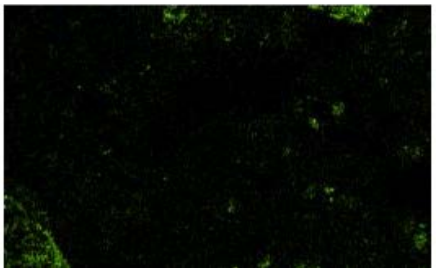

O Kα1

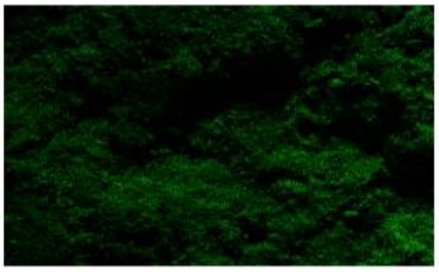

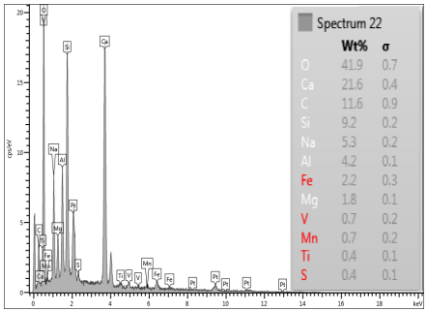

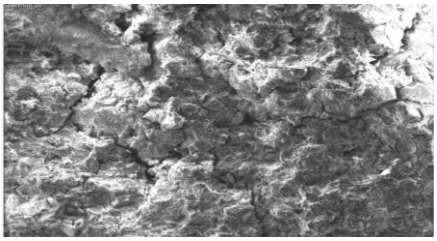

Ca Kα1

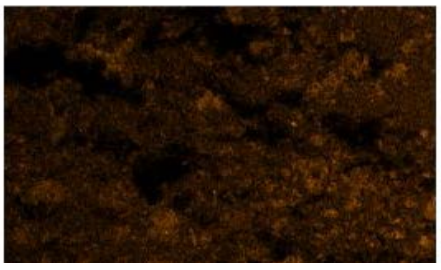

Si Kα1

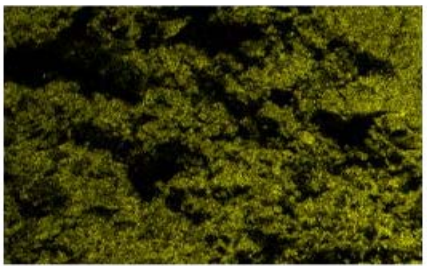

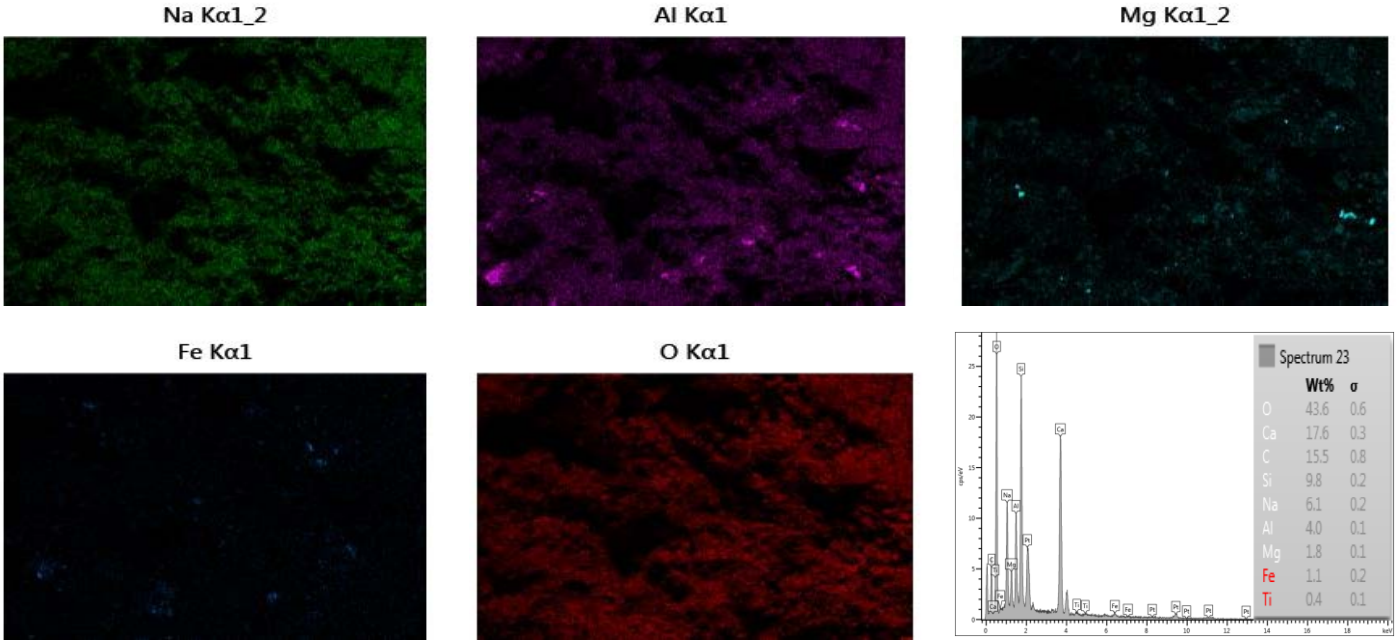

b)

Fig 12.1. The morphology of the mixture G0.5L0.5-6M: a) Carbonated BOF aggregates to binder 3; b) Element map of mixture containing carbonated BOF aggregates to binder 3

a) Fc: 21.08 MPa

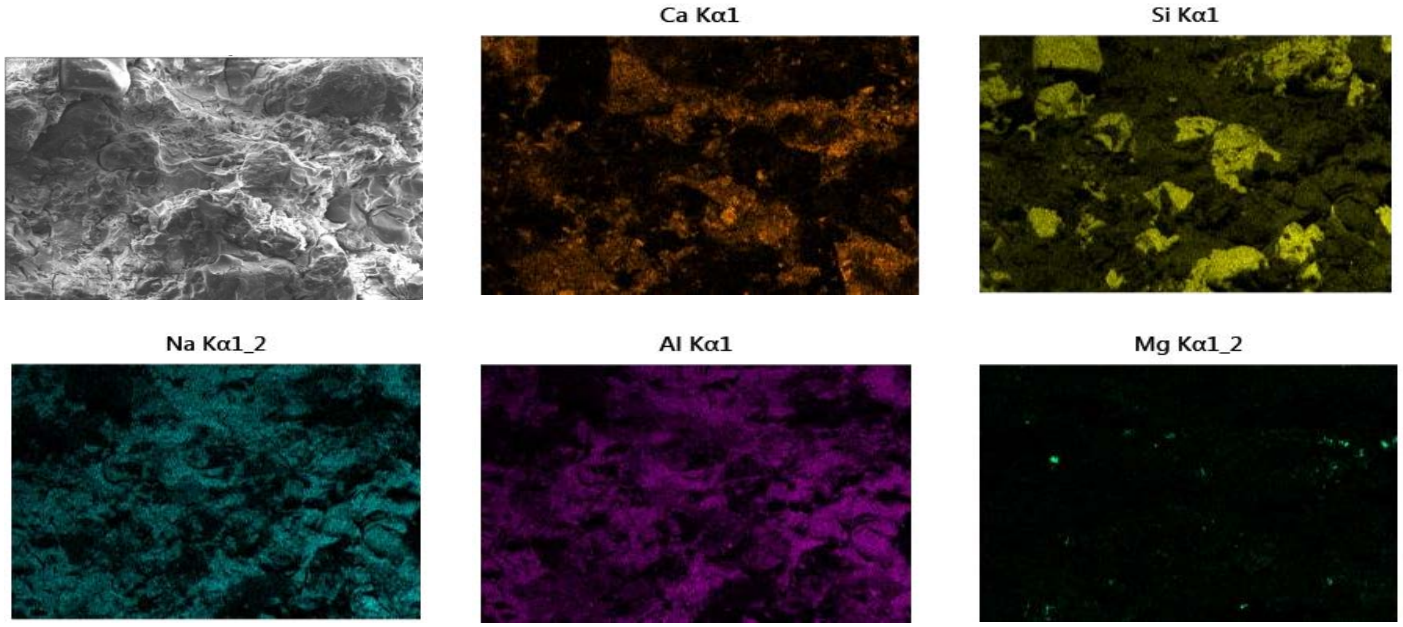

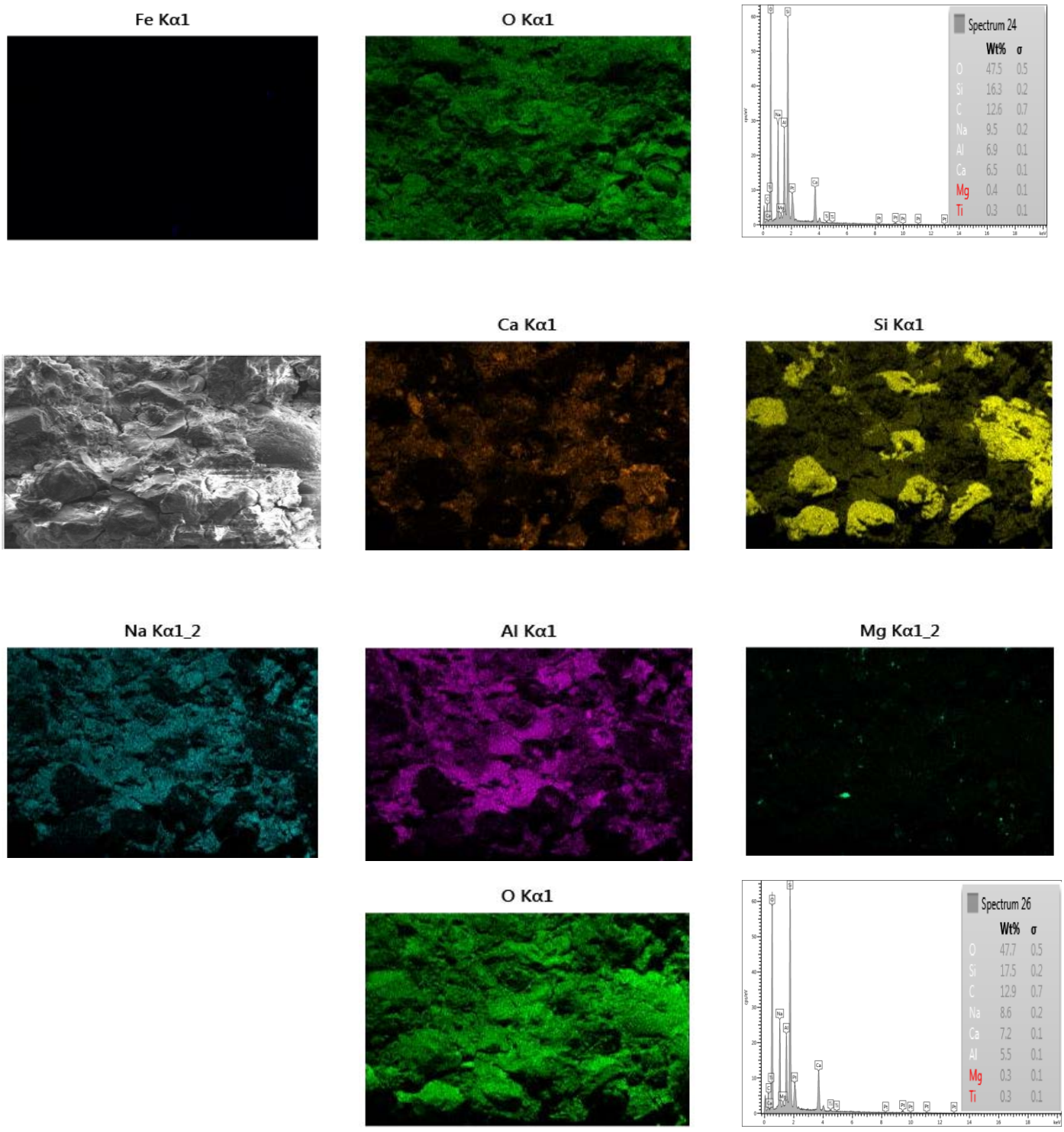

b)

Fig 13.1. The morphology of the mixture L1-10M: a) Normal aggregates to binder 3; b) Element map of mixture containing normal aggregates to binder 3

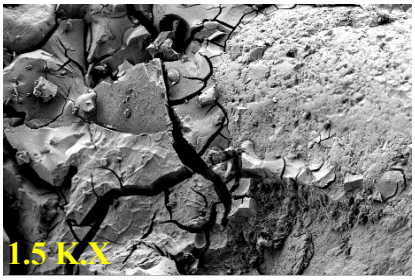

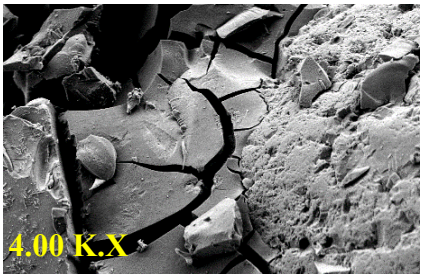

a) Fc: 42.15 MPa

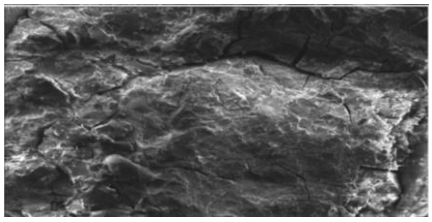

Ca Kα1

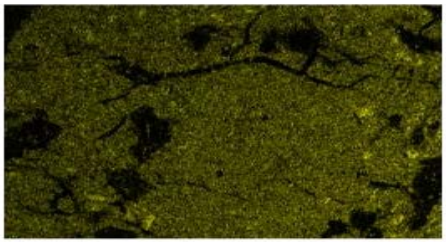

Si Kα1

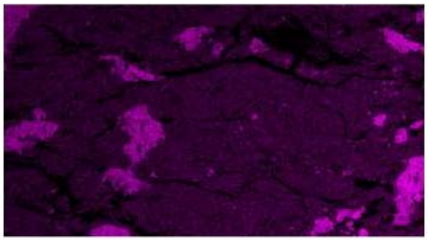

Na Kα1_2

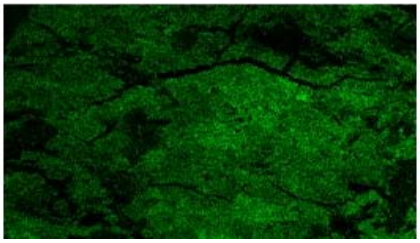

Al Kα1

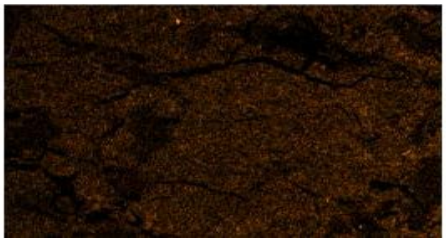

Mg Kα1_2

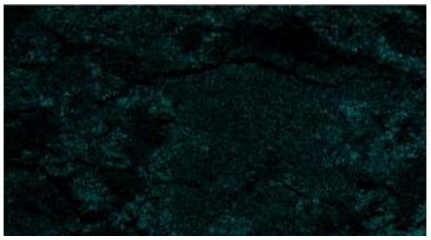

Fe Kα1

O Kα1

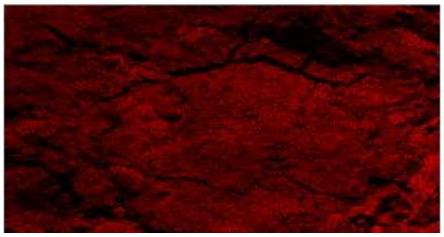

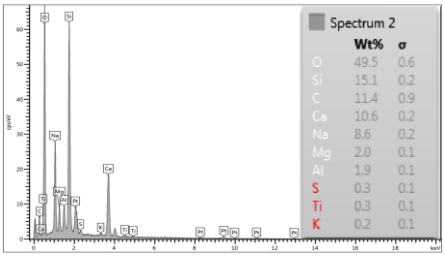

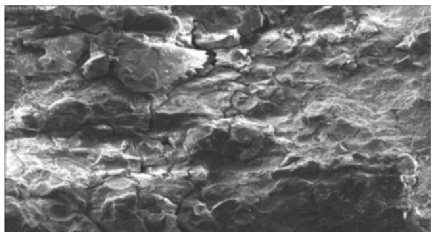

Ca Kα1

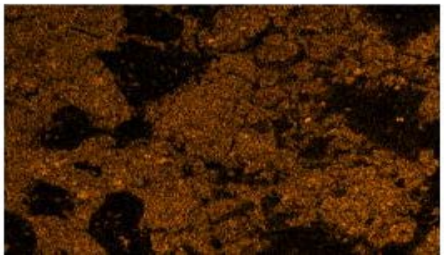

Si Kα1

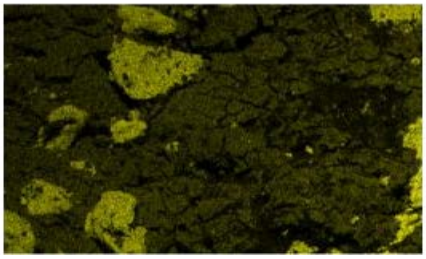

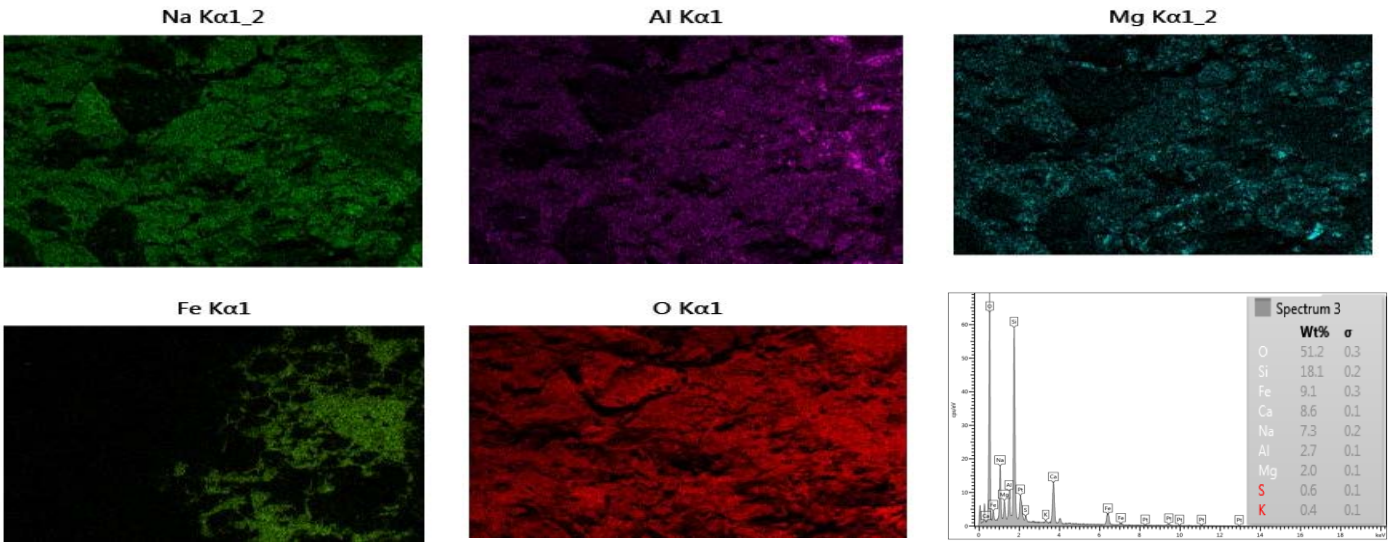

b)

Fig 14.1. The morphology of the mixture G1-10M: a) Normal aggregates to binder 3; b) Element map of mixture containing normal aggregates to binder 3.

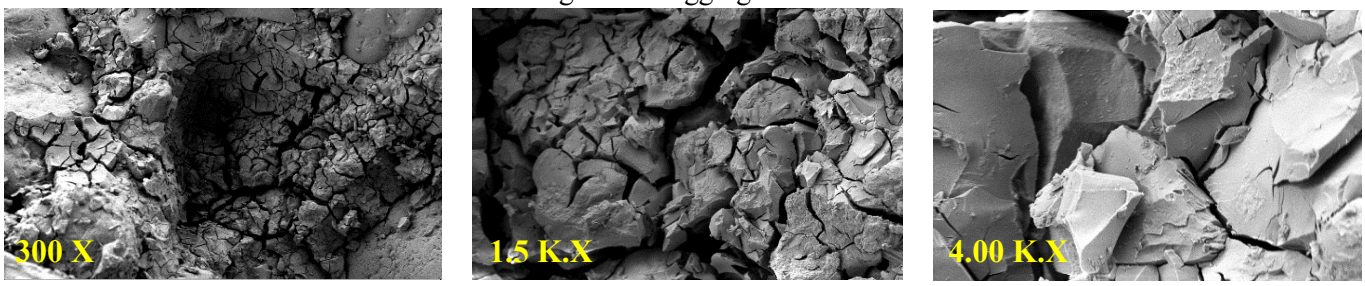

a) Fc: 34.45 MPa

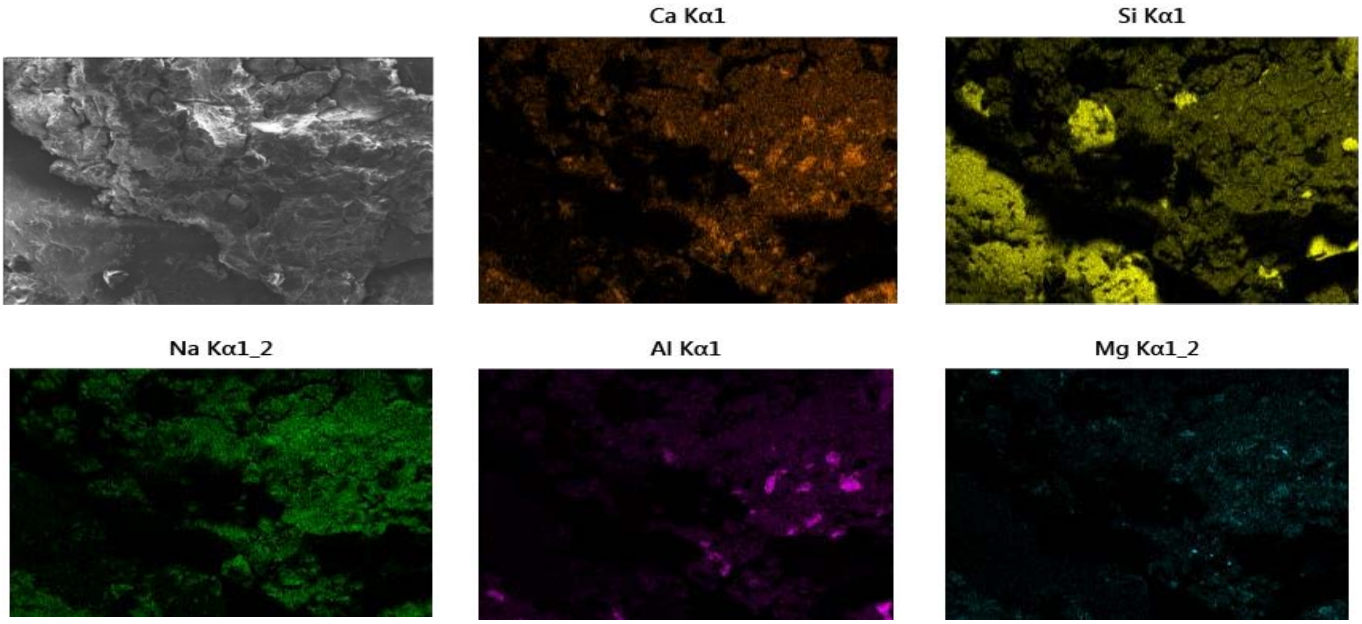

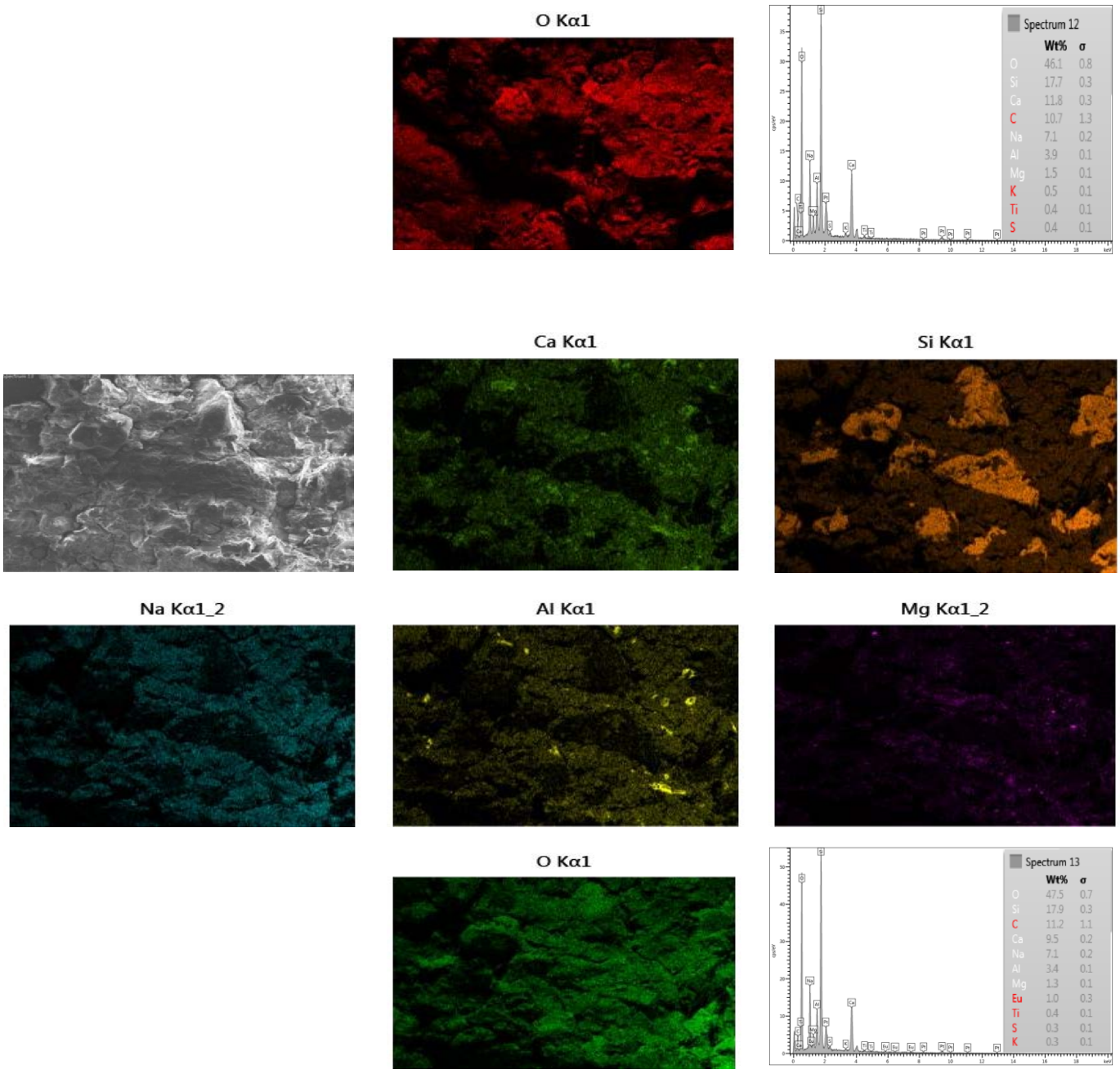

b)

Fig 15.1. The morphology of the mixture G0.5L0.5-10M: a) Normal aggregates to binder 3; b) Element map of mixture containing normal aggregates to binder 3

a) Fc: 21.26 MPa

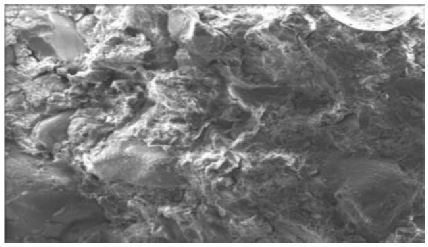

Ca Kα1

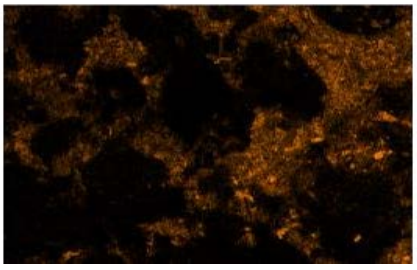

Si Kα1

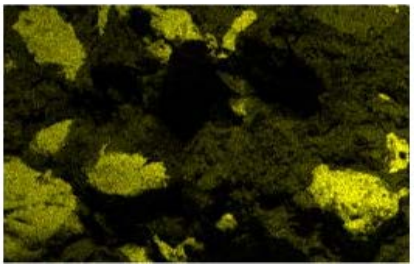

Na Kα1_2

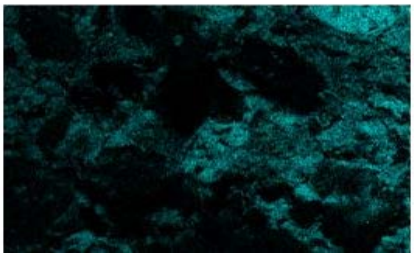

Al Kα1

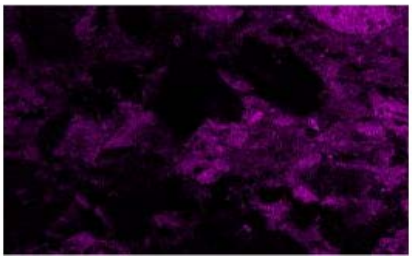

Mg Kα1_2

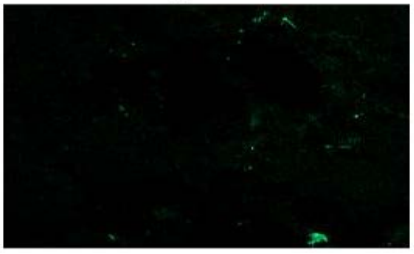

Fe Kα1

O Kα1

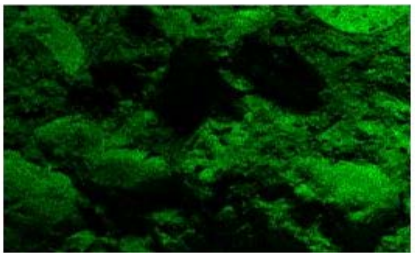

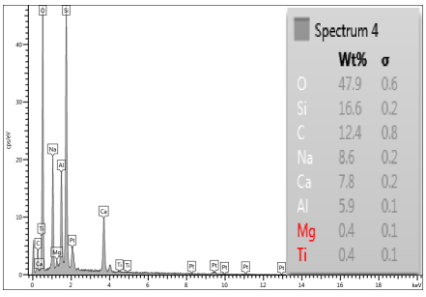

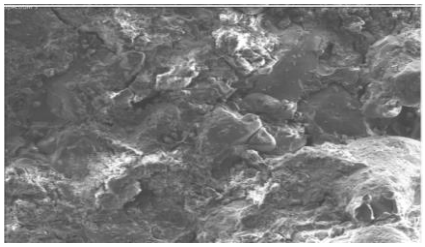

Ca Kα1

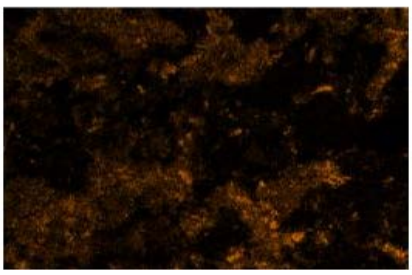

Si Kα1

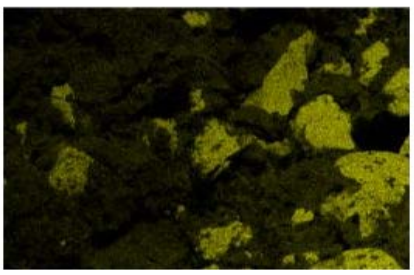

Na Kα1_2

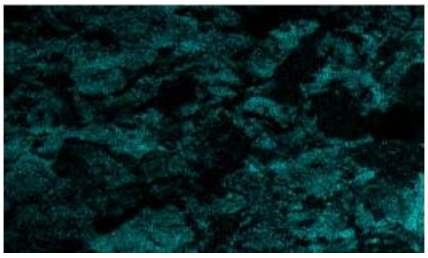

Al Kα1

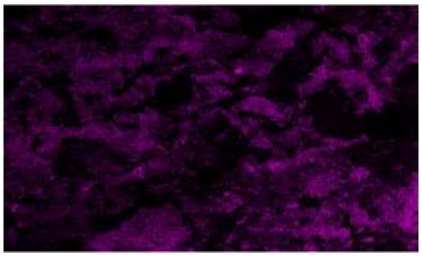

Mg Kα1_2

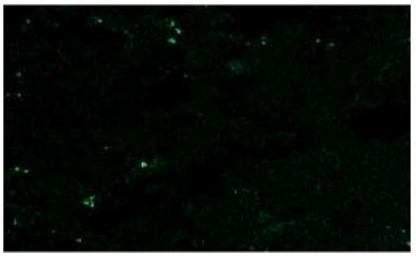

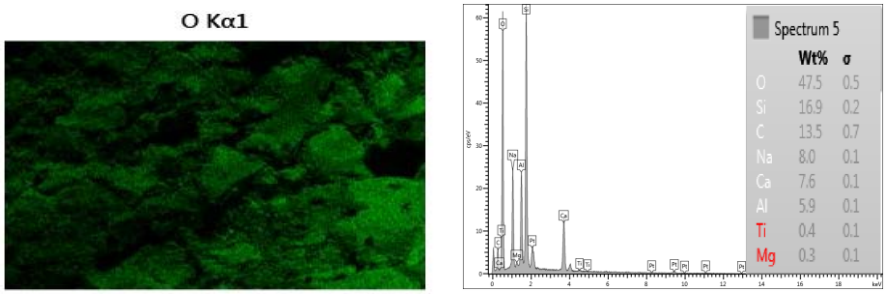

b)

Fig 16.1. The morphology of the mixture L1-8M: a) Normal aggregates to binder 3; b) Element map of mixture containing normal aggregates to binder 3

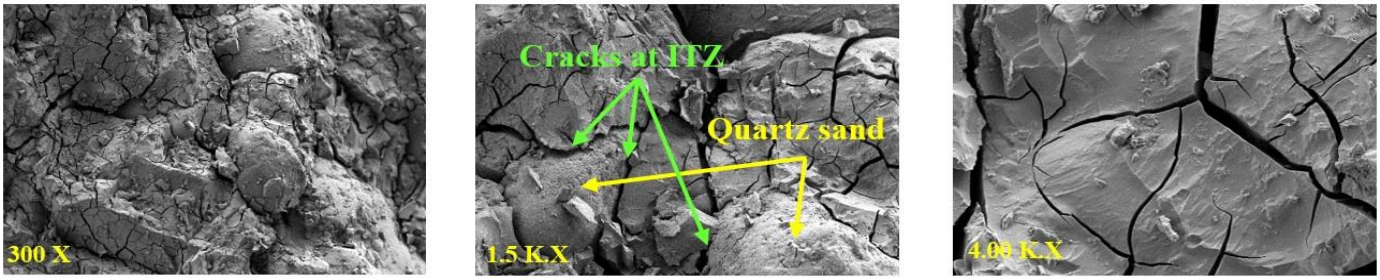

a) Fc: 32.33 MPa

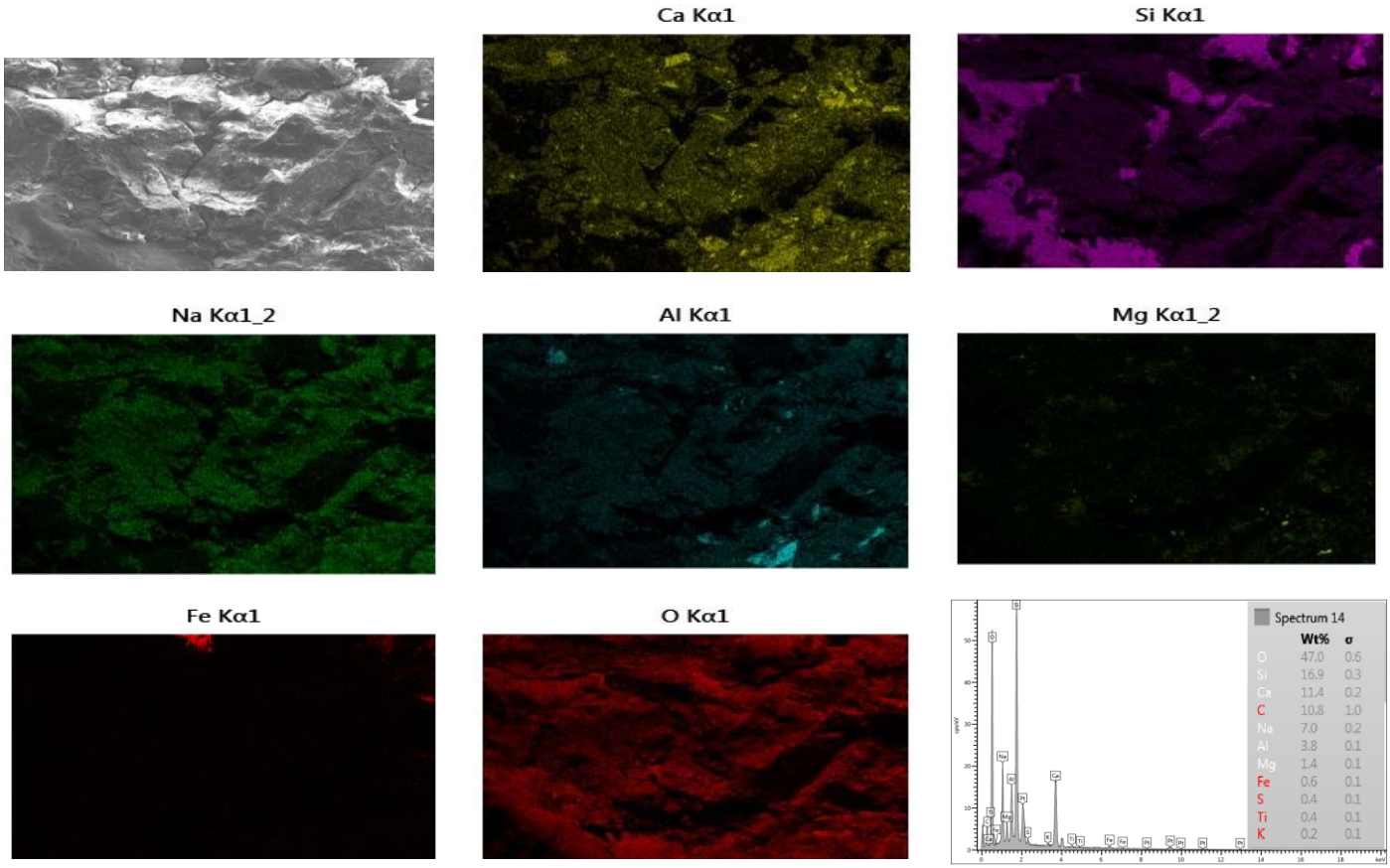

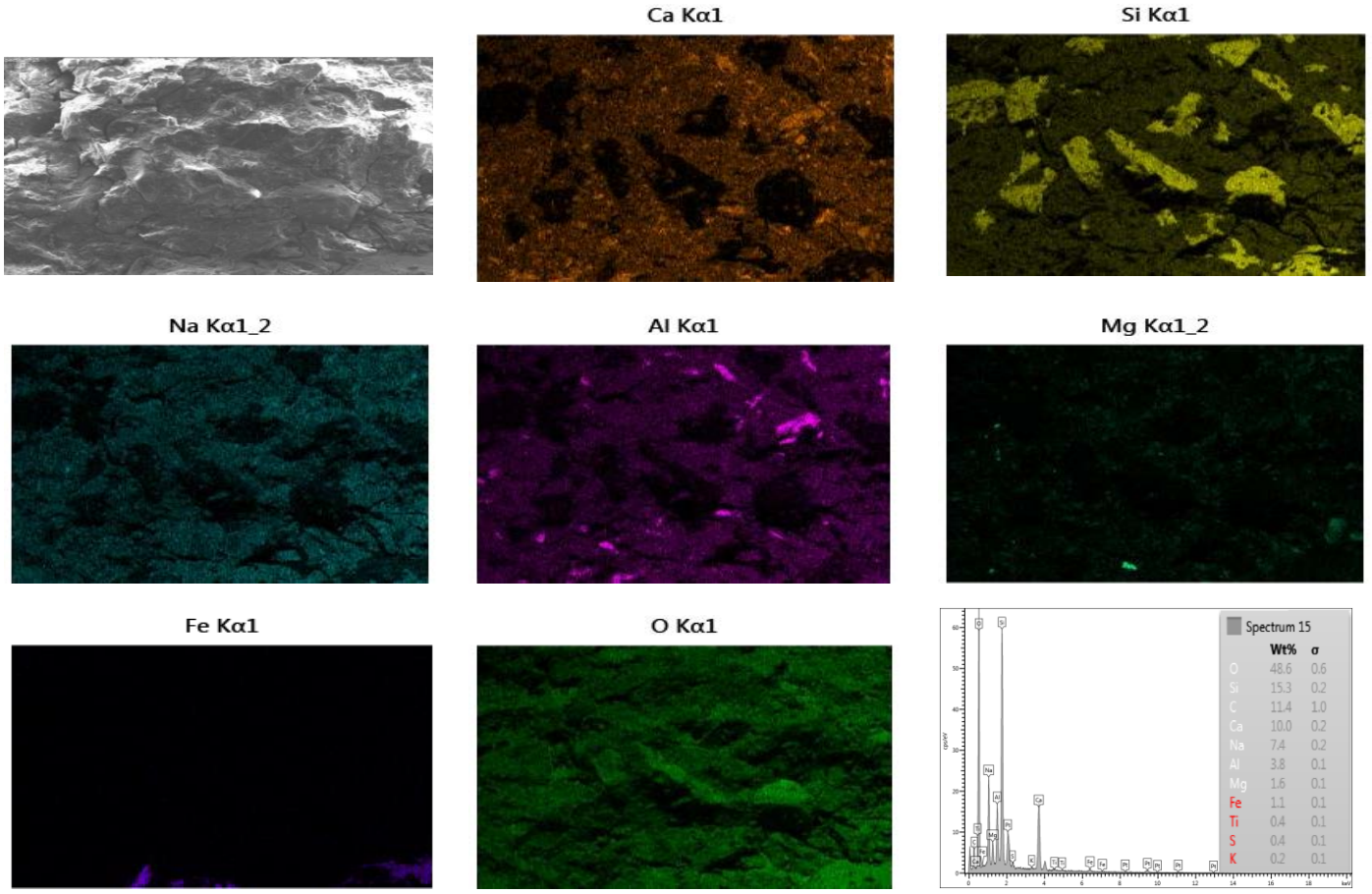

b)

Fig 17.1. The morphology of the mixture G0.5L0.5-8M: a) Normal aggregates to binder 3; b) Element map of mixture containing normal aggregates to binder 3

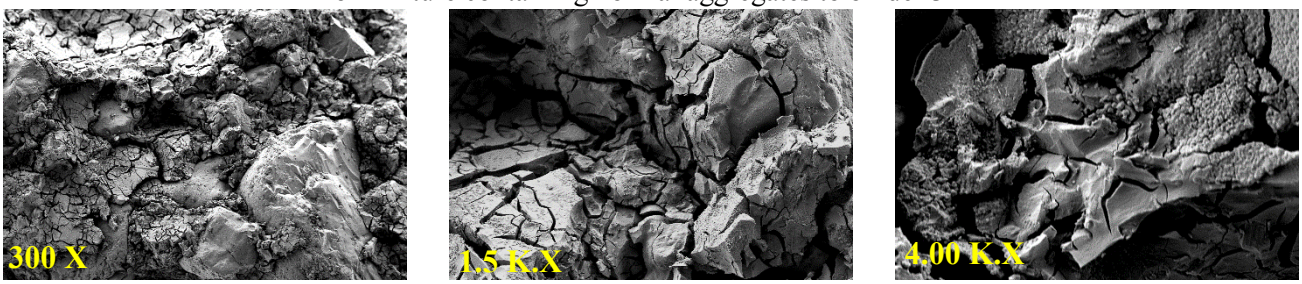

a) Fc: 22.69 MPa

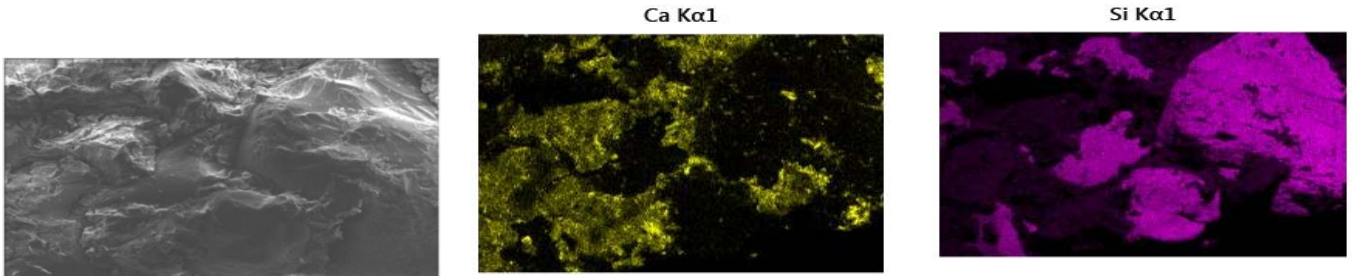

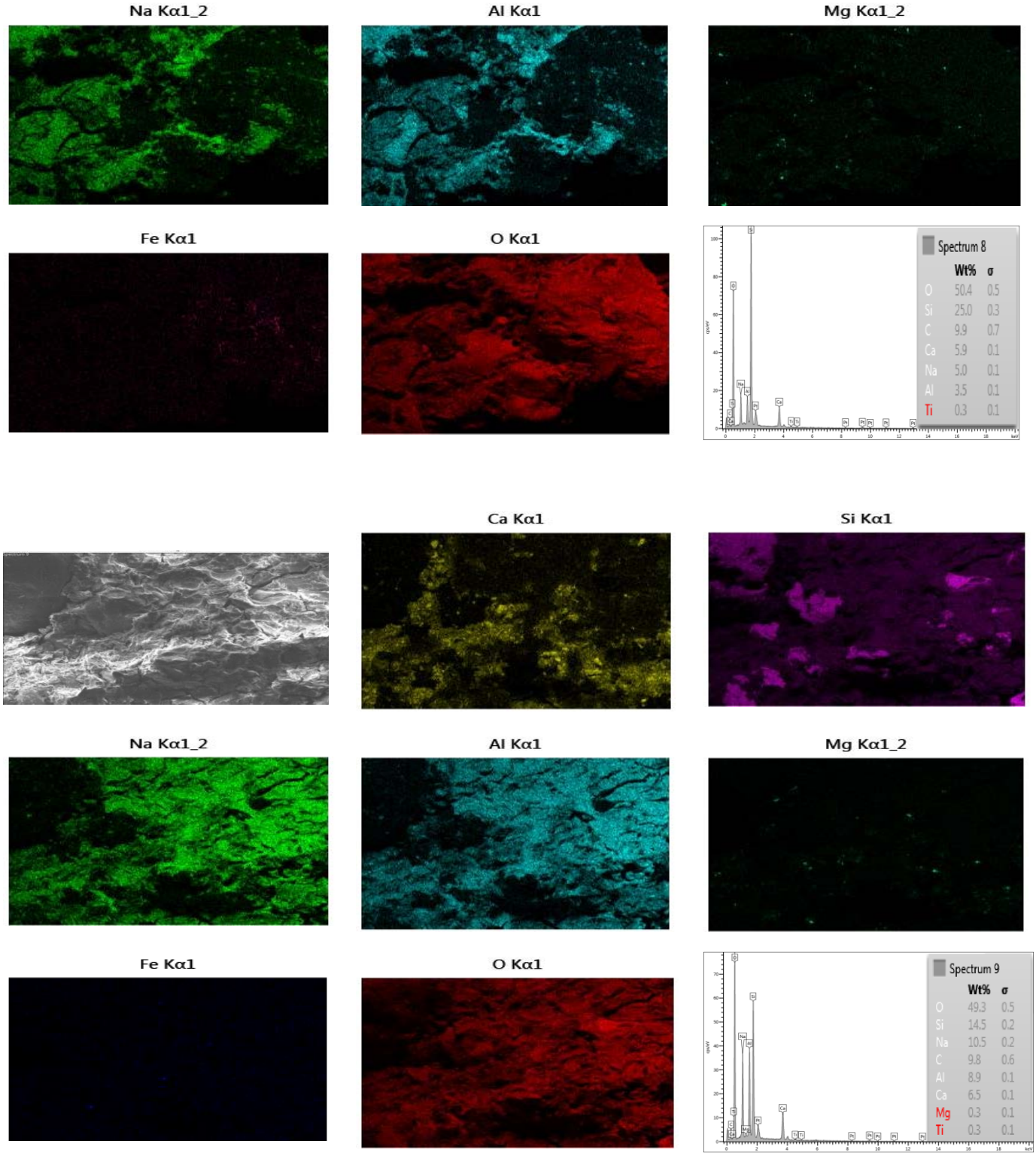

b)

Fig 18.1. The morphology of the mixture L1-6M: a) Normal aggregates to binder 3; b) Element map of mixture containing normal aggregates to binder 3

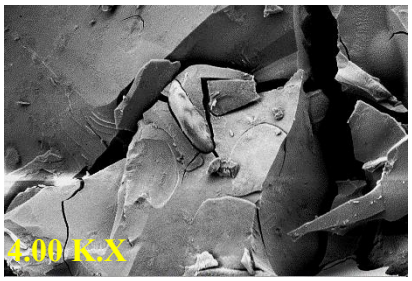

a) Fc: 47.83 MPa

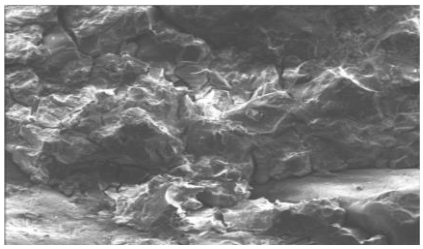

Ca Kα1

Si Kα1

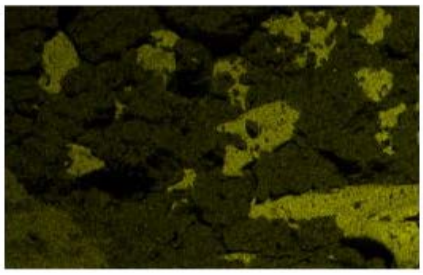

Na Kα1_2

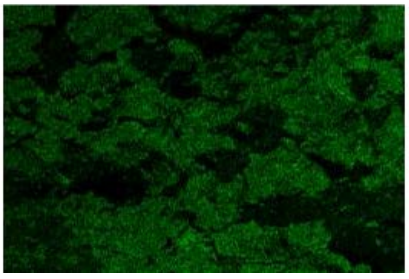

Al Kα1

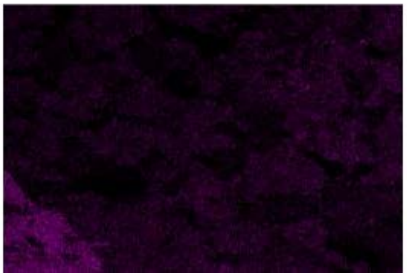

Mg Kα1_2

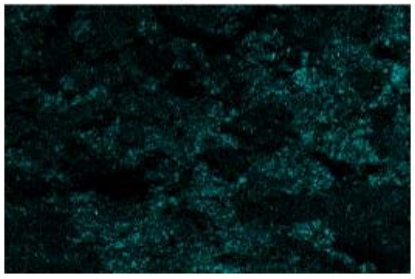

Fe Kα1

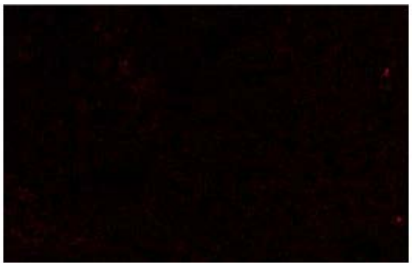

O Kα1

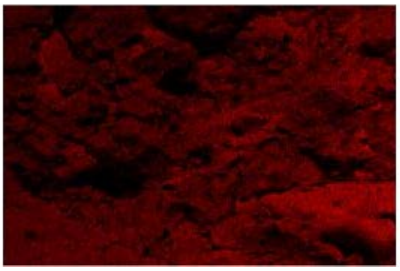

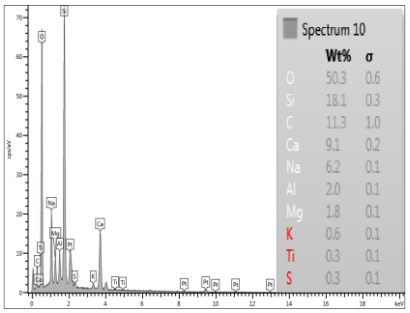

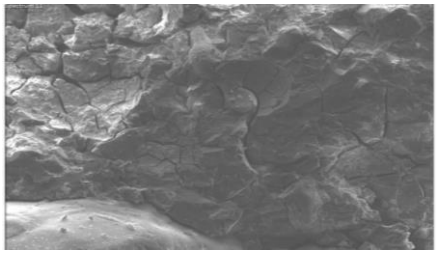

Ca Kα1

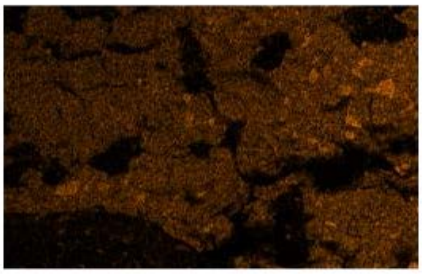

Si Kα1

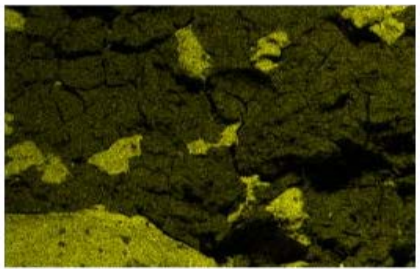

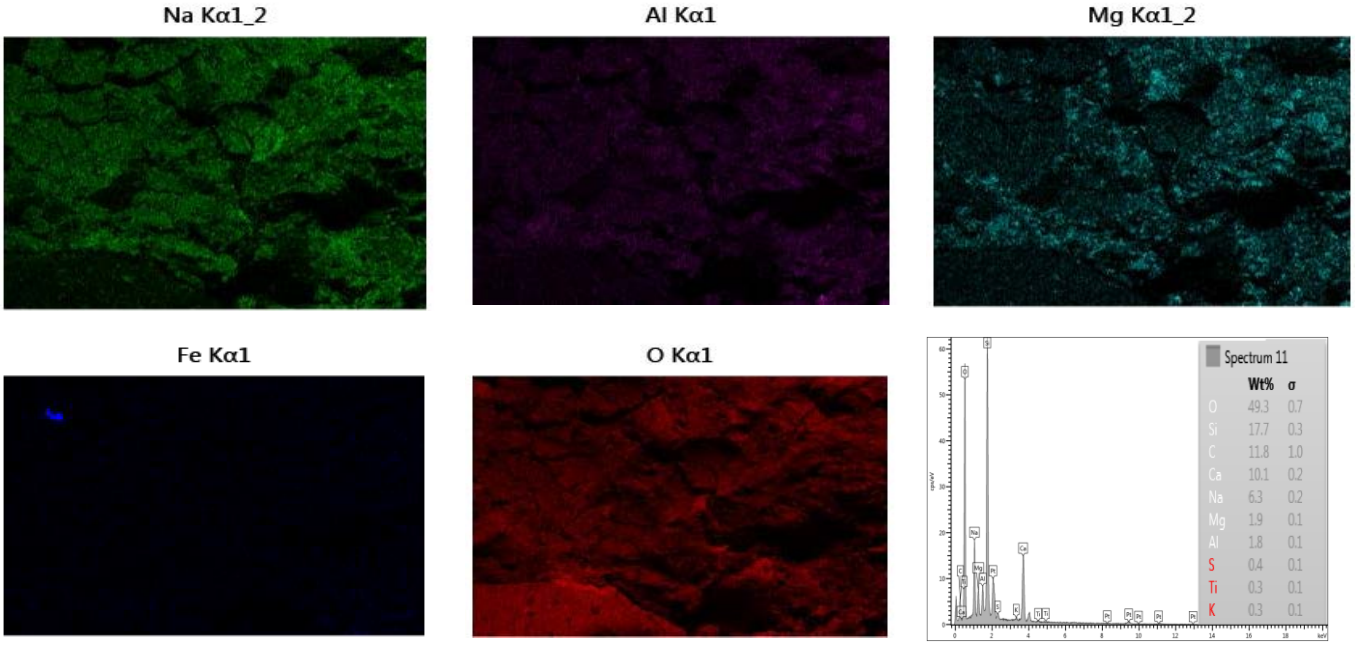

b)

Fig 19.1. The morphology of the mixture G1-6M: a) Normal aggregates to binder 3; b) Element map of mixture containing normal aggregates to binder 3

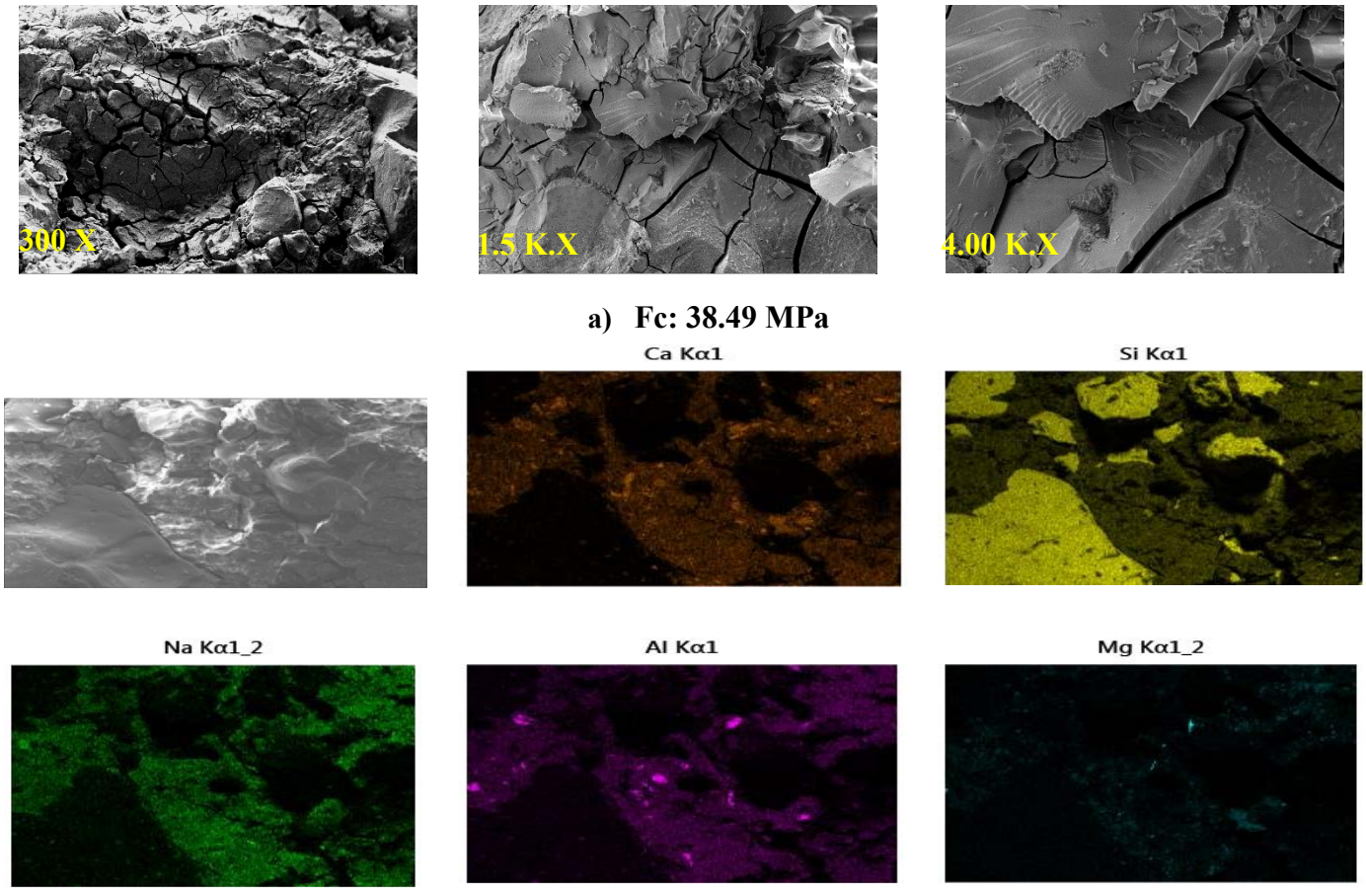

a) Fc: 38.49 MPa

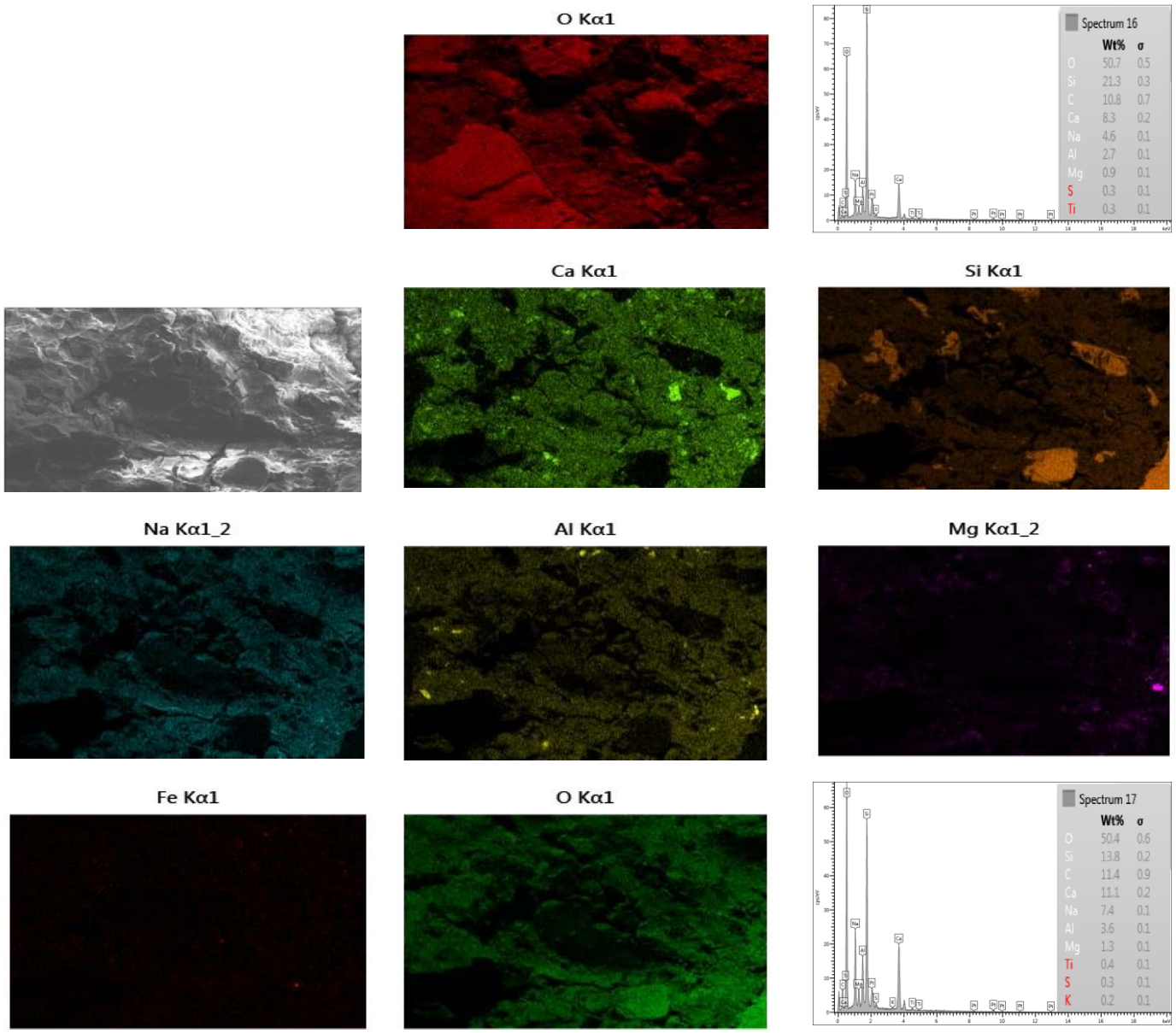

b)

Fig 20.1. The morphology of the mixture G0.5L0.5-6M: a) Normal aggregates to binder 3; b) Element map of mixture containing normal aggregates to binder 3

1.4.3.1 EDS analysis:

The atomic ratios of the carbonated BOF aggregate and normal aggregate are listed in Table 3.1.

Table 3.1. Atomic ratio of a) Carbonated BOF b) Normal aggregate

a)

Atomic ratios	L1-10M (30.47 MPa)			G1-10M (42.04 MPa)			L1-8M (27.34 MPa)			L1-6M (44,66 MPa)			G1-6M (42.51 MPa)			G0.5L0.5-10M (51,84 MPa)			G0.5L0.5-8M (53,89 MPa)			G0.5L0.5-6M (49.94 MPa)		
	ID:1	ID:2	Ave.	ID:1	ID:2	Ave.	ID:1	ID:2	Ave.	ID:1	ID:2	Ave.	ID:1	ID:2	Ave.	ID:1	ID:2	Ave.	ID:1	ID:2	Ave.	ID:1	ID:2	Ave.
SiO_2/Al_2O_3	3.12	2.73	2.93	12.27	11.56	11.91	2.62	2.52	2.57	3.2	3.02	3.11	12.52	11.68	12.10	5.7	5,34	5.52	4.68	4.7	4.6	3.57	4.71	4.14
Al_2O_3/Na_2O	0.61	0.68	0.65	0.17	0.19	0.18	0.71	0.82	0.76	0.51	0.62	0.56	0.24	0.24	0.24	0.32	0,33	0.33	0.45	0.46	0.45	0.67	0.55	0.61
CaO/SiO_2	1.98	1.69	1.84	1.79	1.32	1.56	1.97	2.17	2.07	1.65	2.87	2.26	1.31	1.38	1.34	1.69	1,76	1.76	1.51	1.63	1.57	1.94	1.25	1.6
Na_2O/CaO	0.26	0.31	0.28	0.26	0.33	0.29	0.26	0.22	0.24	0.37	0.18	0.27	0.24	0.25	0.25	0.31	0,31	0.31	0.30	0.28	0.29	0.94	0.30	0.25

b)

Atomic ratios	L1-10M (21.08 MPa)			G1-10M (42.15 MPa)			L1-8M (21.26 MPa)			L1-6M (22.69 MPa)			G1-6M (47.83 MPa)			G0.5L0.5-10M (34.45 MPa)			G0.5L0.5-8M (32.33 MPa)			G0.5L0.5-6M (38.49 MPa)		
	ID:1	ID:2	Ave.	ID:1	ID:2	Ave.	ID:1	ID:2	Ave.	ID:1	ID:2	Ave.	ID:1	ID:2	Ave.	ID:1	ID:2	Ave.	ID:1	ID:2	Ave.	ID:1	ID:2	Ave.
SiO_2/Al_2O_3	4.55	6.13	5.33	15.29	12.9	14.1	5.41	5.51	5.46	13.75	3.13	8.44	17.41	18.93	18.17	8.74	10.13	9.43	8.56	7.74	8.15	15.18	7.38	11.28
Al_2O_3/Na_2O	0.62	0.55	0.58	0.18	0.31	0.25	0.58	0.63	0.61	0.60	0.72	0.65	0.27	0.24	0.25	0.47	0.41	0.43	0.46	0.43	0.44	0.5	0.41	0.45
CaO/SiO_2	0.28	0.29	0.28	0.49	0.33	0.41	0.33	0.32	0.32	0.16	0.31	0.24	0.34	0.39	0.37	0.47	0.37	0.41	0.47	0.45	0.46	0.27	0.56	0.41
Na_2O/CaO	1.27	1.04	1.15	0.7	0.73	0.7	0.96	0.92	0.93	0.73	1.41	1.07	0.62	0.54	0.58	0.52	0.65	0.58	0.53	0.64	0.58	0.48	0.58	0.53

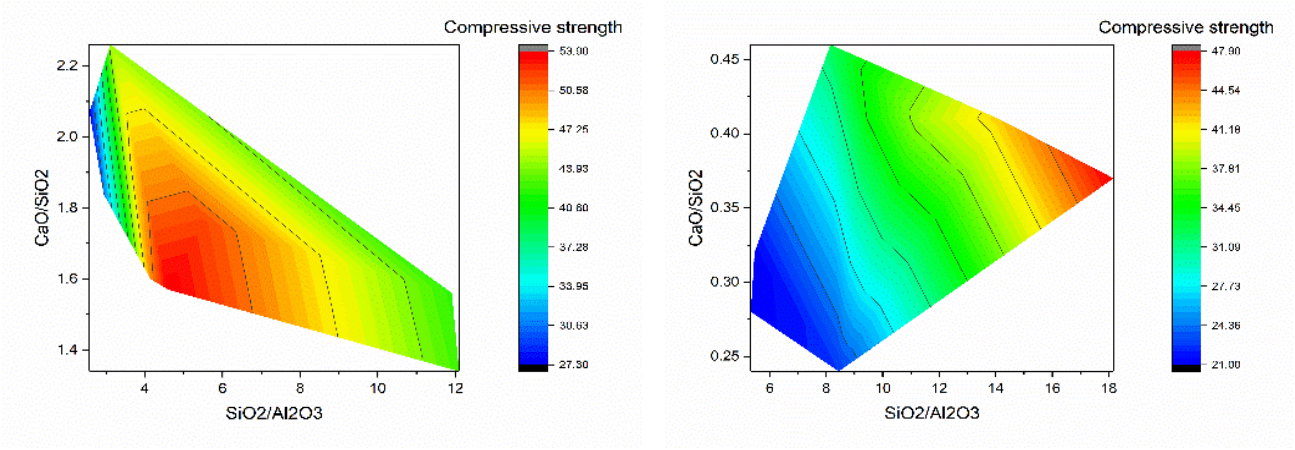

a) Carbonated BOF b) Normal aggregates

Fig 21.1. Correlation between atomic ratio analysis and compressive strength a) carbonated BOF and b) Normal aggregates.

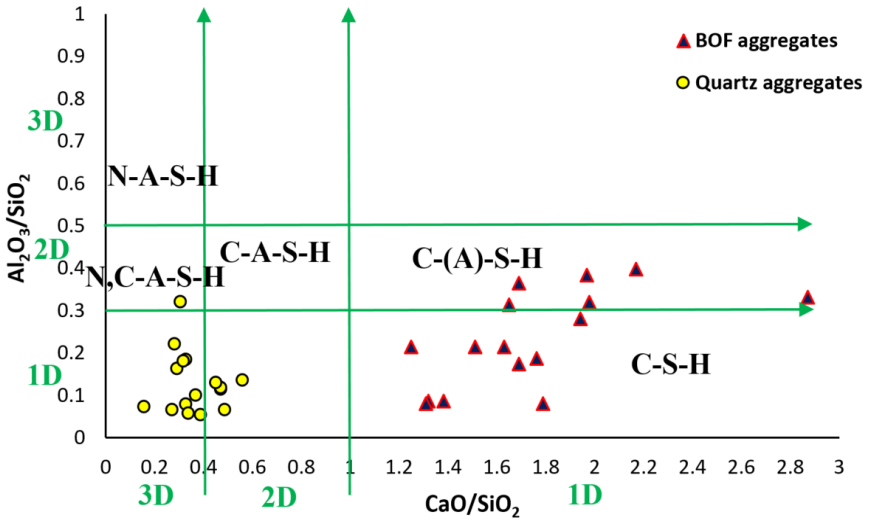

Fig 22.1. Al_2O_3/SiO_2 versus CaO/SiO_2 ratios for gels precipitating in the mixtures (Based on EDS findings)

Fig 21.1 depicts general correlation of the compressive strength to the molar ratios (CaO/SiO_2) and (SiO_2/Al_2O_3) of the mixtures. These correlations were found based on EDS analysis of all studied mixtures in Table 3.1, which contain carbonated BOF and quartz-based aggregates. Interestingly, it was found that the maximum strength in the studied alkali-activated binders containing carbonated BOF aggregates is obtained when $4 < SiO_2/Al_2O_3 < 6$ and $1.5 < CaO/SiO_2 < 1.7$. Since the maximum strength development in alkali-activated binders containing normal aggregates is achieved when $16 < SiO_2/Al_2O_3 < 18$ and $0.35 < CaO/SiO_2 < 0.4$.

CaO/SiO_2 versus SiO_2/Al_2O_3 in all mixtures were illustrated in Fig 22.1. According to the results, a certain (much smaller) number of points were located in the calcium-(sodium) aluminosilicate hydrate (N, C)-A-S-H gel zone due to use of quartz aggregates in alkali-activated binders.

Replacement of quartz (normal) aggregates with carbonated BOF aggregates mainly increased the CaO/SiO_2, therefore, most of the points were positioned in the calcium silicate hydrate (C-S-H) and calcium (aluminum) silicate hydrate C-(A)-S-H gel ranges.

1.4.3.2 XRD analysis

As discussed earlier, regardless of the sodium hydroxide molarity, it was found that using a precursor consists of a combination of ladle slag and GGBFS results in the maximum strength. Therefore, a comparative XRD analysis was carried out in this phase to understand the impacts of formed different crystallization in alkali-activated ladle slag-based binders, alkali-activated GGBFS based binders, and alkali activated ladle/GGBFS slag-based binders. Fig 22.1 shows that mineral patterns of pastes containing different aggregates such as carbonated BOF and normal aggregate with 6M,8M and 10M NaOH. The mixtures showed varying crystalline phases which including K: Katoite; P: Portlandite; C: Calcite; C2S; I: Iron Oxide; S: Srebrodolskite; Ca: Calcio; Cal: Calcium Hydrogen Phosphate; M: monetite for carbonated BOF and Al: Aluminum Oxide Sulfate Hydroxide Hydrate; P: Paranatrolite; q: quartz-alpha for normal aggregate and also shows the quantitative phase analysis of the compositions, which was followed by Rietveld method (Rietveld, 1969). The result indicates that similar XRD patterns are formed in the mixtures, regardless of the differences in the precursor type. Although, the precursor type (ladle slag, GGBFS, and ladle slag/GGBFS) affected the intensity characteristics of the diffraction peaks and higher diffraction peaks formed in mixture of the combination of ladle slag/GGBFS compared to others. Comparing the mixtures with carbonated BOF and normal aggregates show that using carbonated BOF increased significantly the crystallization as well as changing the formed chemical products. This finding is in the line of SEM/EDS analysis.

The increase of the crystallinity could either enhances or degrades mechanical properties, depending on the enough space exists in the mixture to be filled by the formed crystalline phases. The transition of amorphous gels into more ordered structures causes the local microstructure to change, introducing the internal stresses. The matrix would be denser if enough space is existence for the formed crystalline, otherwise crystallizations form micro-cracks (as observed in the Fig 17.1). The differences in the strength development may be justified by the differences in the microscopic analysis.

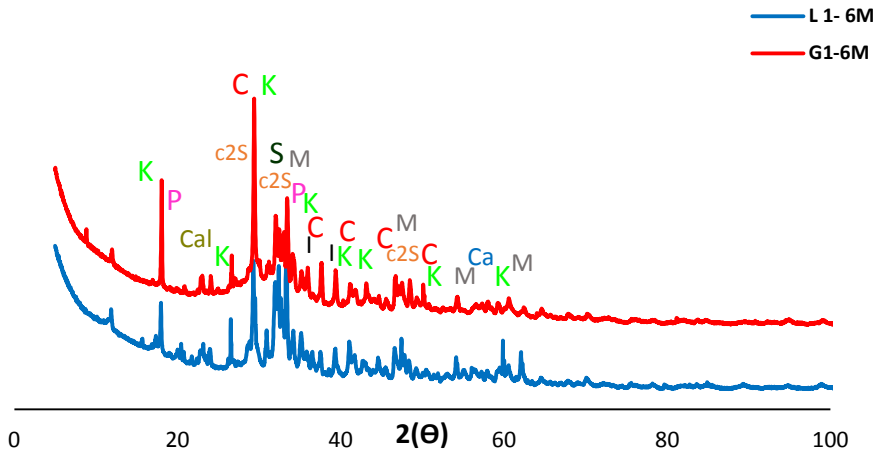
L 1- 6M
G1-6M
2(Θ)

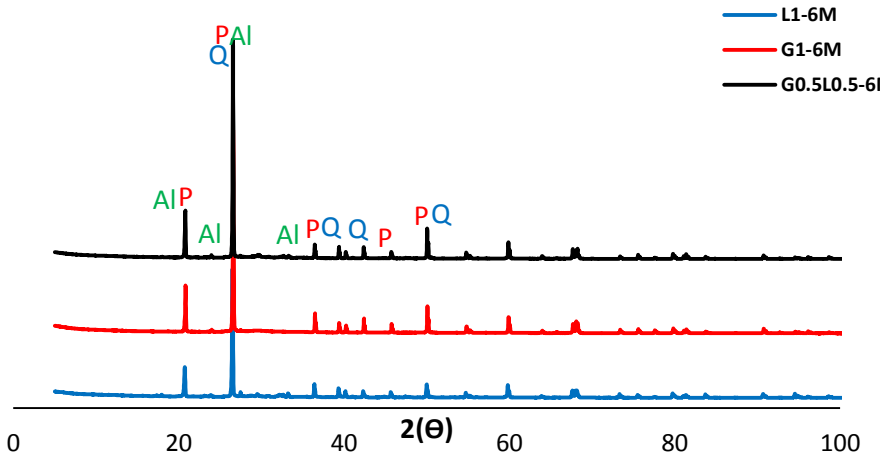
L1-6M
G1-6M
G0.5L0.5-6M
2(Θ)

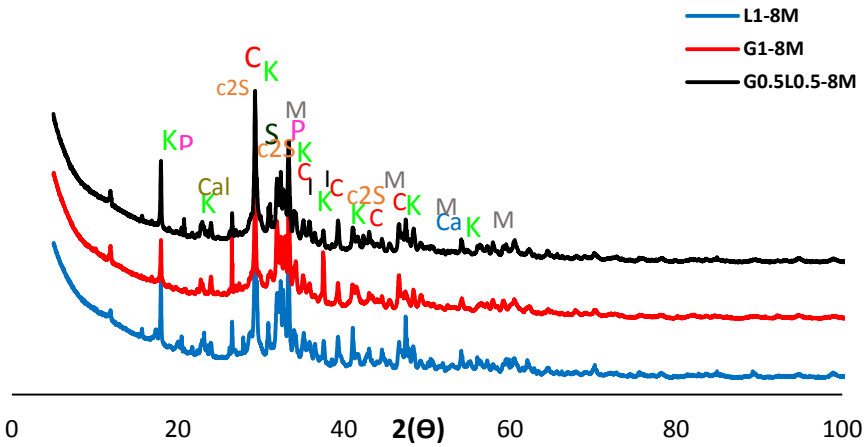
L1-8M
G1-8M
G0.5L0.5-8M
2(Θ)

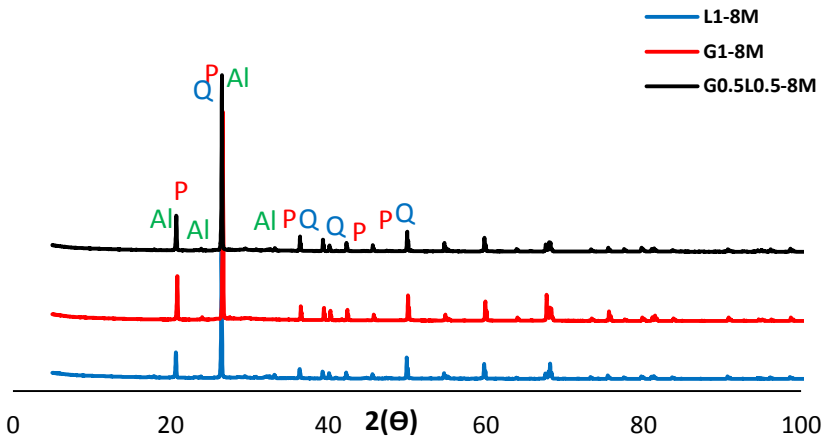
L1-8M
G1-8M
G0.5L0.5-8M
2(Θ)

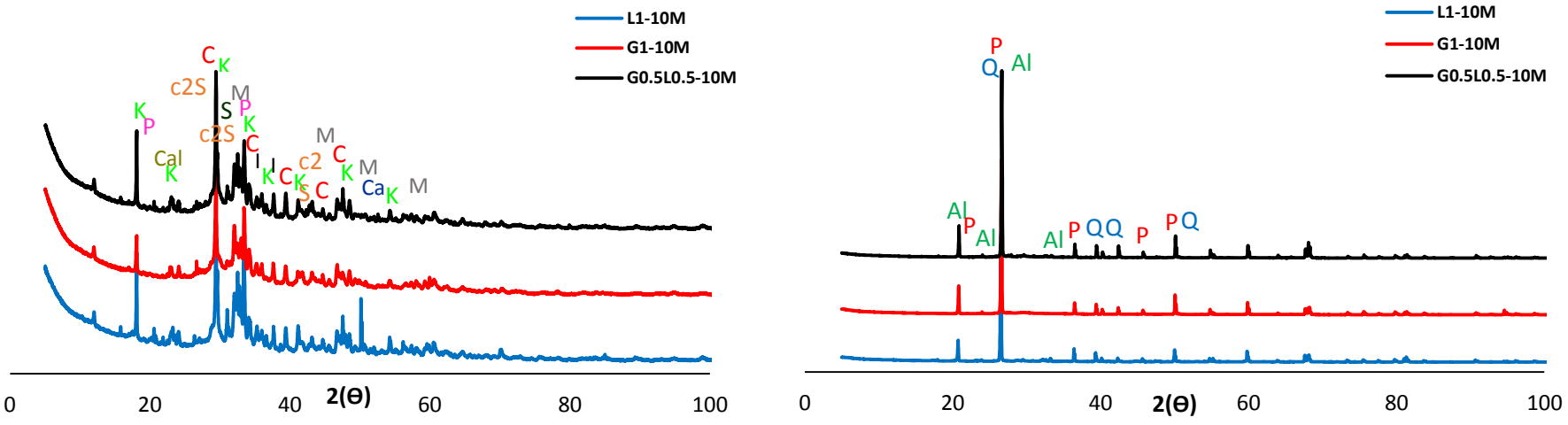
L1-10M
G1-10M
G0.5L0.5-10M
2(Θ)
0
20
40
60
80
100

a)

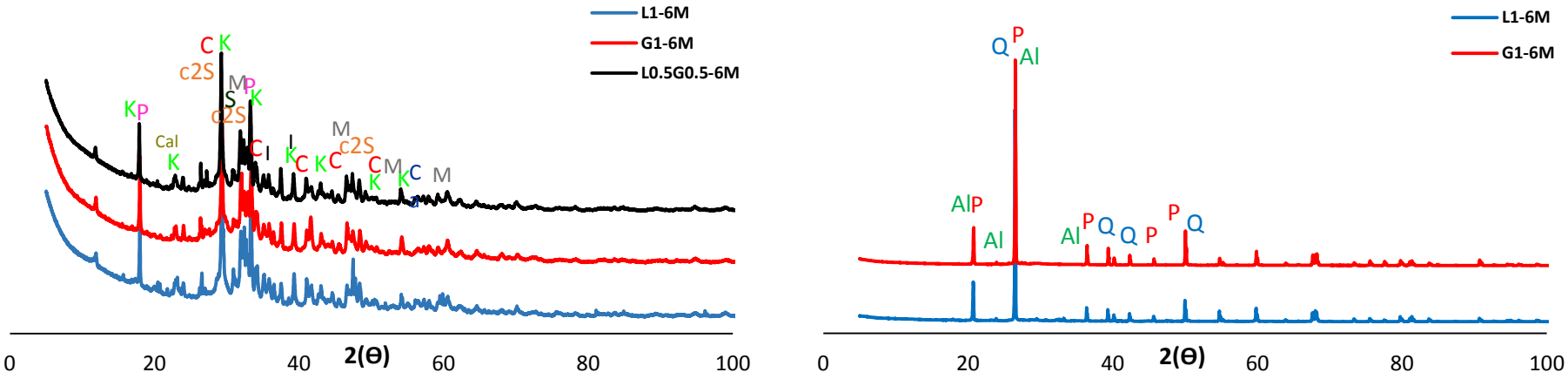
L1-6M
G1-6M
L0.5G0.5-6M
2(Θ)
0
20
40
60
80
100

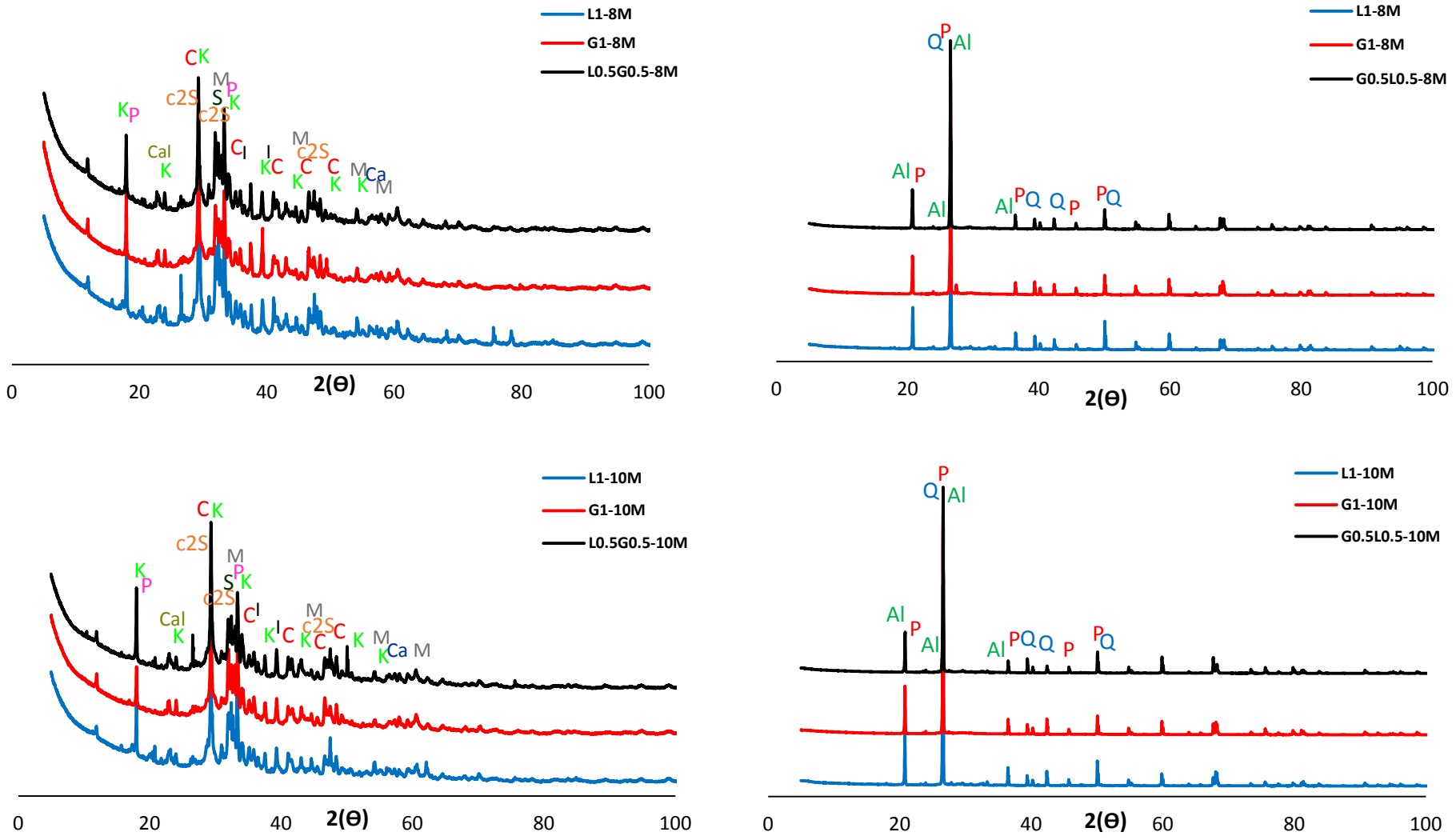
L1-8M
G1-8M
L0.5G0.5-8M
L1-8M
G1-8M
G0.5L0.5-8M
L1-10M
G1-10M
L0.5G0.5-10M
L1-10M
G1-10M
G0.5L0.5-10M
2(Θ)
2(Θ)
2(Θ)
2(Θ)
0
20
40
60
80
100

b)

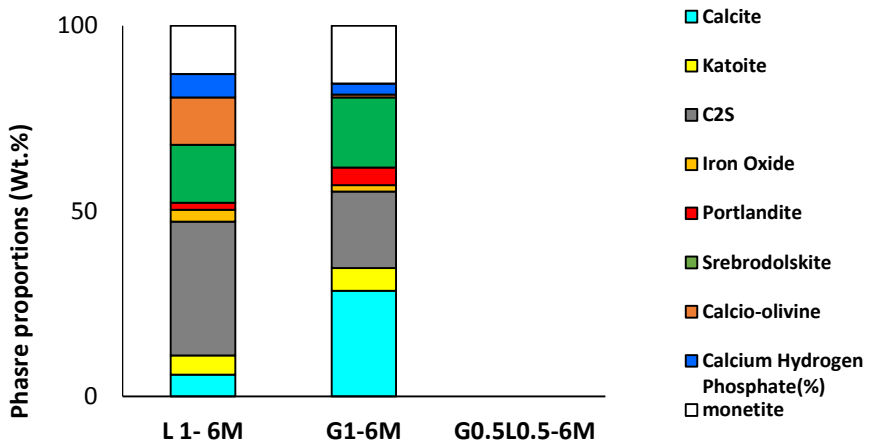
100
50
0
Phasre proportions (Wt.%)
L 1- 6M
G1-6M
G0.5L0.5-6M
Calcite
Katoite
C2S
Iron Oxide
Portlandite
Srebrodolskite
Calcio-olivine
Calcium Hydrogen Phosphate(%)
monetite

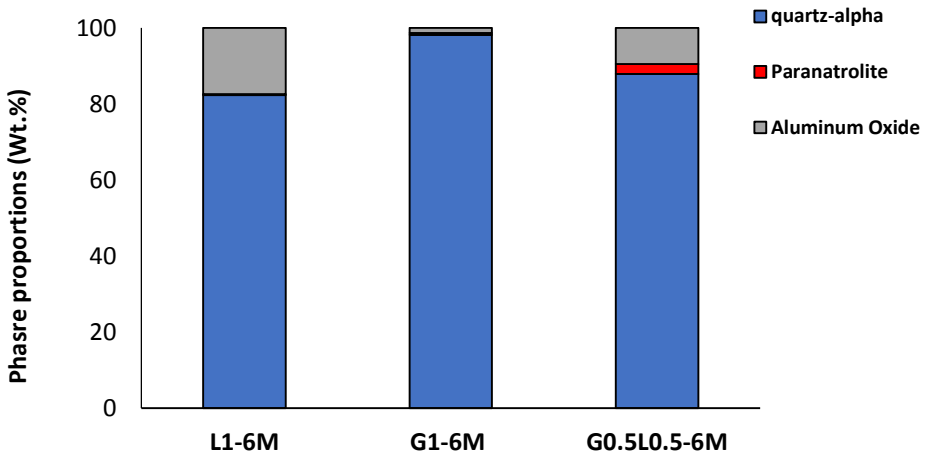
100
80
60
40
20
0
Phasre proportions (Wt.%)
L1-6M
G1-6M
G0.5L0.5-6M
quartz-alpha
Paranatrolite
Aluminum Oxide

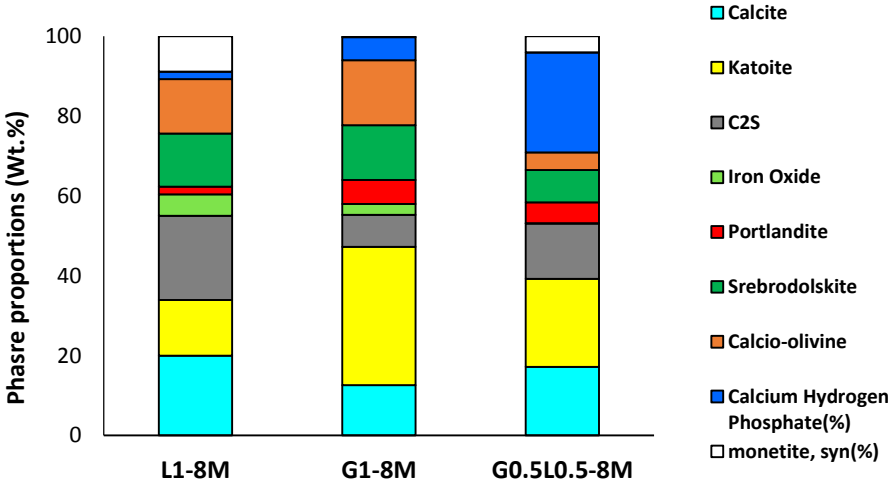
100
80
60
40
20
0
Phasre proportions (Wt.%)
L1-8M
G1-8M
G0.5L0.5-8M
Calcite
Katoite
C2S
Iron Oxide
Portlandite
Srebrodolskite
Calcio-olivine
Calcium Hydrogen Phosphate(%)
monetite, syn(%)

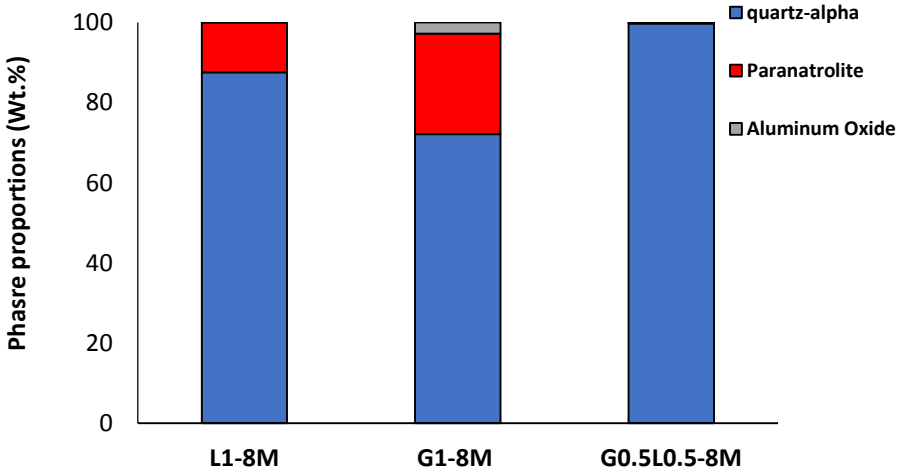
100
80
60
40
20
0
Phasre proportions (Wt.%)
L1-8M
G1-8M
G0.5L0.5-8M
quartz-alpha
Paranatrolite
Aluminum Oxide

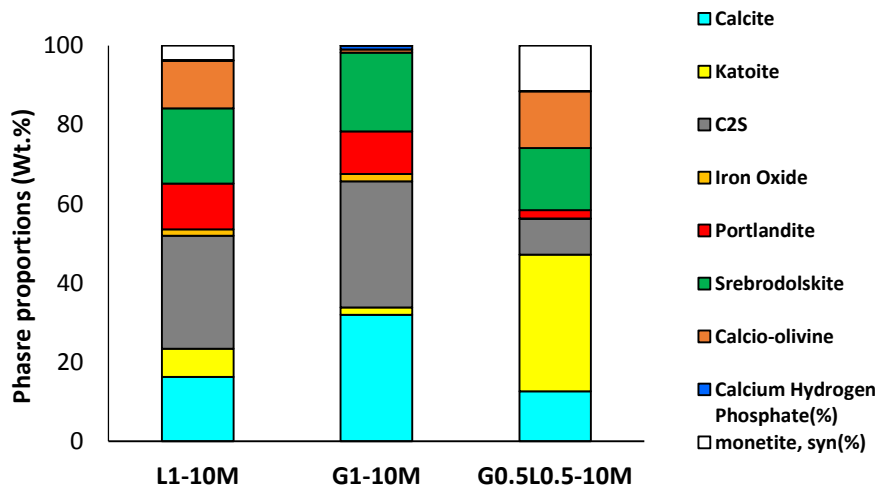
Phasre proportions (Wt.%)
100
80
60
40
20
0
L1-10M
G1-10M
G0.5L0.5-10M
Calcite
Katoite
C2S
Iron Oxide
Portlandite
Srebrodolskite
Calcio-olivine
Calcium Hydrogen Phosphate(%)
monetite, syn(%)

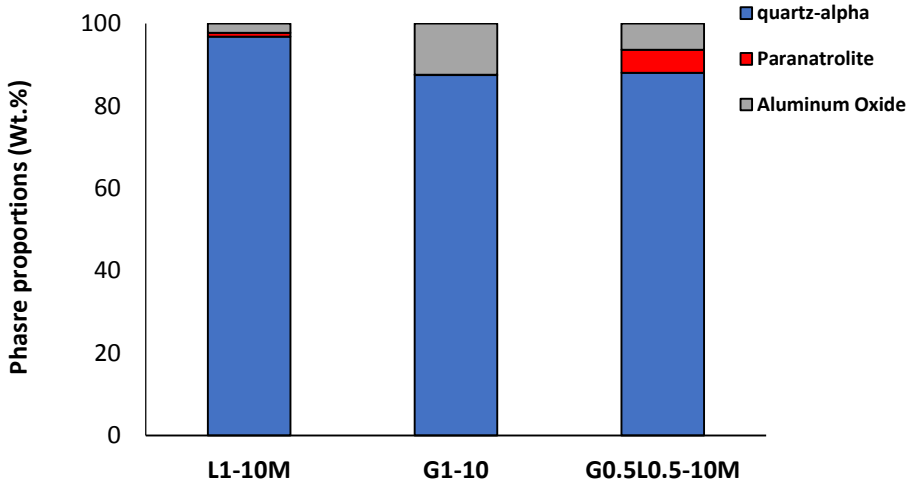
Phasre proportions (Wt.%)
100
80
60
40
20
0
L1-10M
G1-10
G0.5L0.5-10M
quartz-alpha
Paranatrolite
Aluminum Oxide

c)

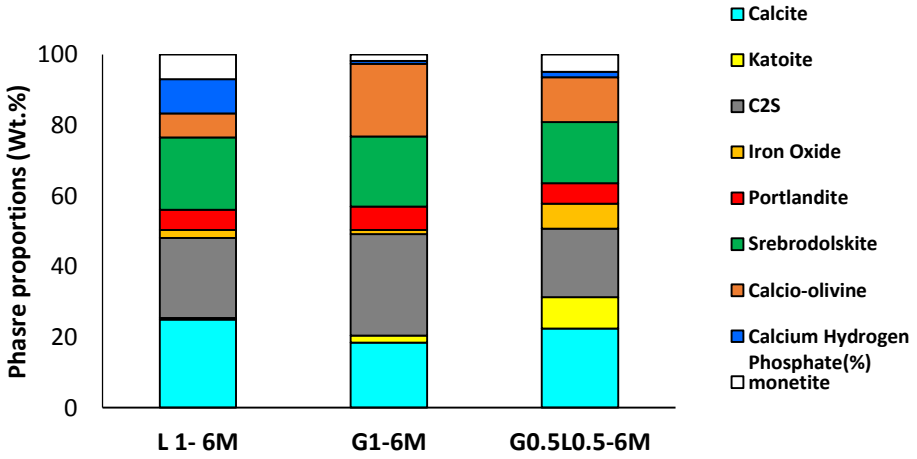
Phasre proportions (Wt.%)
100
80
60
40
20
0
L 1- 6M
G1-6M
G0.5L0.5-6M
Calcite
Katoite
C2S
Iron Oxide
Portlandite
Srebrodolskite
Calcio-olivine
Calcium Hydrogen Phosphate(%)
monetite

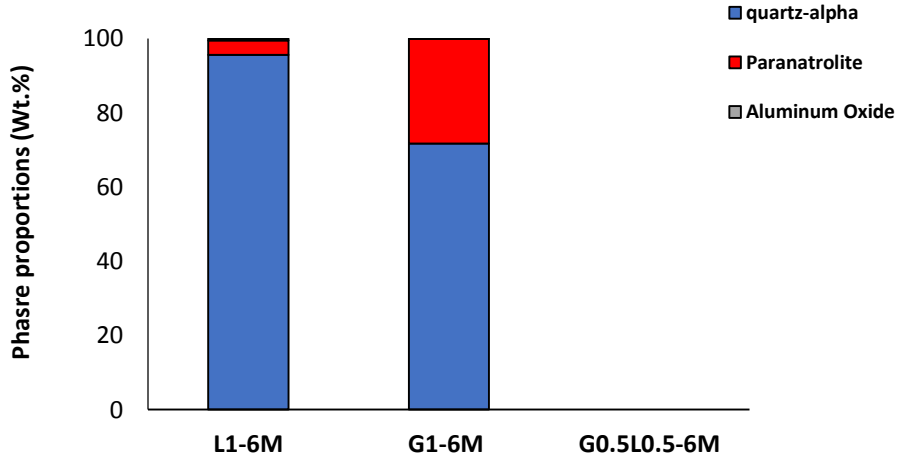
Phasre proportions (Wt.%)
100
80
60
40
20
0
L1-6M
G1-6M
G0.5L0.5-6M
quartz-alpha
Paranatrolite
Aluminum Oxide

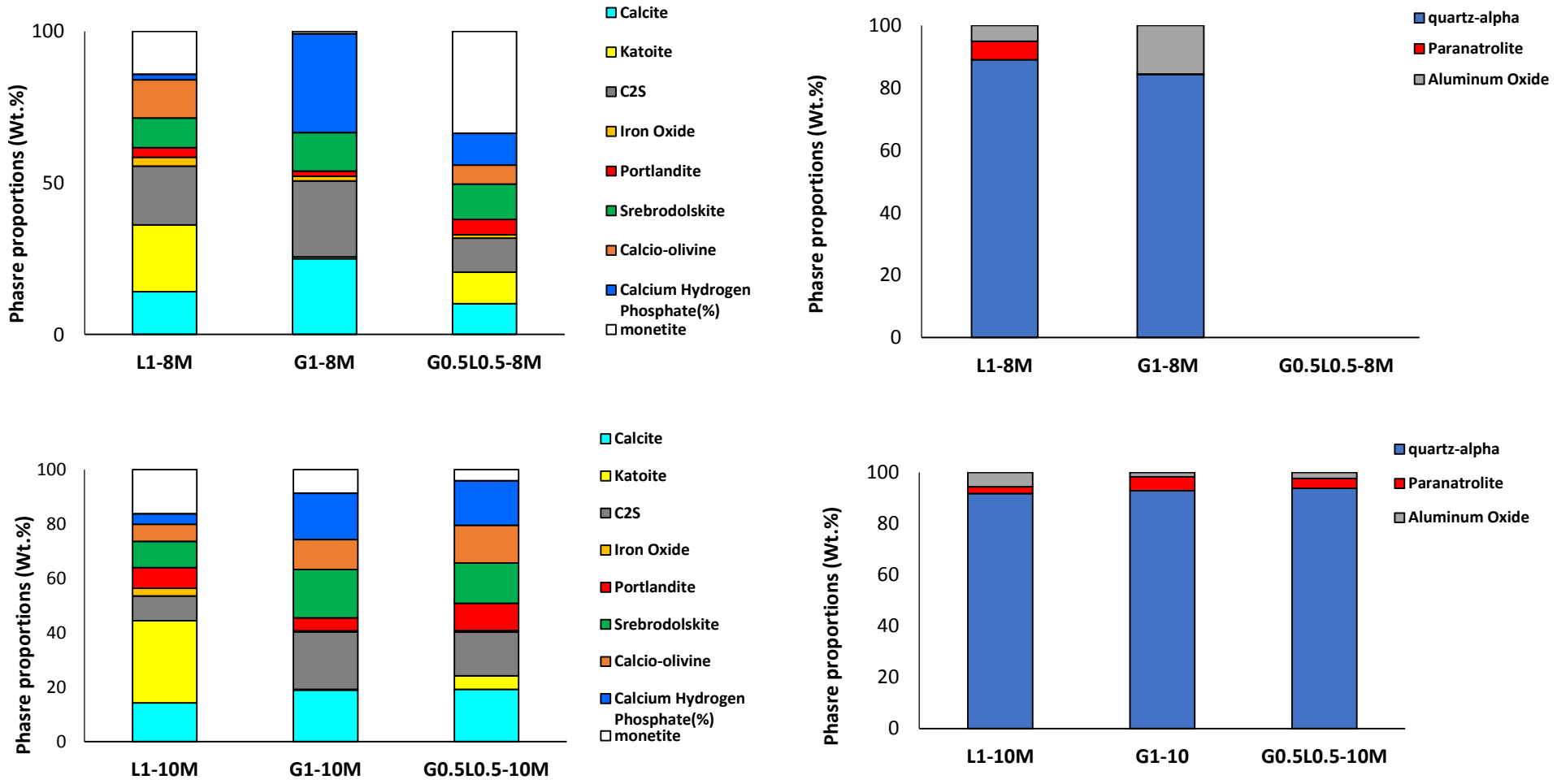

d)

Fig 22.1. XRD patterns of pastes of a) Carbonated BOF (K: Katoite; P: Portlandite; C: Calcite; C2S; I: Iron Oxide; S: Srebrodolskite; Ca: Calcio; Cal: Calcium Hydrogen Phosphate; M: monetite) Normal Aggregate (Al: Aluminum Oxide Sulfate Hydroxide Hydrate; P: Paranatrolite; q: quartz-alpha) with ratio 3; b) carbonated BOF and normal aggregates with ratio of 5 and Quantitative phase analysis of the compositions by the Rietveld method; c) carbonated BOF and normal aggregates with ratio of 3; d) carbonated BOF and normal aggregates with ratio of 5.

1.4.3.3 Thermogravimetric analysis (TGA) and differential thermogravimetry (DTG) analysis

Fig 23.1 depicts the weight loss and the derivative weight of the mixtures. As other microscopic analysis showed, using carbonated BOF aggregates greatly affected the TGA and DTG curves. Weight losses in TGA could be considered in the temperatures from 100 ºC to 800 ºC (Li, et al., 2017). Both free water and structurally bonded water are available at the first stage. The free water could be evaporated up to 100 ºC, and the weight loss from 100 ºC to 800 ºC is attributed to the structural water (Li, et al., 2017). The mass loss rate slowed down after 250 ºC owing to the chemically bonded water and OH groups (Nath, et al., 2016).

According to the TGA results in Fig 23.1(a) and 23.1 (b), higher mass loss was recorded in alkali-activated concretes containing carbonated BOF aggregates compared to normal aggregates. It shows that the mixture with carbonated BOF aggregates possess more chemical products than the mixtures incorporating normal aggregates.

Regarding the DTA curves, three major endothermic peaks at around 180 ºC, 500 ºC, and 780 ºC were observed in the mixtures with carbonated BOF aggregates; the large shoulder just below 200 ºC is attributed to the dehydration of the calcium-rich silicate gel (Alarcon-Ruiz, et al., 2005). The second major endothermic peak could be assigned to Portlandite ($Ca(OH)_2$) (Shaikh & Supit, 2014). The third destruction phase (at 780 ºC) could be attributed to the decomposition of calcite ($CaCO_3$) (Shaikh & Supit, 2014). The differences in the major endothermic peaks of the DTA curves indicate that some additional gel formation may have occurred owing to carbonated BOF aggregates. Since only one major endothermic peak at around 170 ºC was noticed in the mixtures with normal aggregates.

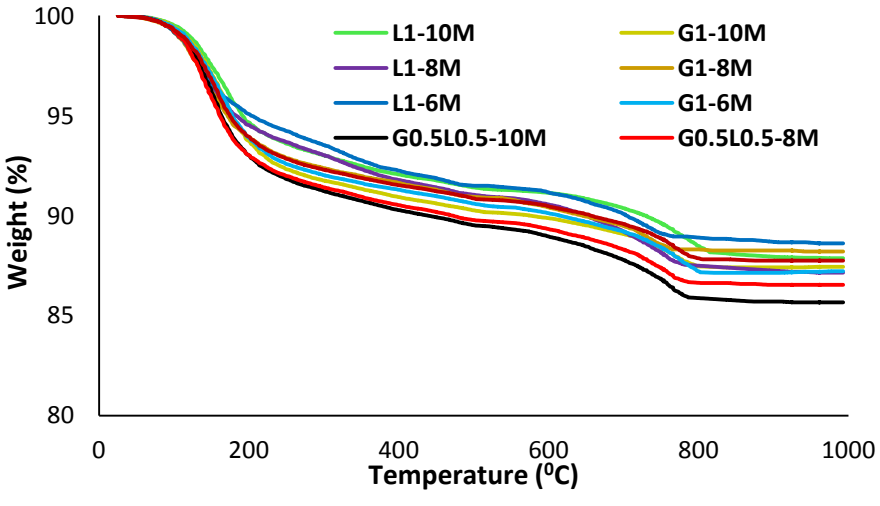

a)

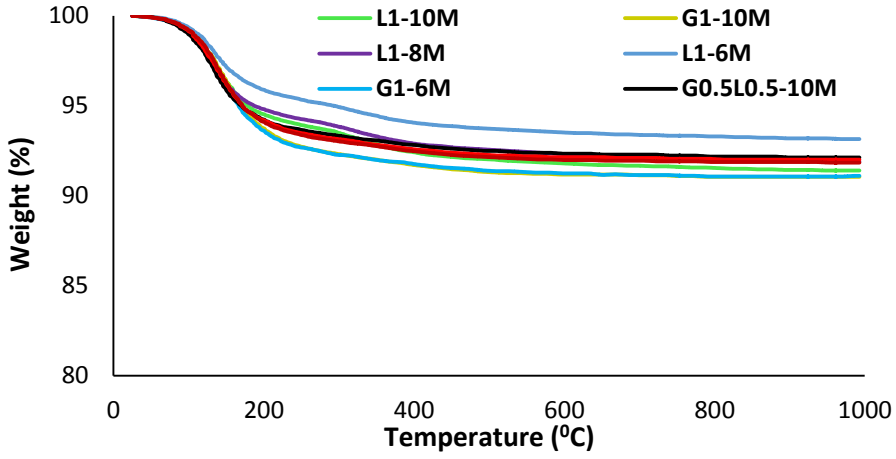

b)

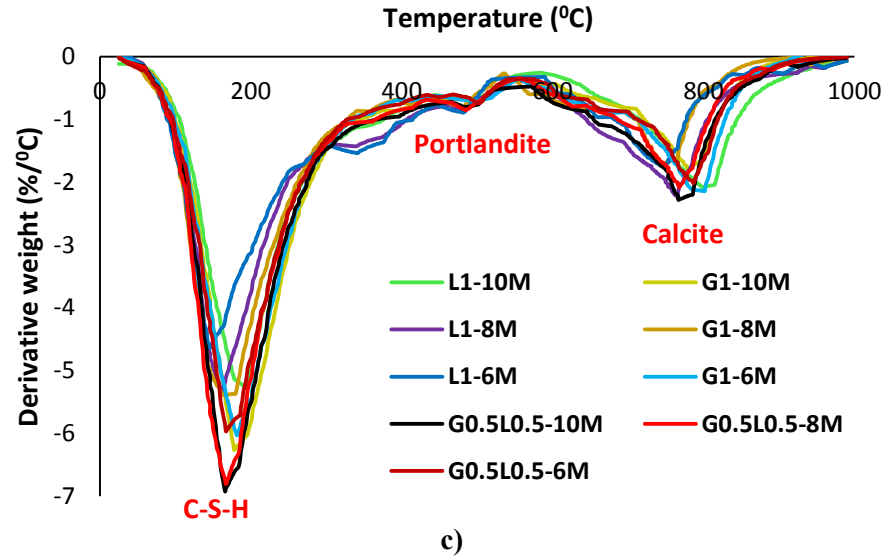

c)

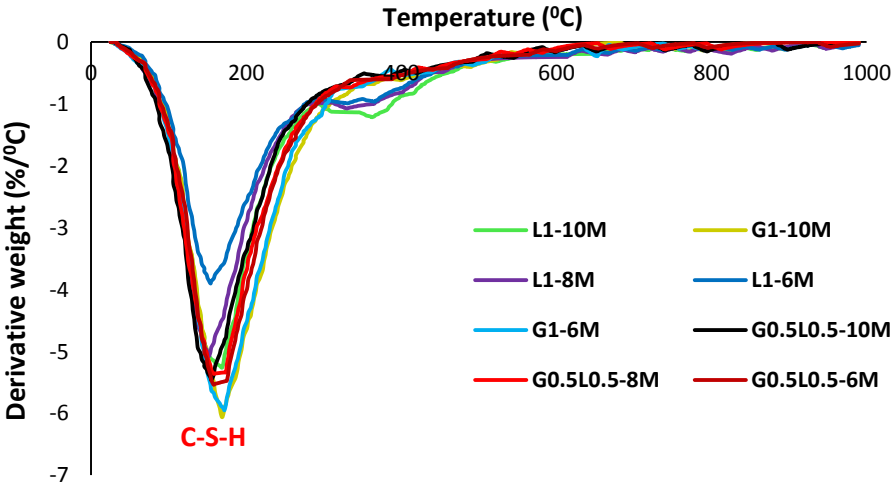

d)

Fig 23.1. a) TGA analysis in alkali activated concretes containing carbonated BOF aggregate to binder ratio of 3; b) TGA analysis in alkali activated concretes containing normal aggregate to binder ratio of 3; c) DTG analysis in alkali activated concretes containing carbonated BOF aggregate to binder ratio of 3; d) DTG analysis in alkali activated concretes containing normal aggregate to binder ratio of 3

1.5 Conclusions

In this chapter, mechanical and microscopic properties of alkali-activated binders with recycled carbonated BOF and natural aggregates were investigated. Regarding the result attained, the following remarks could be highlighted:

Regarding the compressive strength, it was observed that the mixture G0.5L0.5-8M with carbonated BOF to binder ratio of 3 has the maximum strength (54MPa). Replacing carbonated BOF to normal aggregates at the same mix composition reduced 40% (33MPa) of the strength. Although G0.5L0.5-10M mix composition with carbonated BOF to binder 3 ratio also has maximum strength, however, using 8M sodium hydroxide solution is more cost effective.

Regarding EDS analysis, higher molar ratios of CaO/SiO_2 justifies the higher strength in the mixtures which consisting carbonated BOF aggregate compared to natural aggregate.

From XRD analysis, it was observed that carbonated BOF has the significant influence on increase crystalline type and change chemical products.

According to the TGA analysis, higher mass loss was resulted in alkali-activated concretes consisting carbonated BOF aggregates compared to natural aggregates. It indicates that mix composition with carbonated BOF aggregates has more chemical products than the mixtures containing normal aggregates.

CHAPTER 2

Development of alkali activated desulfurization slag concretes containing carbonated BOF aggregates

2.1 Introduction

Desulfurization (DS) slag is known as a by-product of steelmaking industries and produces from ironic minerals. Desulfurizatants can be divided into 4 categories such as a) soda ash, b) calcium carbide, c) lime, and d) magnesium (Huang, et al., 2016). There are several applications of desulphurization slag (DS) such as ground improvement, soil modification, earth backfill and substituent of calcite ($CaCO_3$) for production of cement clinker (Kuo & Tsung-Chin Hou, 2014). Recently, DS has been utilized as an alternative of coarse and fine aggregate in concrete materials (Kuo & Weng, 2009) (Kuo & Shu, 2014) (Kuo, 2015). Use an adequate amount of desulfurization slag instead of natural fine aggregate can enhance the efficiency, reduce the pending time for a testing run and, also minimize the construction time (Huang, et al., 2016)

(Kuo & Tsung-Chin Hou, 2014) found that desulfurization slag can contribute sufficient alkali environment for initiating pozzolanic reactions when worked with GGBFS. They found 17 MPa compressive strength after 28 days which is revealed satisfactory quality to produce non-Portland-cement binders. Other researchers (Huang, et al., 2016) found that use of DS (0%, 10%, 20%, 30%, 40%, and 50%) instead of natural fine aggregate, the compressive strength have decreased from 36.1 to 62.5% per addition of DS but they found satisfactory compressive strength (9 MPa) after 28 days which is adequate strength requirement in Taiwan.

Several studies found that main components of desulfurization (DS) slag are iron (Fe) and iron oxides (FeO, Fe_2O_3, and Fe_3O_4), calcium oxide (CaO), silicon dioxides (SiO_2), magnesium oxide, and aluminum oxide (Kawatra & Ripke, 2002) (Ma & Houser, 2014) (Kuo, et al., 2014). The amount of CaO can be improved to 48-69 wt%, after separated iron-rich component from DS (Kuo, et al., 2014) (Ho, et al., 2017) and some researcher use this slag instead of fine aggregate in a cement-based concrete (Ho, et al., 2017) (Huang, et al., 2016). They detected that the rate of the volume expansion in cementitious mortar has increased by using desulfurization slag. Several investigations found that free CaO and MgO from slag are the reason for the volume expansion problem which will be an essential issue to the resulting properties of construction material (Shen, et al., 2009) (Wang, 2010) (Wang, et al., 2010). So, in order to utilize desulfurization slag in cement, the expansion should be minimized.

After demonstrating the efficiency of using carbonated BOF aggregates in enhancing the properties of alkali-activated binders, in this chapter, the impacts of using different parameters such as using carbonated and non-carbonated desulfurization (DS) slag in alkali activation of mixtures with

carbonated BOF aggregates and sodium hydroxide molarities will be studied and discussed in terms of mechanical properties, efflorescence, and pH experiments.

2.2 Experimental plan

2.2.1 Mix design and designations

The mortars were contained of carbonated desulfurization slag (C-DS), desulfurization slag (DS) as precursor and carbonated recycled BOF as an aggregate. The alkali solution was combined by liquid sodium silicate $\frac{SiO_2}{Na_2O} \approx 2.5$ and sodium hydroxide (with molarity of 6M, 8M, 10M, and 12M). To prepare different molar concentrations of sodium hydroxide, solid Na(OH) pellets were dissolved in water, after that the solution cooled at room temperature (average temperature of 23 ^{0}C). In this chapter, twenty-four mix compositions were prepared and tested. Mix compositions and different mix proportion are shown in Table 1.2.

Table 1.2. Mix compositions of alkali activated desulfurization slag concretes

Specimen designation	Binder	Aggregate/binder	Alkali/binder	SS/SH	Sodium hydroxide (M)
C-DS-6M	1	1 (B1) or 3 (B3) or 5 (B5)	1	2.5	6
C-DS-8M					8
C-DS-10M					10
C-DS-12M					12
DS-6M					6
DS-8M					8
DS-10M					10
DS-12M					12

2.2.2 Carbonated DS

After demonstrating the efficiency of using CO_2 sequestration on the physical and mechanical performance of BOF aggregates, this technique also applied on DS slag, which is used as a binder (see Fig 1.2). Therefore, they were initially sieved to obtain particles size smaller than 0.5 mm. After sieving, desulfurization slag was treated for 48 hours exposed to CO_2 gas with the pressure of 1 bar, 5% CO_2 concentration, temperature 23 ^{0}C, and RH 60%. In order to increase the porosity of the mix composition, the aggregate to binder ratio was varied from 1, 3 and 5.

a)

b)

Fig 1.2. a) Sieved DS slag in carbonation chamber; b) DS slag

2.2.3 Mixing and Aging

In this chapter, 24 mix compositions were prepared with carbonated and non-carbonated desulfurization (DS) slags. Dry ingredient carbonated DS and carbonated BOF were combined for 1 min, next added alkali solutions (sodium hydroxide and sodium silicate) which were stirred for 4 min. Fresh mortars were cast into prismatic molds with dimension (20×20×80 mm). After casting the molds, machine vertical shaker was used for 60 seconds to vibrate the specimens. Then, the mold was kept for 24 hours with covered by plastic (see Fig 2.2.b). After that demolded it and cover the specimens with plastic bag again. Then these samples were stored for 28 days in the ambient temperature of lab (averagely 25 ^{0}C and 40% RH). Same way was followed to prepare the specimen containing normal desulfurization slag and carbonated BOF.

a)

b)

c)

Fig 2.2 a) Mixing; b) wrapping with plastic; c) Demolding

2.3 Test procedures

2.3.1 Flexural strength

Regarding the mentioned mix compositions in Table 1.2, totally seventy-two prismatic beams were tested in this chapter to execute the flexural strength under three-point bending (TPB) test. For each mix composition, flexural strength is obtained by averaging of three prismatic beams. The test was

performed using a load cell of 100 kN and a flexural load with displacement control rate of 0.6 mm/min was imposed to the specimens. Equation 1.1 is used to calculate the flexural strength.

2.3.2 Compressive strength

The broken parts from the flexural test have taken to measure the compressive strength. The result was collected by averaging six parts of prismatic beams of each mix composition. Compressive load with displacement control and speed of 1.8 mm/min assigned to the beams. Equation 2.1 is followed to calculate compressive strength.

2.3.3 Efflorescence

To observe the intensity of efflorescence, one sample from each mix composition was used for efflorescence evaluation (see Fig 3.2). The samples were kept in a plastic tray contact with Deionized (DI) water at the bottom at the ambient temperature (averagely 25 ^{0}C) and visually monitored after 24, 48, and 72hours.

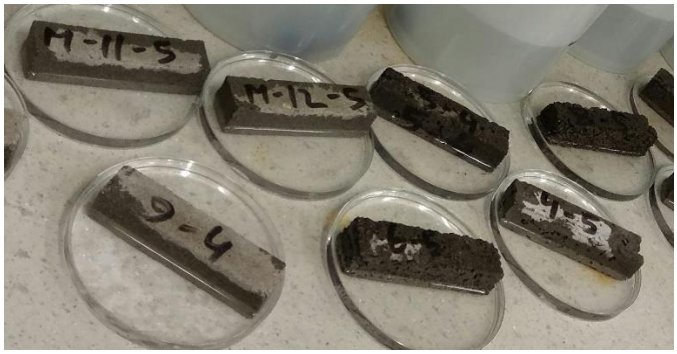

Fig 3.2. Assessment of the efflorescence rates of different mix compositions

2.3.4 pH measurements

The pH of all mix composition was measured by using pH/conductivity meter (Accumet model 20, USA) (see Fig 4.2). All specimens were submerged in DI water and the pH measurements were executed after 24, 48, 72, 96, and 144 hours.

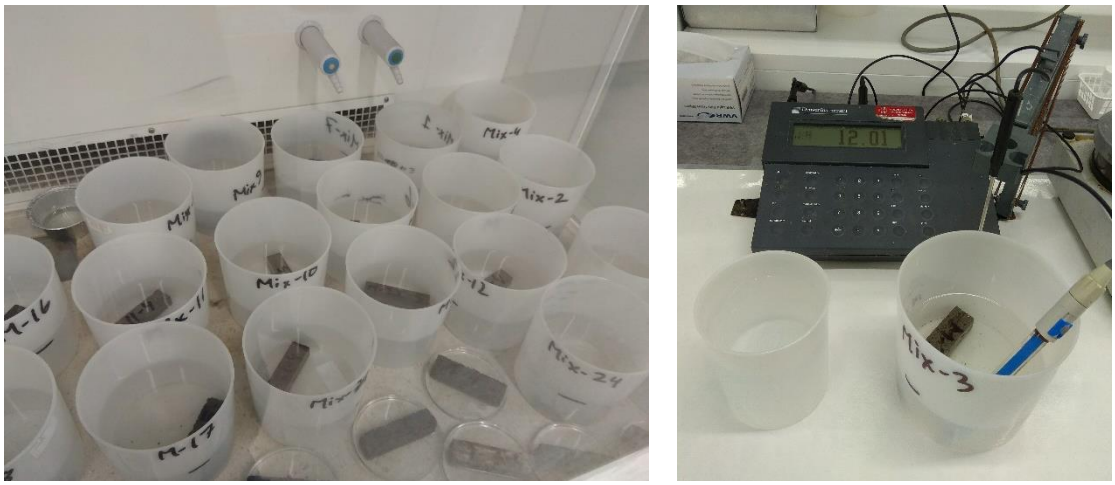

Fig 4.2. pH measurements

2.4 Results and discussion

2.4.1 Flexural strength

The effects of using different parameters on the flexural strength such as different precursor types, carbonated BOF aggregate contents, and sodium hydroxide molarities are shown in Fig. 5.2. According to the results, using non-carbonated desulfurization (DS) slag commonly improved the flexural strength compared to carbonated desulfurization (DS) slag binder. It indicates that increase the amount of carbonated BOF from 1 to 5 improved the flexural strength. Interestingly, the maximum flexural strength resulted in the mixture containing carbonated BOF aggregate to binder ratio of 3. The maximum development was resulted in 3 times in the specimen DS-B3-8M compared to C-DS-B3-8M.

The maximum flexural strength in the mixtures containing non-carbonated desulfurization (DS) slag dependent on carbonated BOF aggregate content, and sodium hydroxide molarities. Regarding the results, it is noticed that the maximum flexural strength was obtained 3.6 MPa in the mixture of DS-B3-8M containing carbonated BOF aggregate to non-carbonated DS binder ratio of 3, while the minimum flexural strength resulted around 1 MPa in the mixture of C-DS-B3-6M with carbonated BOF aggregates to carbonated DS binder ratio of 3.

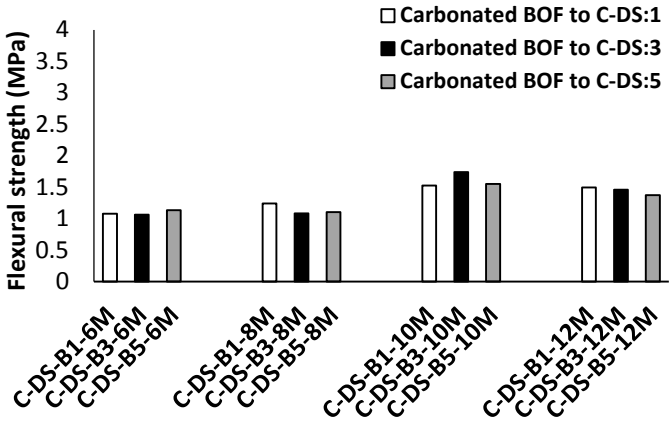

a)

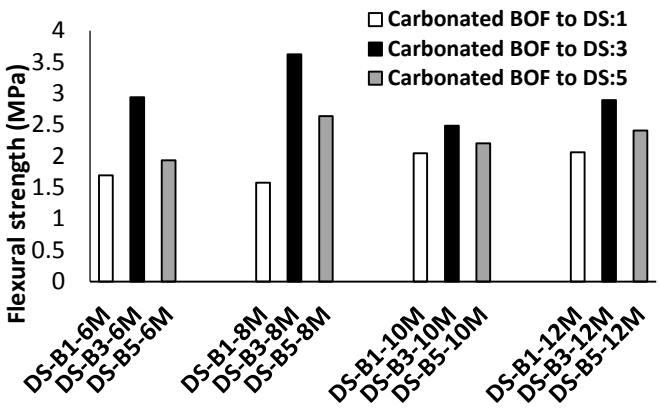

b)

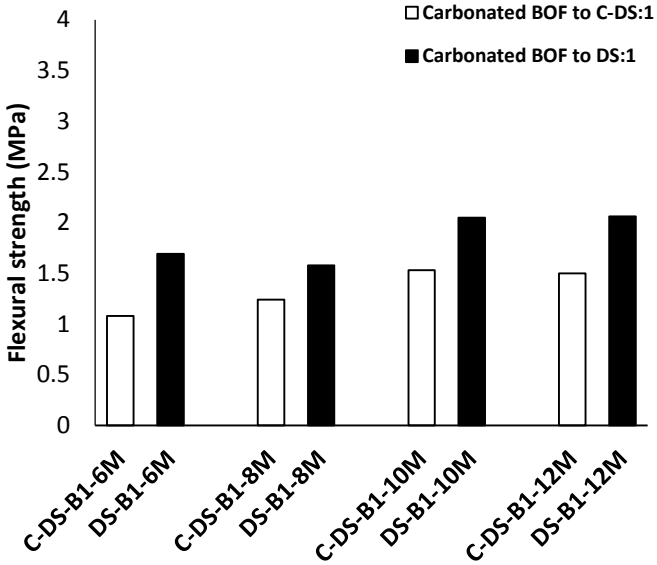

c)

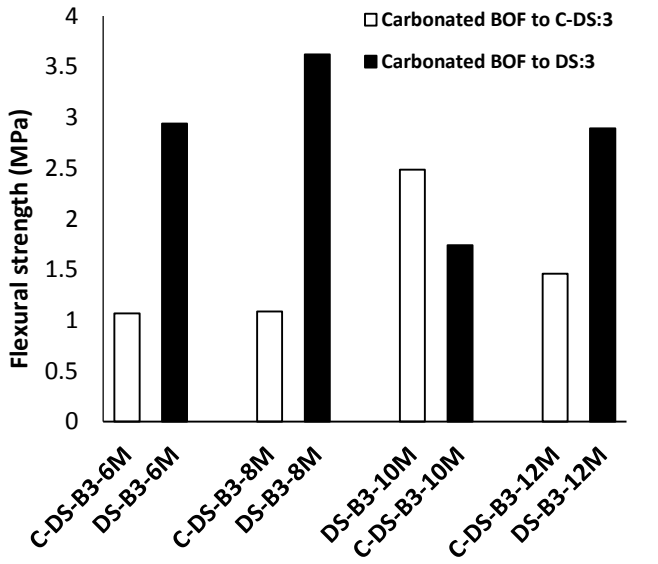

d)

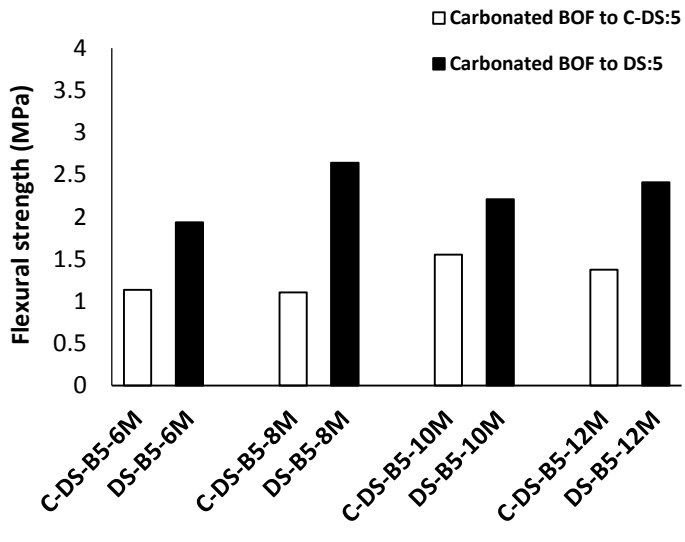

e)

Fig 5.2. a) Effects of using different contents of carbonated DS on the flexural strength; b) Effects of using different contents of non-carbonated DS on the flexural strength; c) comparative effects of using carbonated

BOF to carbonated DS and non-carbonated DS with ratio of 1 on the flexural strength; d) comparative effects of using carbonated BOF to carbonated DS and non-carbonated DS with ratio of 3 on the flexural strength; d) comparative effects of using carbonated BOF to carbonated DS and non-carbonated DS with ratio of 5 on the flexural strength.

2.4.2 Compressive strength

Fig 6.2 depicts the influences of using different variables on the compressive strengths. Regarding the result, using non-carbonated desulfurization (DS) slag instead of carbonated desulfurization (DS) slag commonly increased the compressive strength, which the maximum increment was in the mixture consist of carbonated BOF aggregate to binder ratio of 3 with 8M NaOH. In the mixture of DS-B3-8M the maximum improvement was recorded around 5 times compared to the mixture C-DS-B3-8M.

Similar to the flexural strength, it indicates that, maximum compressive strength highly dependent on the precursor types, carbonated BOF aggregate content, and sodium hydroxide molarities. According to the results, the maximum increase of the compressive strength was measured around 10.5 MPa in the mixture containing carbonated BOF aggregate to non-carbonated DS binder ratio of 3 with 8M NaOH (DS-B3-8M). On the other hand, the minimum strength was achieved around 1.8 MPa in the specimen C-DS-B3-8M with carbonated BOF aggregate to carbonated DS binder ratio of 3.

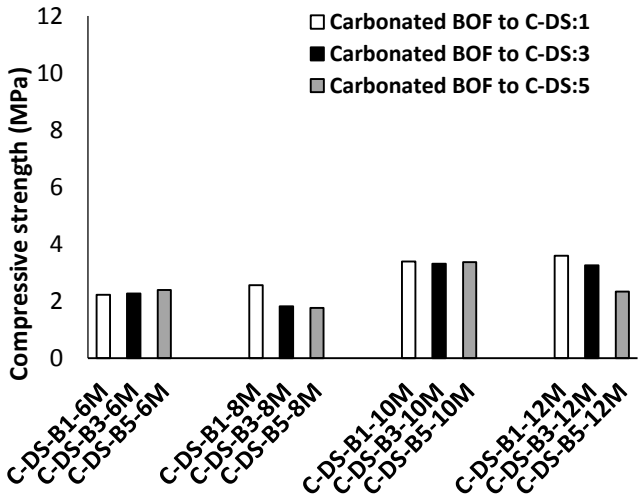

a)

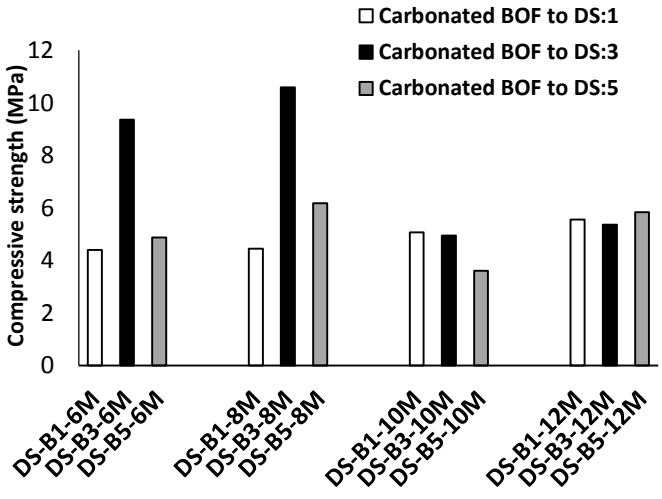

b)

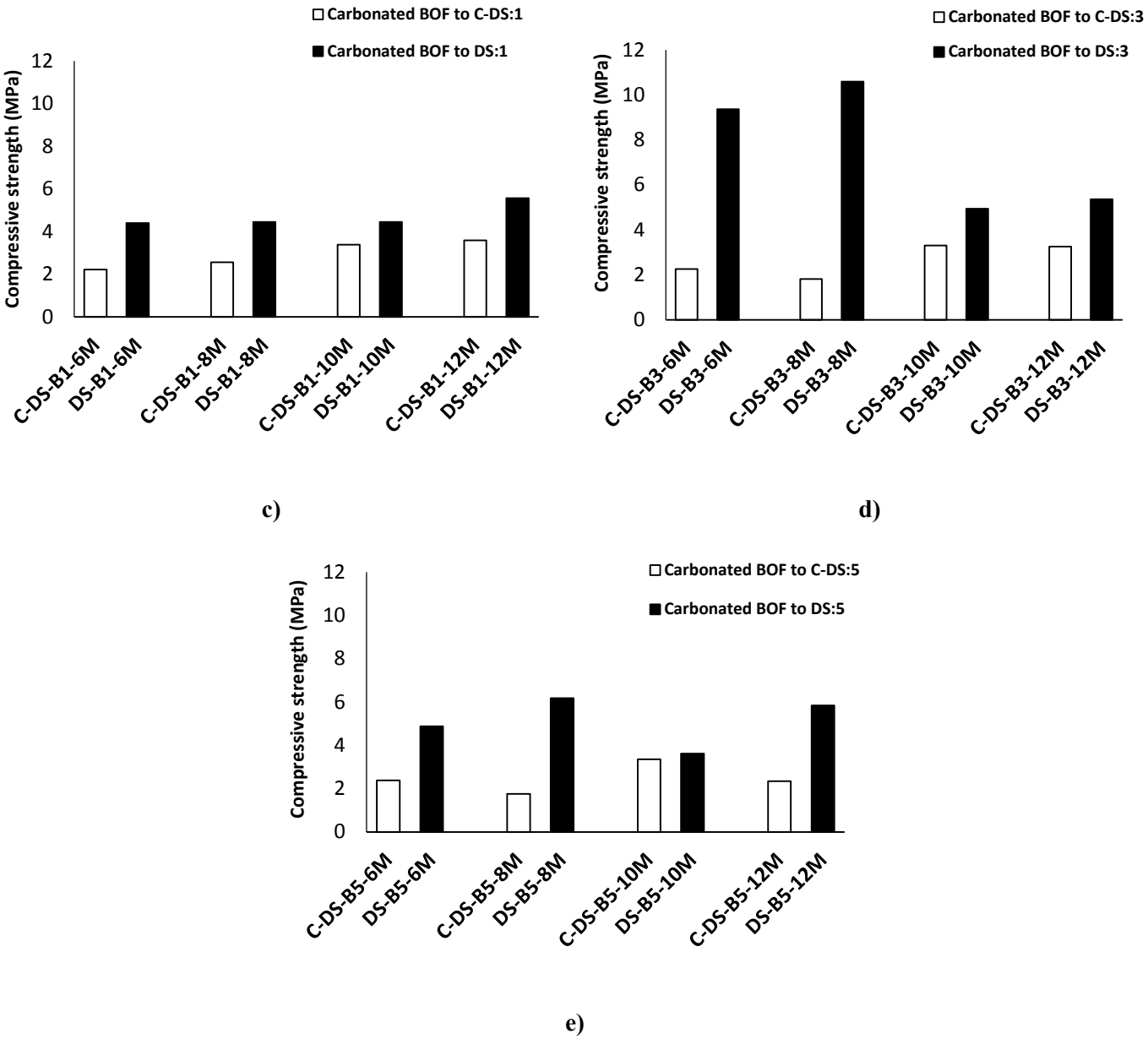

Fig 6.2. a) Effects of using different contents of carbonated DS on the compressive strength; b) Effects of using different contents of non-carbonated DS on the compressive strength; c) comparative effects of using carbonated BOF to carbonated DS and non-carbonated DS with ratio of 1 on the compressive strength; d) comparative effects of using carbonated BOF to carbonated DS and non-carbonated DS with ratio of 3 on the compressive strength; d) comparative effects of using carbonated BOF to carbonated DS and non-carbonated DS with ratio of 5 on the compressive strength.

2.4.3 Efflorescence

Alkali activated binders contain much higher amount of soluble alkali metal concentration compared to OPC, so when the specimens are exposed to the humidity or in contact with water, efflorescence (is formed due to formation of sodium carbonates) could be an important issue (Škvára, et al., 2009). (Zhang, et al., 2014) showed that efflorescence rate depends on activation conditions such as alkali contents which cured at ambient temperature. Therefore, to assess the

potential of forming efflorescence in alkali-activated binders, all mixtures were contacted to water. Fig. 7.2 illustrates the effects of using different precursor types, sodium hydroxide molarities, and carbonated BOF aggregate contents. It observed that the specimen's surfaces, which used carbonated DS had more potential of efflorescence than those ones used non-carbonated DS. To compare the mixture DS-8M-B3 with C-DS-8M-B3, it revealed that C-DS-8M-B3 has much higher efflorescence rate than DS-8M-B3.

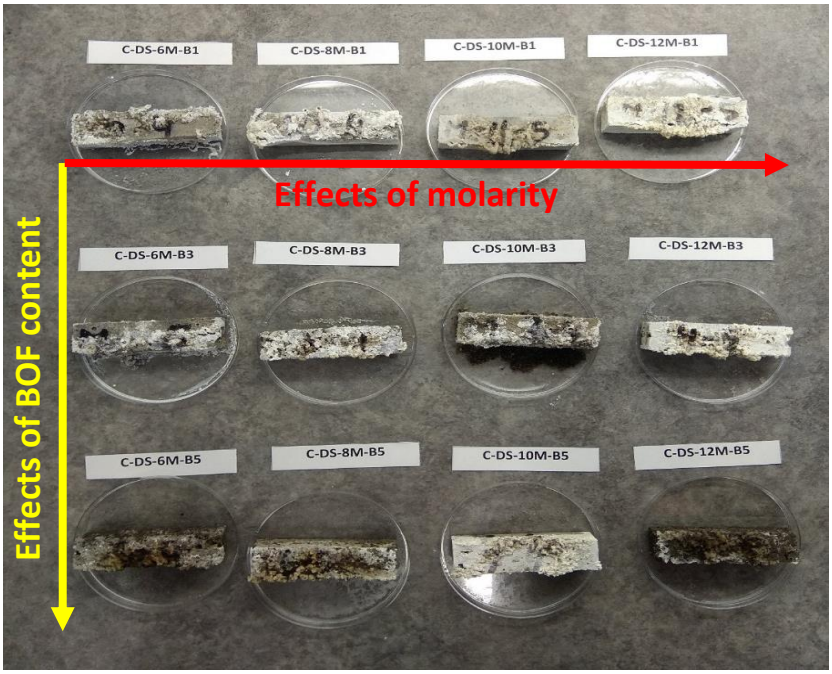

a)

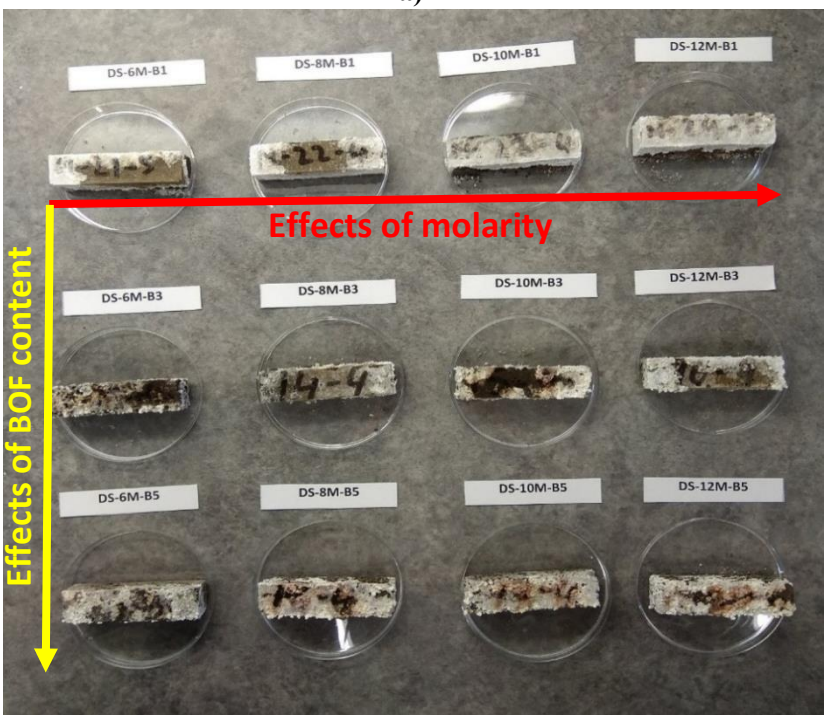

b)

Fig 7.2. Comparative effects of efflorescence in the compositions containing: a) carbonated desulfurization slag; b) desulfurization slag

2.4.4 pH measurements

Fig. 8.2 shows the pH variations of the mix compositions containing carbonated DS and non-carbonated DS precursors. Maximum pH values were obtained after 24 hours, and values of all mixtures were almost similar. After 144 h, it decreased slowly to around 1.5 and 1.1 of the samples containing carbonated DS and non-carbonated DS, respectively. On average, the pH value decreased of using the carbonated DS is 11 and non-carbonated DS is 11.6. Therefore, it could be concluded that the pH values of non-carbonated DS are slightly higher than those of the carbonated DS.

2.5 Conclusions

The effects of using different parameters such as different precursor types (carbonated and non-carbonated DS), carbonated BOF aggregate contents, and sodium hydroxide molarities have been investigated based on strength development, efflorescence, and pH values. The following conclusion can be drawn from this chapter:

Regarding the compressive strength, it is noticed that non-carbonated DS slag with carbonated BOF to binder ratio 3 and 8M NaOH has nearly 9 times higher compressive strength compared to carbonated DS slag. In general, replacing non-carbonated DS to carbonated DS binder increased the mechanical strength.

From the visual observations of efflorescence, it observed that the carbonated DS had more intensity of efflorescence than using non-carbonated DS.

According to the pH values, it showed that the pH values of non-carbonated DS are slightly higher than carbonated DS.

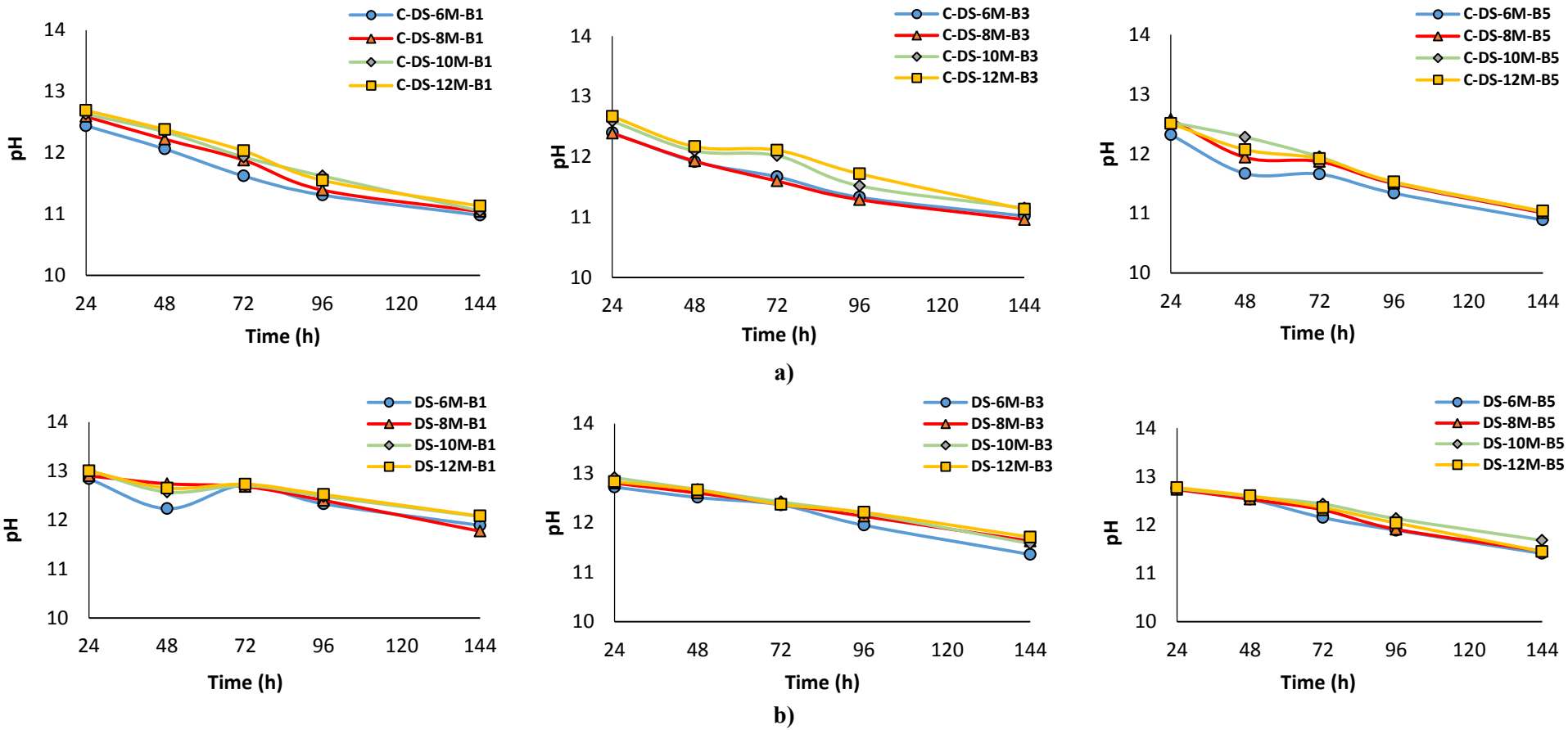

Fig 8.2. Comparative effects of pH in the mix compositions containing: a) carbonated desulfurization slag; b) desulfurization slag.

CHAPTER 3

Development of fiber reinforced alkali activated desulfurization slag concretes containing carbonated BOF aggregates

3.1 Introduction

According to the findings in the previous chapter on desulfurization (DS) slag, one of the major drawbacks of using desulfurization (DS) slag is efflorescence. To improve mechanical properties and minimize the efflorescence, different fibers were used to reinforce the mixtures.

The effects of adding fibers to alkali activated desulfurization slag concretes with carbonated BOF aggregates were investigated by introducing different fibers in the mixture and evaluation of strength development and efflorescence.

3.2 Fibers used to reinforce the mixtures

3.2.1 Basalt

Basalt fibers are manufactured by melting basalt rock which is one of the common rocks in the earth's crust. The primary element of basalt is SiO_2, it has a similar chemical composition of the glass. There are two methods, which are followed to produce the fibrous product, including the Junkers and the Spinneret. It is noticed that when hardening, the density of basalt could not allow it to be drowned to the base or rise to the top. (Kiisa, et al., 2016)

3.2.2 Polyvinyl Alcohol (PVA) fiber

Polyvinyl Alcohol (PVA) fibers are widely used for reinforcing concrete due to their good physical and mechanical properties. According to the (Abdollahnejad, et al., 2018), the maximum compressive strength was recorded more than 50% in the mixture containing 1% PVA fiber compared to the reference mixture which cured in the water. Their findings also showed that increasing the amount of PVA fiber from 0.5% to 1% improved 15% of the flexural strength. In addition, 1% PVA fiber with sealed in a plastic bag had increased 5% water absorption compared to the plain mixture. However, 6% water absorption had reduced in the mixture containing 0.5% PVA fiber which cured in water.

3.2.3 Polypropylene (PP) fiber

Polypropylene (PP) fiber has been broadly utilized in the reinforced concrete and cement industries because of its high toughness and anticorrosion ability. (Abdollahnejad, et al., 2018) found that the highest reduction resulted in the mixture reinforced with PP fiber. The surface of the PP fibers is smooth, as a result, they would not able to make strong bond at fiber/matrix interface (Mastali, et al., 2016) (Mastali & Dalvand, 2017).

3.2.4 Cellulose fiber

Cellulose fiber for concrete is 100% sole cellulose fiber which has a patented alkaline resistant coating manufactured by ISO 9001 certified facility. This fiber gives excellent added reinforcement performance by close fiber spacing, high fiber surface area, excellent bonding ability with the cement matrix, high fiber tensile strength, and ideal distribution in concrete so it is always positioned correctly. It is safe, easy to use, and offers superior finishability. (Inforce, 2019)

Cellulosic fiber is known as environment-friendly which is widely used within the cementitious compositions. Nowadays, the applications of cellulose fiber and their fabric reinforced polymer composites as reinforced materials are getting popular because of their mechanical performance and reasonable costs. This fiber type consists of sisal, flax, cannabinus, hibiscus, eucalyptus pulp, jute, coir, hemp, malva, pineapple leaf, sansevieria leaf, abaca leaf, bamboo, banana, and palm and sugarcane fibers, etc. (Yan, et al., 2016)

3.3 Experimental plan

3.3.1 Mix design and designations

According to the result from the chapter 2, the mixture DS-B3-8M was selected to perform further studies with different fiber types. In this chapter, 4% fiber (in mass) was used for improving the mechanical properties of the proposed mix compositions. Four different fibers (Basalt, PVA (8mm), Cellulose, and PP) were selected in this chapter. Moreover, in this work, 8% and 4% hybrid PVA and Basalt mix compositions also studied. Table 1.3 shown the physical and mechanical properties of used fibers. Mix compositions and different mix proportion with fibers are shown in Table 2.3.

Table 1.3. The physical and mechanical properties of the fibers

Fiber type	Length / Diameter (mm/mm)	Elastic modulus (GPa)	Tensile strength (MPa)	Elongation at break (%)	Density (g/cm^3)
PVA	200	41.0	1600	6	1.30
PP	833	9.6	910	<12	0.91
Basalt	333	100.0	4500	3.1	2.63
Cellulose	117	8.5	750	-	1.10

Table 2.3. Mix compositions

Specimen designation	Desulfurization (DS) slag	Aggregate/binder	Alkali/binder	SS/SH	Sodium hydroxide (M)	Fiber (%)
Basalt	1	3	1	2.5	8	4
PVA 8mm						4

Cellulose						4
PP						4
hybrid PVA and Basalt						4
hybrid PVA and Basalt						8

a) **b)** **c)** **d)**

Fig 1.3. Used fibers: a) Basalt b) PVA 8mm c) PP d) Cellulose

3.3.2 Casting and curing regime

Firstly, dry ingredients non-carbonated desulfurization (DS) slag and carbonated BOF was mixing for 1 min. Then alkali solutions (sodium hydroxide and sodium silicate) added and mixed up to 2 min to ensure proper mix, after that fiber was used gradually and mixed for 2 min. Then the mixture was cast into standard prismatic molds (40×40×160 mm). The mold was filled in two steps. First, it filled up with half and then shaker was used for 60 seconds. After that, the mold is filled, and shaker was used in a same way. All prismatic beams were cured 7 days at the lab condition.

a) **b)** **c)** **d)**

Fig 2.3. Schematic view of the fiber reinforced specimens after demolding a) Basalt b) PVA 8mm c) PP d) Cellulose

3.4 Test procedures

3.4.1 Flexural strength

Regarding the proposed mix composition in Table 1.2, total of six samples were tested to perform the flexural strength under three-point bending test. In this chapter, obtaining flexural strength of each mix compositions is done by one specimen. The test was measured using a load cell of 100 kN and load displacement rate of 0.6 mm/min was attributed to the beams. Equation 1.1 is followed to calculate the flexural strength.

3.4.2 Compressive strength

The broken portion of prismatic beams from the flexural test have taken to measure the compressive strength. Compressive load with displacement control and speed of 1.8 mm/min imposed to the specimens. The compressive strength is calculated by averaging two pieces of prismatic beams, equation 2.1 is used for calculation.

3.4.3 Visual observation of efflorescence

One sample from each mix composition was used to observe the intensity of efflorescence. The samples were kept half of Deionized (DI) water in a tray at the ambient condition (averagely the temperature of 25 ^{0}C) and observed after 24, 48, 72 and 120 hours.

3.5 Results and discussion

3.5.1 Flexural strength

The influences of adding different fibers on the flexural strength of the prismatic beams are shown in fig 3.3. According to the results, the fluctuations in the effect of fibers depend on different fiber types and content of each mixture. The flexural strength of reinforced mixtures with 4% hybrid PVA/basalt, PVA, basalt, and cellulose fibers increased, regardless the fiber content. Interestingly, the maximum improvement was obtained around 70% (2.6 MPa) in the mixture reinforced with cellulose fiber compared to the reference mixture. Additionally, 5%, 30%, and 50% flexural strength increased by using 4% hybrid PVA/basalt, PVA, basalt fibers, respectively.

On the other hand, maximum reduction of the flexural strength resulted around 40% (1 MPa) in the mixture containing PP fiber compared to the plain mixture. PP fiber has a smooth surface, as a result it creates week bond and interaction at fiber/matrix interface during debonding

(Abdollahnejad, et al., 2018). Moreover, using 8% hybrid PVA/basalt also decreased the flexural strength compared to the reference.

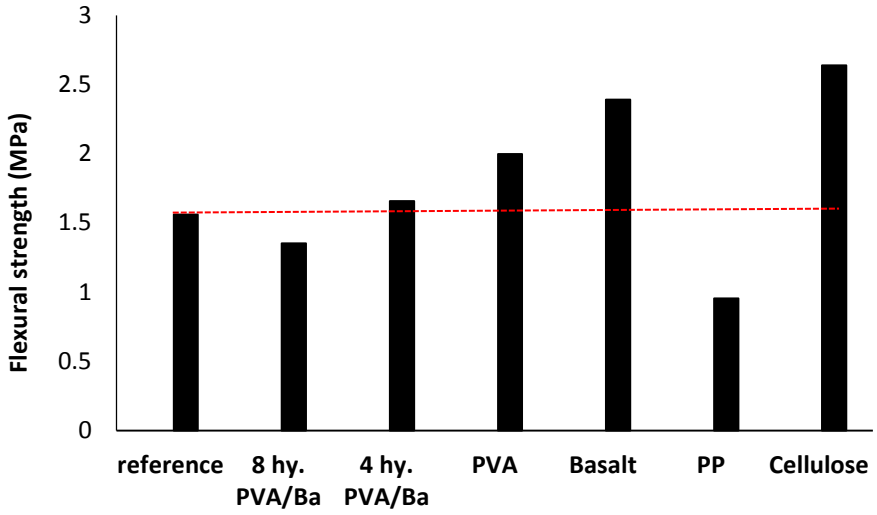

Fig 3.3. Effects of using different fibers on the flexural strength

3.5.2 Compressive strength

Fig 4.3 presents the impacts of introducing different fibers on the compressive strength. It is expected that addition of fiber can minimize crack propagation by increasing air voids in the mixtures. The internal pore structure of mixes depends on fibers content and type, content of binder and aggregate. These different parameters could impact on increasing or decreasing the compressive strength. The results presented that the further crack opening could be arrested by adding of fibers; as a result, it increases the compressive strength (Mastali, 2019).

Concerning the results, the maximum increase of the compressive strength was measured around 40% (11 MPa) in the reinforced mixture with cellulose fiber compared to the plain mixture. In addition, mixture reinforced with basalt fiber 15% increased the compressive strength.

According to the result, it was observed that mixture containing PP, PVA, combination of PVA/basalt (8% and 4%) fibers, significantly reduced the compressive strength. Moreover, the lowest increment of the compressive strength resulted in the reinforced composition containing 8% hybrid PVA/basalt fibers.

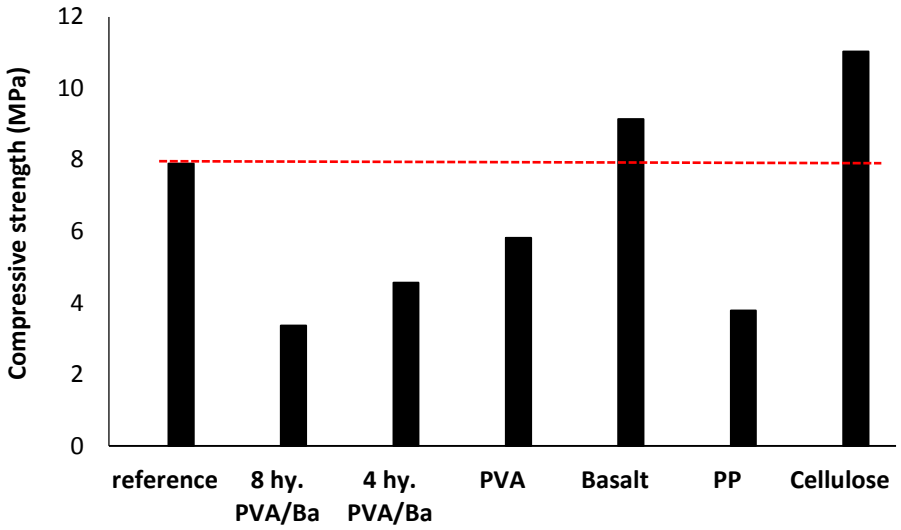

Fig 4.3. Effects of using different fibers on the compressive strength

3.5.3 Visual observation of efflorescence

Fig 5.3 illustrates the comparative effects of efflorescence in the mixtures reinforced with different fibers. Fibers could have different impacts on the efflorescence rates, depending on the fiber type, length, and shape. Regarding the fiber dispersions, fibers could physically provide a confinement around the specimens and affect the efflorescence rates.

It is observed that significant efflorescence did not form after 24 hours contact with water, in the reinforced mixtures with cellulose, PVA 8mm and hybrid 8% fibers. Afterward, it observed that the reinforced mixtures with cellulose, basalt, PVA fibers have lower efflorescence intensity rate than compared to other mixtures until 72 hours. Regardless of the fiber type, reinforcing mixtures could successfully mitigated the efflorescence rates compared to the plain mixtures, as shown in Fig 7.2.

0 hour

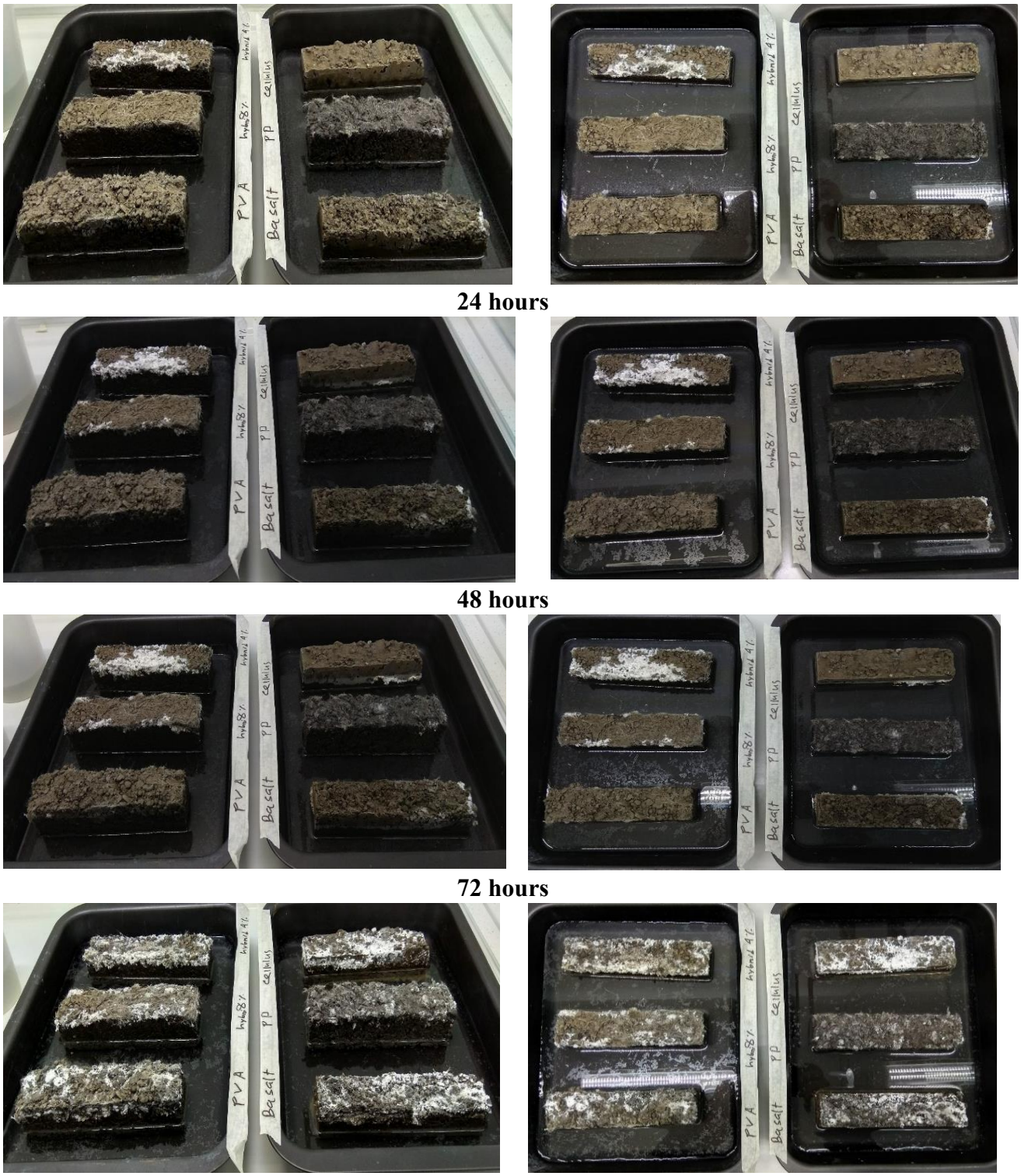

24 hours

48 hours

72 hours

120 hours

Fig 5.3. Comparative effects of using different fibers on the efflorescence rates

3.6 Conclusions

A comparative experimental study was carried out to investigate the influences of using different fiber types on the hardened state properties of the mix composition of DS-B3-8M in terms of strength development and efflorescence. The main results are summarized as follows:

From mechanical testing, it revealed that reinforcing the mixture DS-B3-8M with basalt and cellulose fibers had significant impacts on improving the strength compared to reference, while the maximum reduction in the mechanical strength was observed in the reinforced mixtures with PP fibers.

Promising results were achieved in reducing the efflorescence rates by adding fibers, however, this rate was governed by fiber type, shape, length. Moreover, it was shown that mixtures reinforced with cellulose, basalt, PVA fibers had much lower efflorescence rates than others reinforced fibers.

CHAPTER 4

Hardened state properties of fiber reinforced alkali activated desulfurization slag concretes containing carbonated BOF aggregates to produce bricks

4.1. Introduction

In this chapter, the effects of adding fibers (basalt, cellulose) on the selected mixture (DS-B3-8M) were explored by evaluating mechanical strength, effects of carbonation, water absorption by capillarity, water absorption by immersion, efflorescence, ultrasonic pulse velocity, shrinkage, high temperature, freeze-thaw experiments. The main aim in this chapter is to develop bricks to use in the construction sectors. Therefore, various experiments were carried out to assess the feasibility of using the developed materials in the production of bricks.

4.2 Experimental plan

4.2.1 Mix design and designations

According to the results, basalt and cellulose fibers were selected in this chapter to reinforce the mixture of DS-B3-8M, which containing carbonated BOF aggregates to desulfurization (DS) slag 3. Particle size distributions of carbonated BOF aggregates were larger than 0.5 mm and DS smaller than 0.5 mm. 4% fiber (in mass of binder) was used to add in this study. Three mix compositions were prepared, mixed, and tested as listed in Table 1.4.

Table 1.4. Mix compositions

Specimen designation	DS	Carbonated BOF aggregate/binder	Alkali solution/ binder	SS/SH	Sodium hydroxide (M)
Reference	1	3	1	2.5	8
Basalt					
Cellulose					

4.2.2 Curing and Aging

In total, seventy-two prismatic beams and six cubes were prepared. First, dry ingredients such as DS slag and carbonated BOF aggregates were combined for 1 min. Then, alkali solutions (combination of sodium hydroxide and sodium silicate) was added to the dry mixture and mixed for another 2 minutes. Afterward, fibers added gradually and stirred for more 2 minutes. the molds were filled by fresh concretes and then the specimens were vibrated for 60 seconds. The dimension of the used prismatic beams and cubes were (40×40×160 mm) and (100×100×100 mm), respectively (see Fig 1.4). Then, the molds are covered with plastic for 24 hours. After one day, it was demolded and again sealed with plastic bag and kept in the ambient conditions of lab (averagely 25 ^{0}C and 40% RH) till the test day (28 days).

a) b)

Fig 1.4. Specimens after demolding: a) prismatic beams; b) cubes

4.3 Test procedures

4.3.1 Flexural strength

To compare the effects of introducing the basalt and cellulose fibers to reference (DS-B3-8M) mix composition, total nine sample (40×40×160 mm) were prepared and assessed under three-point bending test (see Fig 2.4). Load was submitted to the middle of the beams and a displacement load with rate of 0.6 mm/min imposed to the specimens. The shear span was 100 mm. The flexural strength was collected by averaging three prismatic beams and equation 1.1 was used for computing the flexural strength. It is worth stating that the UPV was carried out before execution of the flexural test.

Fig 2.4. Adopted flexural test setup

4.3.2 Compressive strength

The compressive strength was performed in broken portions of beams from flexural strength. The compressive load with displacement rate of 1.8 mm/min released to the beams (see Fig 3.4). Equation 2.1 is used to calculate the result and it is done by averaging six parts of broken beams.

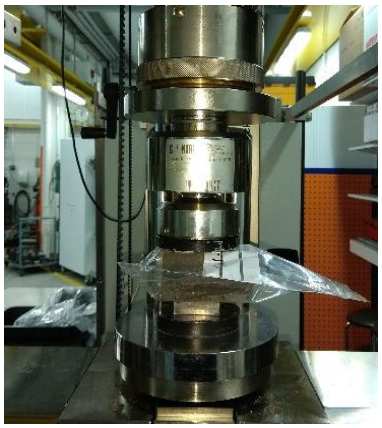

Fig 3.4. Imposed the compressive load

4.3.3 Carbonation test

Three samples from each mix compositions were prepared and then cured in the carbonation chamber for 7 days (see Fig 4.4). The condition of the chamber was CO_2 gas with pressure of 5%, temperature of 23 ^{0}C, and the relative humidity (RH) 67%. After cured in CO_2 chamber, total nine prismatic beams were performed in flexural and mechanical strength. In addition, mass and UPV were measured before and after the carbonation process.

Fig 4.4. Inside the carbonation chamber

4.3.4 Water absorption by capillarity

EN 1015-18:2002 is followed to test water absorption by capillarity rise. Two cubic specimens from each three mix compositions with the size of (100×100×100 mm) were cast and prepared. A silicon layer covered the lateral surface of cubic specimens because the silicon layer helps to avoid water evaporation and humidity transportation over the lateral surface. After polishing the lateral surface, bottom one surface is positioned to contact with water (see Fig 5.4), and the mass of water absorption by capillary rise was measured throughout 96 hours. Equation 3 was used to find coefficient of capillary water absorption.

$$A_w = \frac{\Delta B}{A\sqrt{t}} \qquad (1.4)$$

where A_w represents water absorption coefficient ($kg/m^2/H^{0.5}$), ΔB is for mass of absorbed water and A is the surface area (m^2). The gradient of straight line acquired through plotting cumulative mass of absorbed water which is used to evaluate the mass of water entering the cubic specimen per unit of area and time (Mastali, et al., 2018).

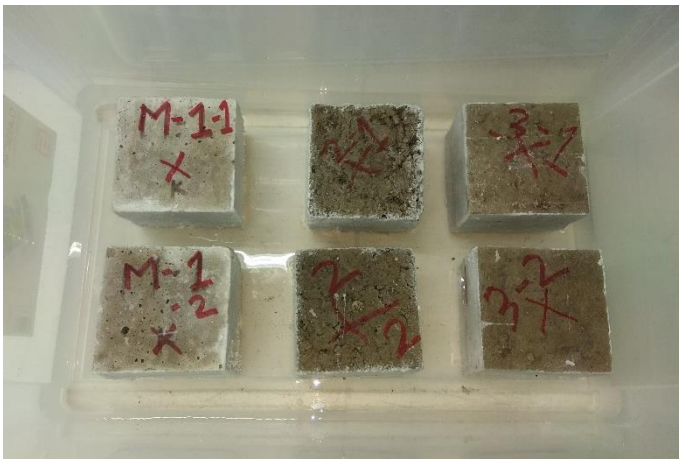

Fig 5.4. Water absorption by capillarity

4.3.5 Water absorption by immersion

Total six prismatic specimens were prepared for water absorption by immersion test after 28 days age. The beams were fully submerged in a plastic water tank at room temperature for 24 hours where average water temperature of water is 20 ^{0}C (see Fig 6.4(a)). After 24 hours, beams were removed from water and keep on a wire mesh for 1 min which helps drain out the water. In addition, rest of water which is visible in the surface of specimen was wiped off by a damp cloth, then measured the mass as W_{sat} (saturated weight). After that, all prismatic beams were kept in an oven at 100 ^{0}C for 24 hours (see Fig 6.4(b)). After healing in the oven, the mass of dried specimens was noted as W_{dry} (oven-dry weight). After measured dried and saturated masses, water absorption by immersion was calculated through following equation (Mastali, et al., 2018).

$$\text{Water absorption} = \frac{W_{sat} - W_{dry}}{W_{dry}} \times 100 \qquad (2.4)$$

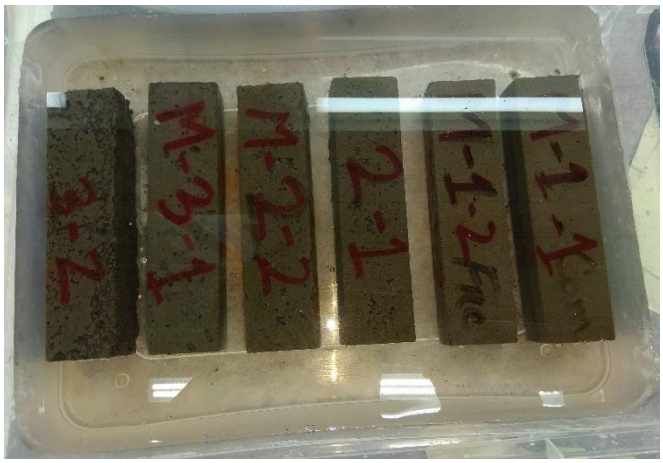

a)

b)

Fig 6.4. Water absorption by immersion a) immersed in a water tank; b) heated in oven at 100 ^{0}C

4.3.6 Efflorescence rates

One specimen from each mix composition was selected for efflorescence test. Prismatic beams were kept in half of DI water in a tray at room temperature and continually observed after 24, 48, 72 and 120 hours.

4.3.7 Ultrasonic pulse velocity

Air voids and compactness of concrete which are influenced by fiber length, type and concentration. UPV test is a non-destructive in-situ test that is used to analyses to find the influences of fibers on compactness and quality of mixtures. The two transducers that are used to measure ultrasonic pulse which is passed through the concrete (see Fig 7.4) (Mastali, et al., 2018). Following equation is used to calculate UPV.

$$V = \frac{L}{T} \qquad (3.4)$$

Where, V is pulse velocity (m/s), L is distance between two transducers (mm), and T is transmission time (μsec).

Fig 7.4. Measuring ultrasonic pulse velocity

4.3.8 Drying shrinkage

Three specimens from each mix composition were prepared for assessing the drying shrinkage. Digital strain gauge was used to measure the length specimens, as shown in Fig 8.4. The drying shrinkage is measured every day in first week, then every second day in second week and lastly did one day per week, this way is continued for at least two months.

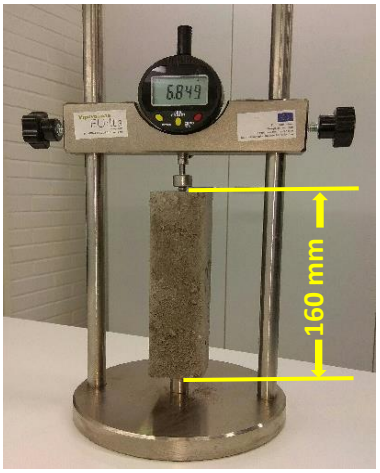

Fig 8.4. Drying shrinkage measurement

4.3.9 High-temperature resistance

Total 27 prismatic beams were prepared for three different high temperature (400 ^{0}C,600 ^{0}C, and 800 ^{0}C) investigation. In this experiment, rising time for high temperature was 3 hours and specimens were kept 4 hours at high temperature (400 ^{0}C,600 ^{0}C, and 800 ^{0}C) (see Fig 9.4). Fig 10.4 shows the condition of specimens before and after high-temperature experiment. Mass and UPV measured before and after high temperature test.

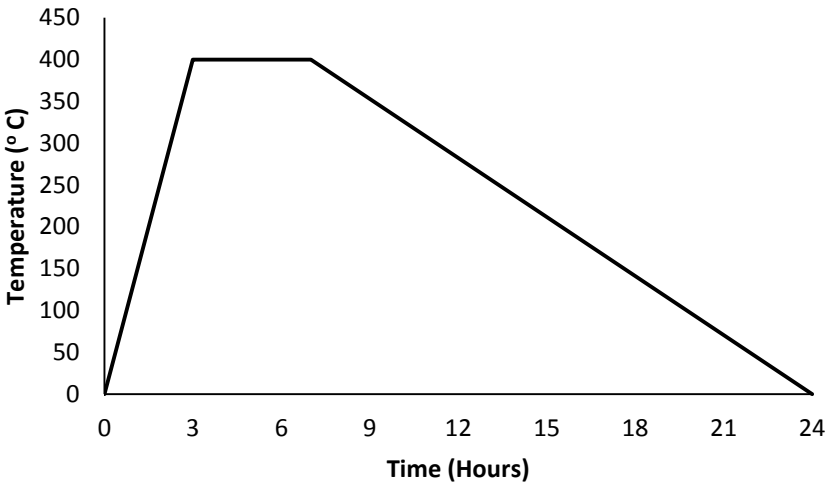

Fig 9.4. Temperature variation for 400^{0}C

a) **b)** **c)** **d)**

Fig 10.4. a) Oven used for high temperature (400 ^{0}C, 600 ^{0}C, and 800 ^{0}C); b) inside the oven; c, d) the curved reference beams after imposing high temperature.

4.3.10 Freeze-thaw resistance

Total six prismatic beams were prepared and performed freeze-thaw test. The specimens were kept in a tray with half of water. According to PD CEN/TS 12390-9:2016 standard, temperature range was +15 ^{0}C to -20 ^{0}C (Mastali, et al., 2018). For 24 hours there is three cycles in the system, in one cycle the specimens were kept 2 hours in -20 ^{0}C, the changes of temperature from plus to minus and minus to plus degree it took 4 hours and next 2 hours it kept in +15 ^{0}C. After 28 days aging, specimens were kept in freeze for 7 days (see Fig 11.4).

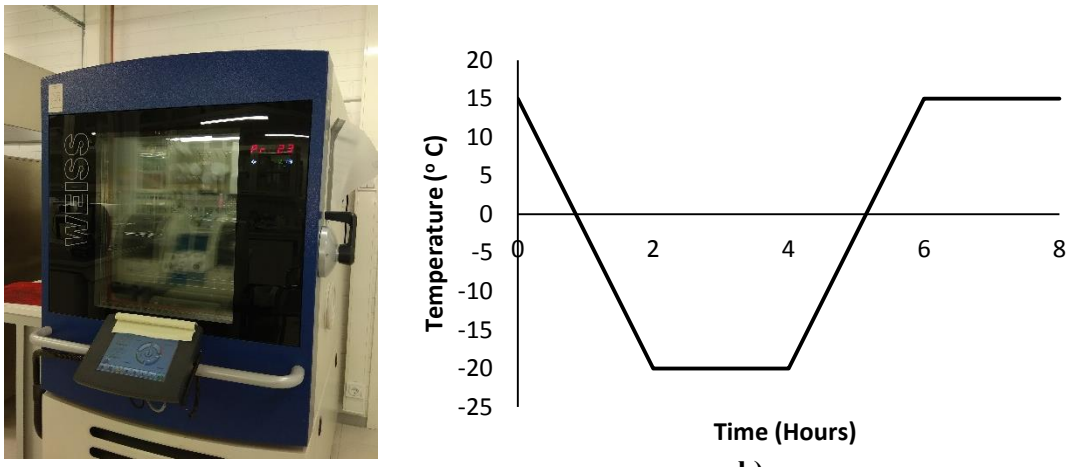

Fig 11.4. a) Equipment for testing the freeze-thaw resistance; b) Temperature variation for one freeze-thaw cycle

4.4 Results and discussion

4.4.1 Ultrasonic pulse velocity (UPV)

Fig. 12.4. shows the result of the UPV test of reference and the mix compositions reinforced with basalt and cellulose fibers. It shows that the addition of fiber could decrease or increases air voids, therefore, the UPV had no specific trend (Mastali, 2019). It is noticed that the reinforced mix composition with cellulose fiber had almost 10% higher UPV than the reference mixture, whereas using basalt fiber decrease the UPV slightly (< 1%).

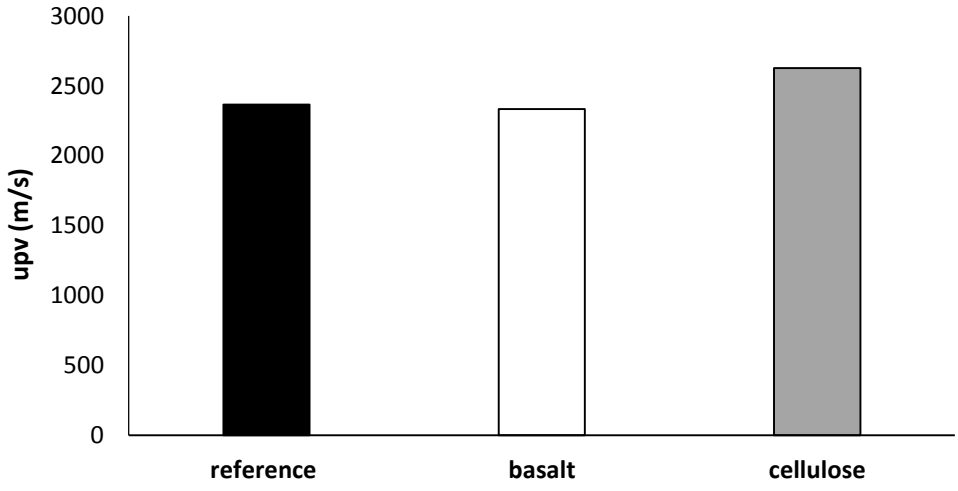

Fig 12.4. Effects of using DS and BOF on the UPV of the fiber reinforced mixtures

4.4.2 Flexural strength

Influence of adding basalt and cellulose fibers to reference mix composition on flexural strength are shown in Fig 13.4. It indicates that, fiber bridging action slightly improved the flexural strength. According to the figure it shows that maximum enhancement was resulted in mixture reinforced with basalt fiber around 10% (2 MPa) of the flexural strength, as compared to the reference mixture (1.8 MPa). In addition, mixture reinforced with cellulose fiber slightly increased the flexural strength which is around 5% (1.9 MPa) than the plain mixture.

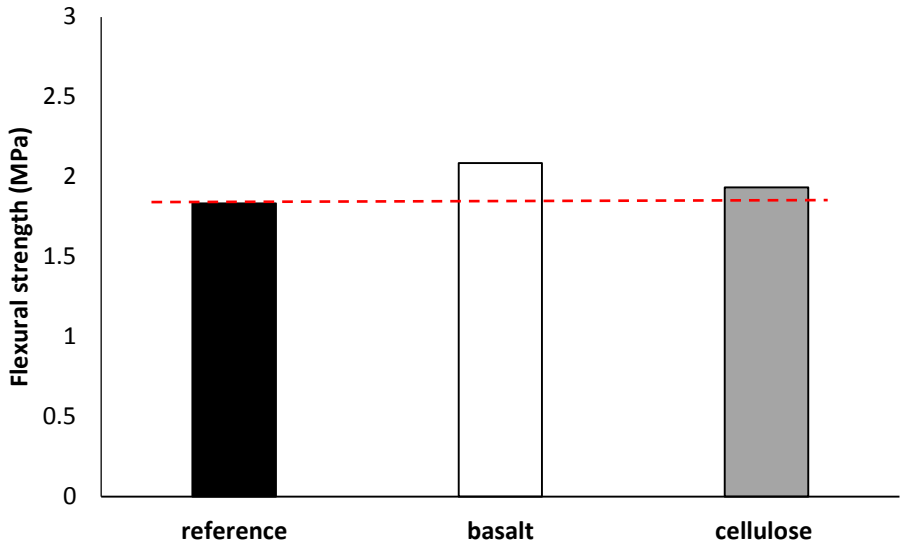

Fig 13.4. Influences of using different fibers on flexural strength

4.4.3 Compressive strength

Fig 14.4 presents the effects of introducing different fibers (basalt and cellulose) on the compressive strength. It is expected that adding fibers could increase the air voids which helps to decrease crack propagation. The internal pore structure of the mixture influenced by containing fiber content, binder, and aggregate. Therefore, capacity of fiber could arrest the further crack opening (Mastali, 2019). According to the figure, it shows that there is slightly increase of compressive strength after adding fibers. It is noticed that approximately 15% (9 MPa) strength achieved in the mixture reinforced with cellulose compared to the plain mixture (8 MPa). On the other hand, basalt indicated similar compressive strength, which was about 8.85 MPa.

.

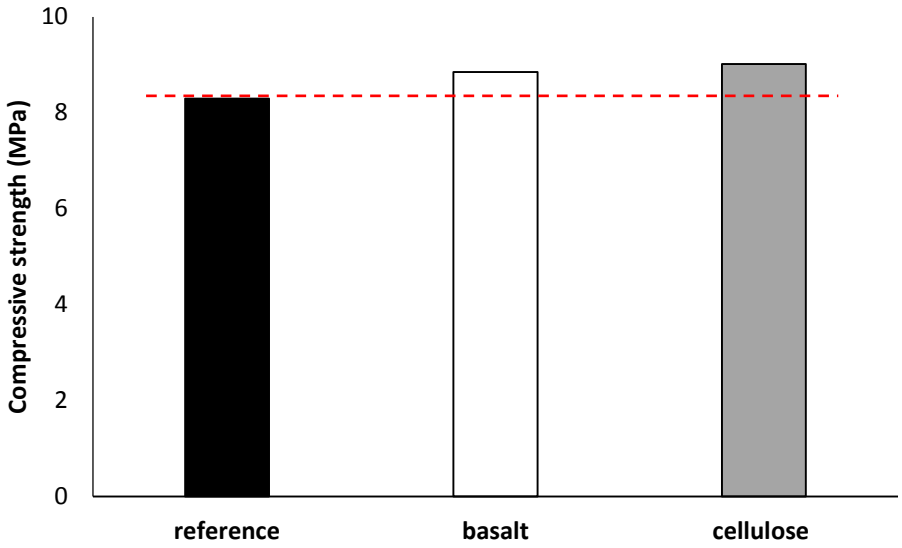

Fig 14.4. Influences of using different fibers on the compressive strength

4.4.4 Effects of carbonation

Fig 15.4 depicts the effects of carbonation on the UPV of mixtures including basalt and cellulose fibers. Generally, it indicates that carbonation has significant impacts on UPV, after carbonation process it observed that all mixes reduced the UPV. The maximum reduction of UPV occurred in the mixture reinforced with cellulose, it was decreased 30% compared to before carbonation process. In addition, around 25% reduction resulted the mixture reinforced with basalt fiber. After carbonation the maximum UPV was recorded 1895 m/s of plain mixture which is decrease around 15% compared to the UPV before carbonation.

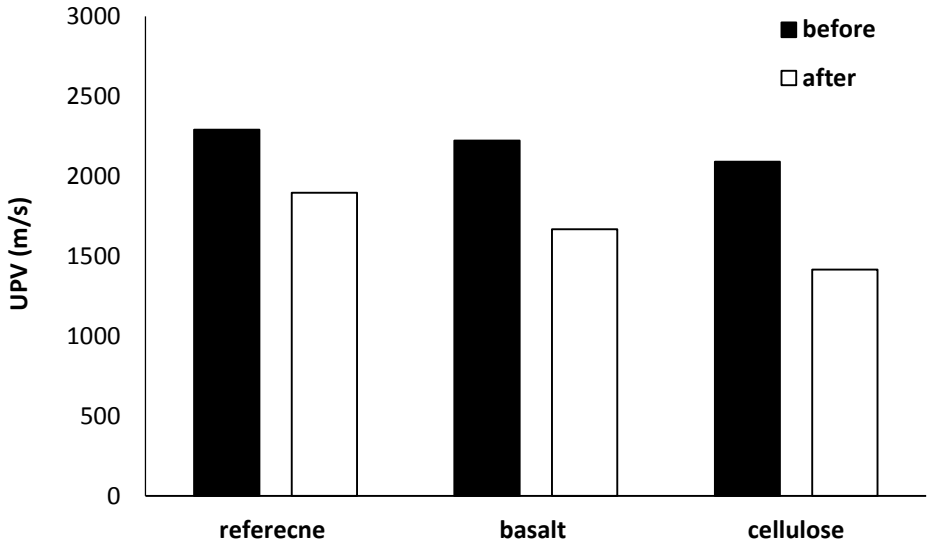

Fig 15.4. Effects of carbonation on the UPV of the mixtures

Effects of carbonation on the specimen's mass are shown in the fig 16.4. According to the result, it indicates that there is no significant change of mass after carbonation process. It slightly decreased the mass from all the mixtures, including reinforced mixture with basalt and cellulose fiber.

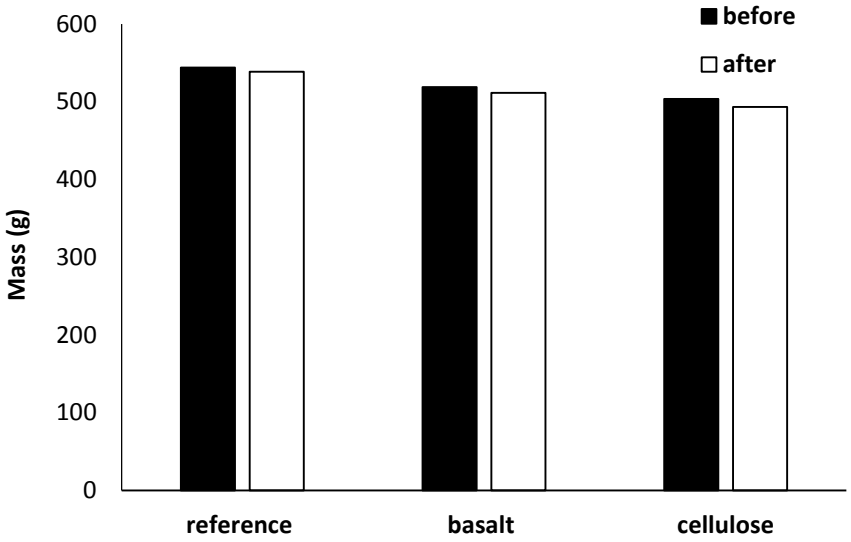

Fig 16.4. Mass changes before and after execution of the carbonation test

Fig 17.4 presents influence of the carbonation on the flexural strength of the reference and reinforced mixtures with fibers (basalt and cellulose). It shows that carbonation has significant impacts on the flexural strength. The maximum reduction of the flexural strength was observed on the mixture reinforced with cellulose, it resulted 47% of loss of the flexural strength. Around 33% loss was resulted both plain mixture and mixture reinforced with basalt fiber.

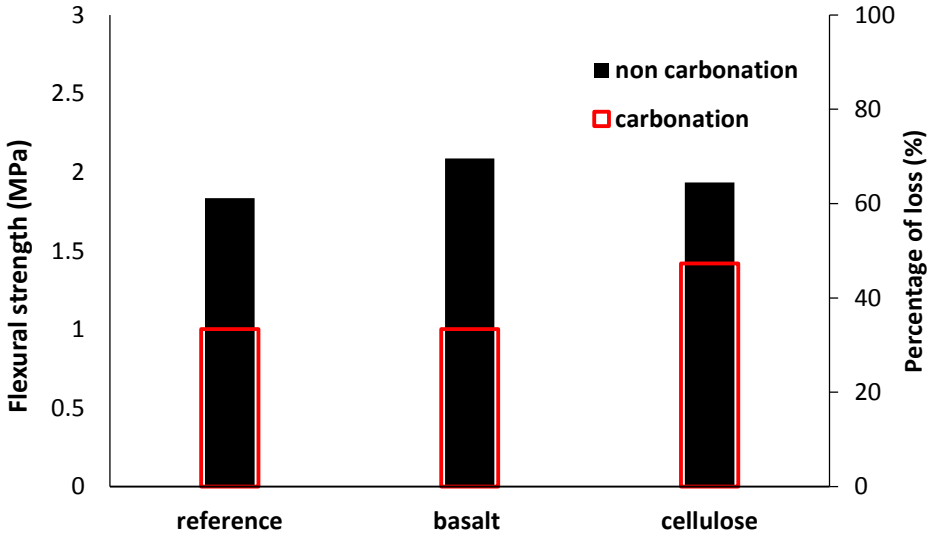

Fig 17.4. Influence of the carbonation on the flexural strength

The impacts of the carbonation on the compressive strength of the reference and reinforced mixtures with fibers (basalt and cellulose) are shown in Fig 18.4.

Similar to the flexural strength, the highest percentage of loss around 60% has recorded the mixture reinforced with cellulose. On the other hand, the minimum loss (40%) resulted in the plain mixture. About 50% loss was recorded on the mixture reinforced with basalt (4.3 MPa).

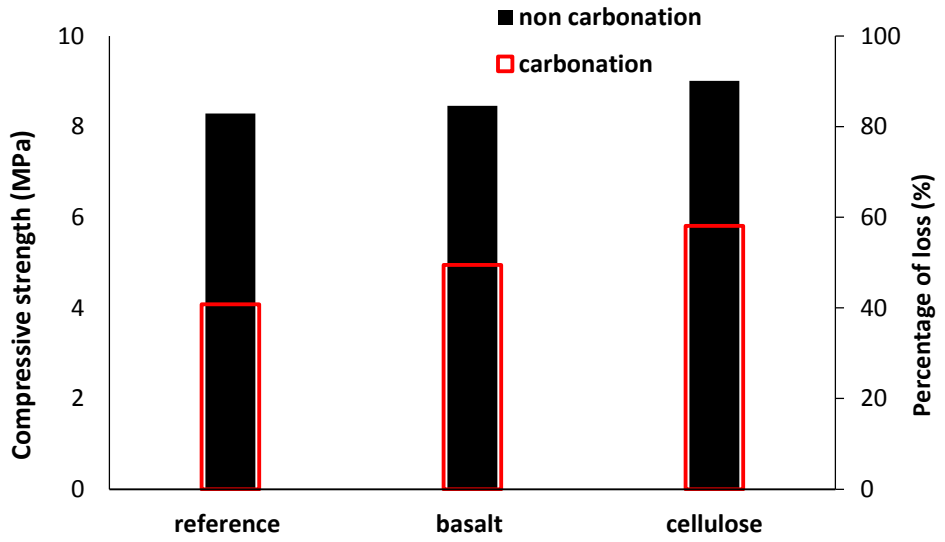

Fig 18.4. Influence of the carbonation on the compressive strength

4.4.5 Water absorption by capillarity

The influences of using desulfurization (DS) slag binder with 4% fiber reinforcement on the internal pore structure of reinforced mixtures was investigated through cumulative mass of water and the capillary coefficient of the mixtures. Fig 19.4 illustrates that mixture reinforced with cellulose fiber reduced the cumulative mass of water compared to plain mixture. On the other hand, mixture reinforced with basalt fiber increased cumulative mass of absorbed water which is same as the reference mix composition. In addition, capillary coefficient was reduced by using cellulose fibers compared to plain mixture. The maximum reduction recorded in cellulose fiber (15%) and same capillary coefficient resulted in the mixture reinforced with basalt compared to reference mixture. Capillary coefficient was found around 0.62 $kg/m^2H^{0.5}$ for both reference and mixture reinforced with basalt and 0.53 $kg/m^2H^{0.5}$ for cellulose fiber.

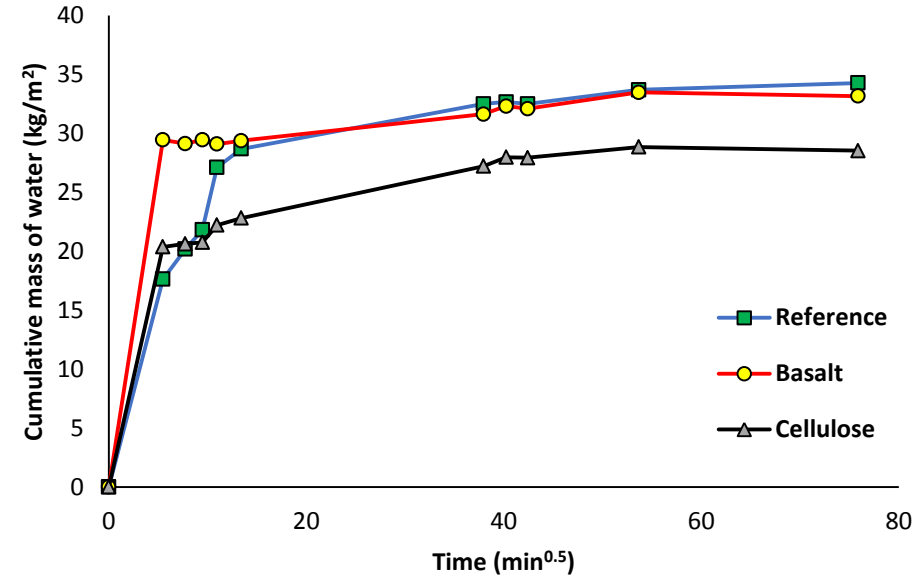

a)

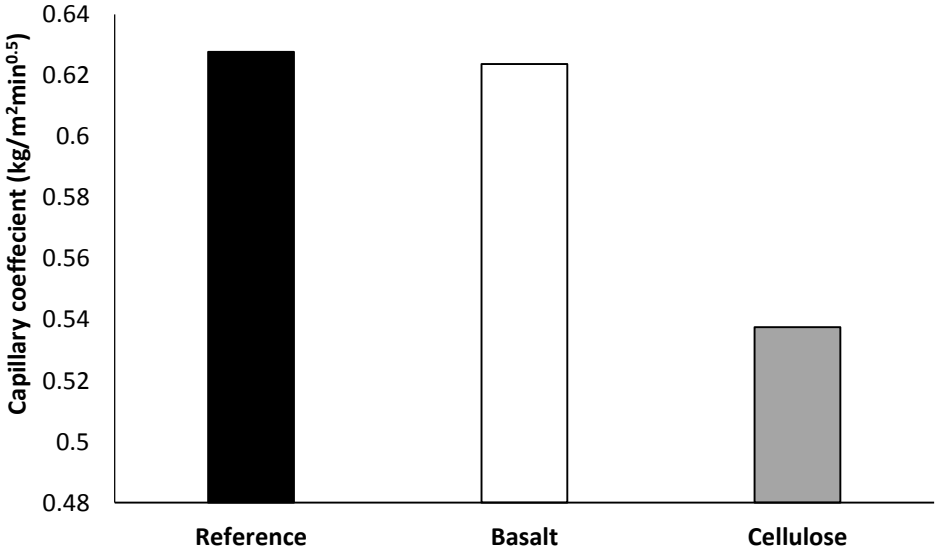

b)

Fig 19.4. a) Cumulative mass of water in the mixtures reinforced with 4% basalt and cellulose b) capillary coefficient.

4.4.6 Water absorption by immersion

The impacts of using fibers on water absorption by immersion are depicted in Fig 20.4. Investigation by this experiment, the information about permeable pore volume in the concrete and pores conductivity could be found (Mastali, 2019). The mixture reinforced with cellulose fiber has 5% increased water absorption compared to the plain mixture. According to the result, it shows that mixture reinforced with cellulose fiber has much porosity than basalt fiber, so it increased the water absorption.

A comparison of the results showed that the using fibers had significant effects on water absorption through immersion than did the reference mixture. This finding can make co-relation with freeze/thaw experiment.

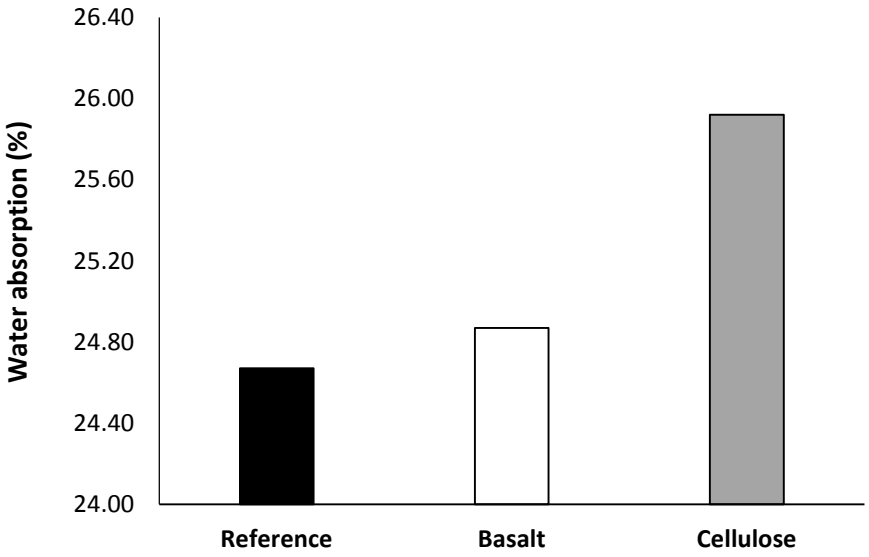

Fig 20.4. Water absorption by immersion

4.4.7 Visual observation of efflorescence

Fig 21.4 depicts the comparative effects of efflorescence rates in the reference, reinforced mixtures with basalt and cellulose fibers. After 24 hours, the reference and in the mixture reinforced with basalt fiber had much slat shape materials on their surfaces rather than the mixture reinforced with cellulose fiber. After 72 and 120 hours, it observed that the mixture reinforced with cellulose fiber has lower efflorescence intensity than other two samples.

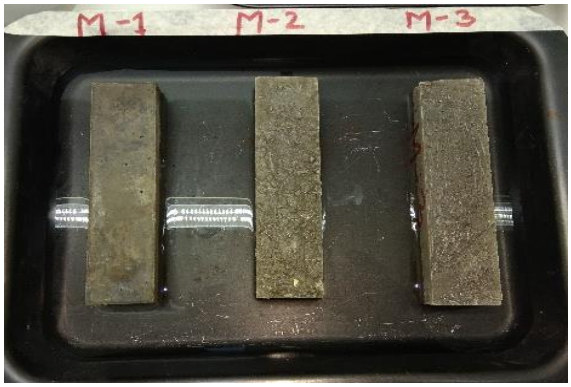

0 hour

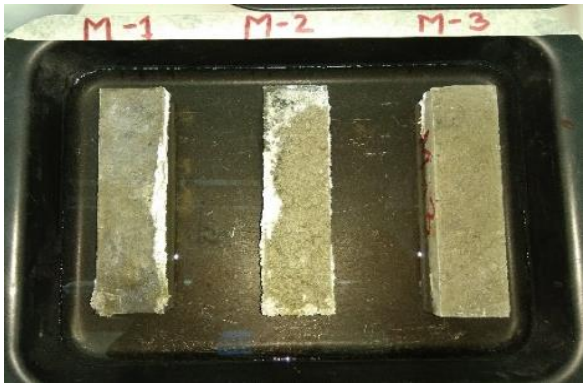

24 hours

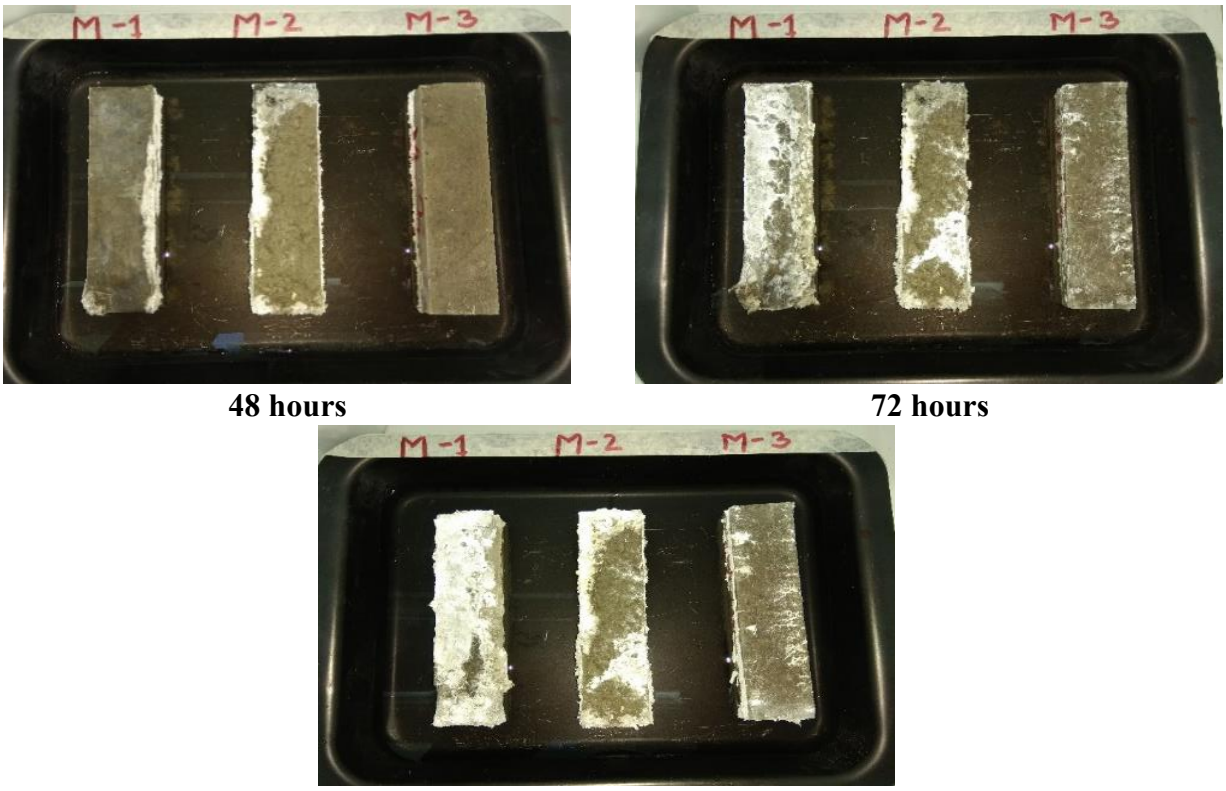

48 hours **72 hours**

120 hours

Fig 21.4. Comparative effects of efflorescence in M-1: Reference, M-2: Reinforced with basalt, M-3: Reinforced with cellulose fiber.

4.4.8 Drying shrinkage

Fig 22.4 illustrates the impacts of using fibers on the drying shrinkage of the plain mixture and the mixtures reinforced with basalt and cellulose fibers. Promising results were achieved in controlling the drying shrinkage due to use of fibers compared to the plain mixture, particularly when basalt fiber is used (≈35% reduction). It is noticed that, mixture reinforced with basalt fiber has decreased the drying shrinkage rate compared to use of cellulose fiber.

4.4.9 High temperature resistance

Fig 23.4. and Fig 24.4 shows the effects of high temperatures (400 ^{0}C, 600 ^{0}C, 800 ^{0}C) on the UPV and the changes of mass before and after high temperature, respectively. According to the result, high temperature could impose some several internal damages to the matrix and fibers. In some case fibers were burned and their space increased the porosity.

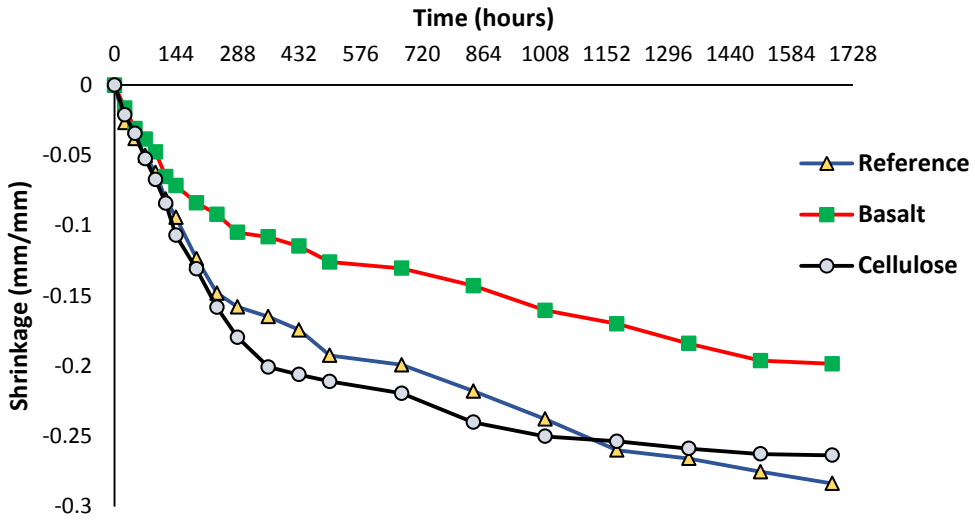

Fig 22.4 Shrinkage of reference, basalt and cellulose mixtures.

Therefore, the UPV greatly reduced compared to un-heated conditions. Moreover, heating led to evaporate water and reducing the mass of specimens.

High-temperature effects on the flexural strength are shown in the Fig 25.4. According to the results, high temperature has significant impacts on the flexural strength of the mixture including reinforced mixture with basalt and cellulose fiber. Fig 28.4(a) illustrates that after 600 ^{0}C, all mixtures have loss the strength around 90% compared to the unheated flexural strength and this loss increases with temperature. Regarding the result, high temperature leads to increase the internal damages and burning the fibers, so that the temperature greatly reduced the flexural strength.

Fig 26.4 presents the influence of high temperature on the compressive strength. Similar to the flexural strength, high temperature significantly reduced the compressive strength of the plain mixture as well as reinforced mixture with basalt and cellulose fiber. According to the result, averagely 95% loss resulted every level of temperature (400 ^{0}C, 600 ^{0}C, and 800 ^{0}C).

4.4.10 Freeze and Thaw resistance

Fig 27.4 presents the effects of temperature variations on the plain mixture and mixture reinforced with basalt and cellulose fiber. Temperature variations had significant effects after 7 days. Regarding the result of water absorption by immersion, it was found that the mixture reinforced with cellulose fiber has much porosity than other samples, so it was expected to observe more damages than other samples with lower porosity. According to the figure, after 3 freeze-thaw cycles, the mixture reinforced with cellulose fiber had much visible cracks than others. Finally, it

was noticed that all mixtures were damaged under different freeze/thaw cycles after 7 days (21 freeze-thaw cycles).

a)

b)

Fig 27.4. Condition of after a) 3 freeze-thaw cycles and b) 21 freeze-thaw cycles, M-1=Reference, M-2=Mixture reinforced with basalt fiber, M-3= Mixture reinforced with cellulose fiber

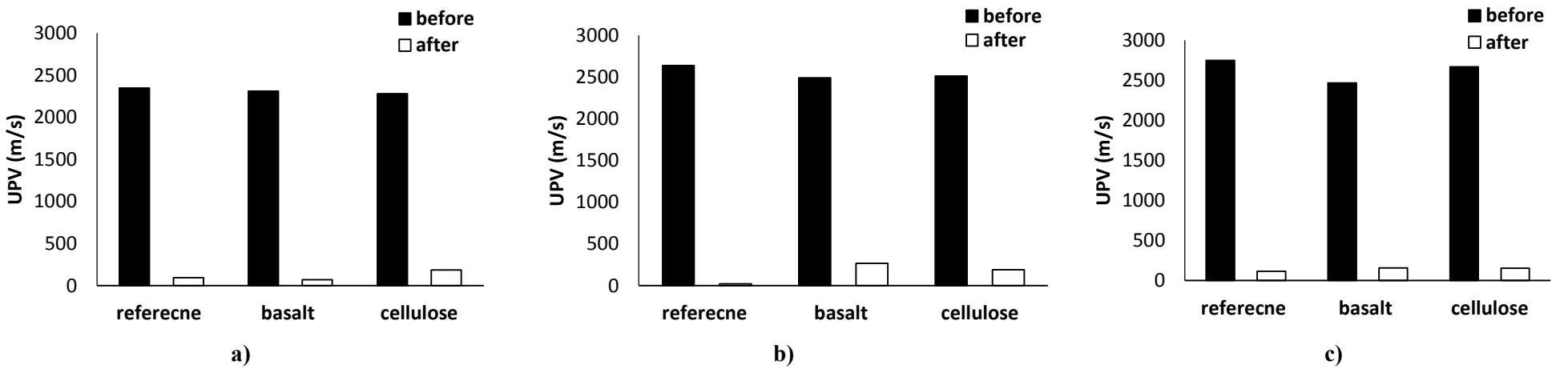

Fig 23.4. High temperature effects at a) 400 ^{0}C; b) 600 ^{0}C; and c) 800 ^{0}C on the UPV of mixtures

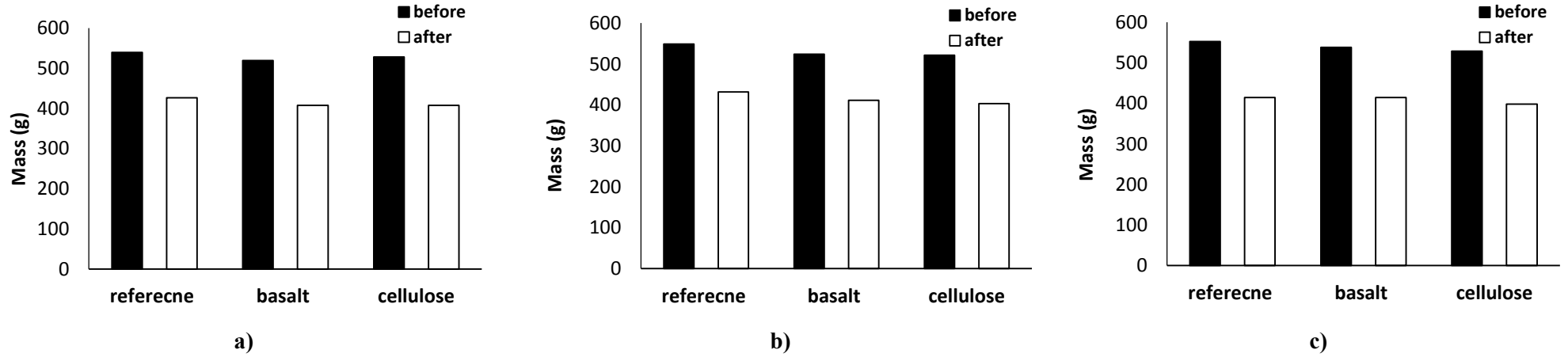

Fig 24.4. Effect of high temperature a) 400 ^{0}C; b) 600 ^{0}C; and c) 800 ^{0}C on the mass of mixtures

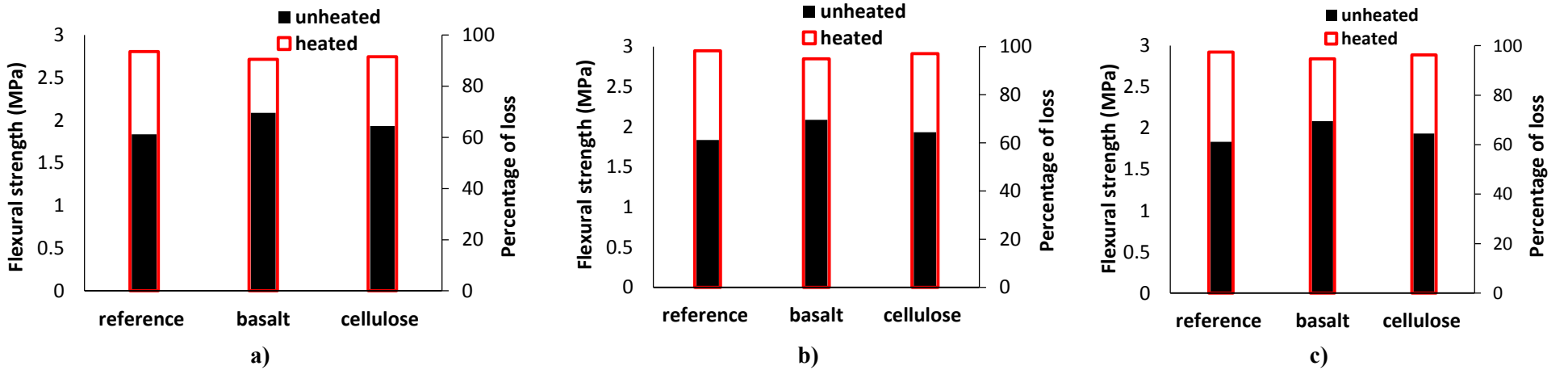

Fig 25.4. High temperature effects on the flexural strngth a) 400 ^{0}C; b) 600 ^{0}C; and c) 800 ^{0}C

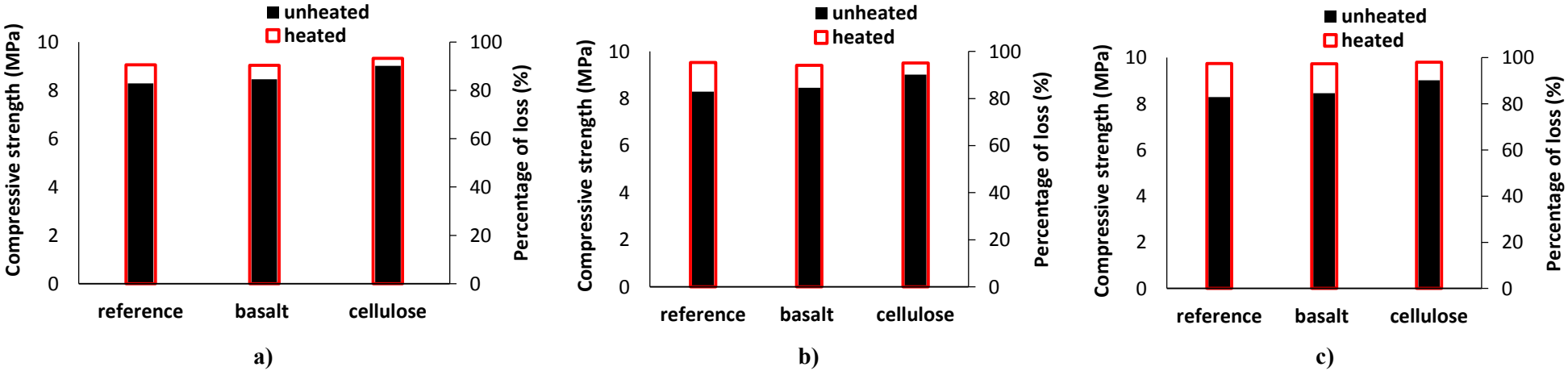

Fig 26.4. High temperature effects on the compressive strngth a) 400 ^{0}C; b) 600 ^{0}C; and c) 800 ^{0}C

4.5 The production of the bricks

The trial bricks were made by using the reference mixtures and the reinforced mix compsotions with basalt and cellulose fibers. They are shown in Fig 27.4. From the result and discussion, it is revealed that, the mixture containing basalt and cellulose fiber have satisfactory quality to produce bricks for construction sector. It is worth mentioning that the density of the produced bricks were around 1.7 g/cm^3.

a) **b)** **c)**

Fig 27.4. Produced trail bricks with dimension of 160×80×40 mm: a) reference; b) basalt; c) cellulose

4.6 Conclusions

In this study, the effects of applying fiber reinforcement (basalt and cellulose) on the plain mixture has been investigated based on the mechanical strength, carbonation, water absorption by capillarity, water absorption by immersion, efflorescence, ultrasonic pulse velocity, shrinkage, high temperature, freeze-thaw experiments. Regarding the result, the following conclusion could be highlighted:

Introducing basalt and cellulose fiber slightly improved the flexural and compressive strengths.

In the carbonation process, the compressive and flexural strength losses obtained in the mixture reinforced with cellulose were around 60% and 45%, respectively, while, comparatively lower strength losses were recorded in the mixture reinforced with basalt.

From water absorption by capillary assessment, it showed that the mixture reinforced with cellulose fiber reduced the cumulative mass of water compared to plain mixture. Besides, the capillary coefficient was decreased by 15% of using cellulose fiber compared to the reference. On the other hand, mixture containing basalt fiber obtained similar water absorption compared to plain mixture.

According to the result from water absorption by immersion, it noticed that using fibers increased the water absorption compared to the plain mixture. According to the result, the water absorption

increased 1% in the mixture reinforced with basalt and 5% in the mixture reinforced with cellulose fiber.

In general, a positive impact on minimizing the efflorescence rates was noticed by introduction of fibers.

The promising result was achieved in controlling the drying shrinkage due to the use of fibers. The minimum shrinkage (0.198 mm/min) was observed in the reinforced mixtures with the basalt fibers.

Great impact was observed due to expose specimens to the high temperatures. Averagely, 90% loss was recorded after high-temperature treatment in both flexural and compressive strength.

Exposing above 21 cycles of freeze and thaw treatment imposed significant damages.

References

Abdollahnejad, Z. et al., 2018. Fiber-reinforced one-part alkali-activated slag/ceramic binders. *Ceramics International, ,* Volume 44(8), pp. 8963-8976.

Adesanya, E., Ohenoja, K. & Kinnunen, P., 2017. Alkali activation of ladle slag from steel-making process. *Journal of Sustainable Metallurgy,* Volume 3(2), pp. pp.300-310..

Adesanya, E. et al., 2018. Ladle slag cement–Characterization of hydration and conversion. *Construction and Building Materials,* Volume 193, pp. 128-134.

Alarcon-Ruiz, L., Platret, G., Massieu, E. & Ehrlacher, A., 2005. The use of thermal analysis in assessing the effect of temperature on a cement paste. *Cement and Concrete research,* Volume 35(3), pp. 609-613.

Anastasiou, E., Liapis, A. & Papayianni, I., 2015. Comparative life cycle assessment of concrete road pavements using industrial by-products as alternative materials. *Resources, Conservation and Recycling,* Volume 101, pp. 1-8.

Andreas, L., Diener, S. & Lagerkvist, A., 2014. Steel slags in a landfill top cover–Experiences from a full-scale experiment. *Waste management,* Volume 34(3), pp. 692-701.

Andrew, R., 2018. Global CO2 emissions from cement production. *Earth Syst. Sci. Data,* Volume 10, p. 195–217.

Arbi, K., Nedeljković, M., Zuo, Y. & Ye, G., 2016. A review on the durability of alkali-activated fly ash/slag systems: advances, issues, and perspectives. *Industrial & Engineering Chemistry Research,* Volume 55(19), pp. 5439-5453.

Aydın, S. & Baradan, B., 2012. Mechanical and microstructural properties of heat cured alkali-activated slag mortars. *Materials & Design,* Volume 35, pp. 374-383.

Bakharev, T., Sanjayan, J. & Cheng, Y., 2002. Sulfate attack on alkali-activated slag concrete. *Cement and Concrete Research,* Volume 32(2), pp. 211-216.

Belhadj, E., Diliberto, C. & Lecomte, A., 2014. Properties of hydraulic paste of basic oxygen furnace slag. *Cement and Concrete Composites,* Volume 45, pp. 15-21.

Bentchikou, M. et al., 2012. Effect of recycled cellulose fibres on the properties of lightweight cement composite matrix. *Construction and Building Materials,* Volume 34, pp. 451-456.

Bernal, S. A., 2015. The resistance of alkaliactivated activated cement-based binders to carbonation. *Handbook of Alkali-Activated Cements, Mortars and Concretes,* pp. 319-332.

Bertos, M., Simons, S., Hills, C. & Carey, P., 2004. A review of accelerated carbonation technology in the treatment of cement-based materials and sequestration of CO2. *Journal of hazardous materials,* Volume 112(3), pp. 193-205.

Carvalho, S. et al., 2018. Reducing environmental impacts: the use of basic oxygen furnace slag in portland cement. *Journal of Cleaner Production,* Volume 172, pp. 385-390.

Collins, F. & Sanjayan, J., 2000. Effect of pore size distribution on drying shrinking of alkali-activated slag concrete. *Cement and Concrete Research,* Volume 30(9), pp. 1401-1406.

Collins, F. & Sanjayan, J., 2001. Microcracking and strength development of alkali activated slag concrete. *Cement and Concrete Composites,* Volume 23(4-5), pp. 345-352.

Das, B., Prakash, S., Reddy, P. & Misra, V., 2007. An overview of utilization of slag and sludge from steel industries. *Resources, conservation and recycling,* Volume 50(1), pp. 40-57.

Davidovits, J., 1991. Geopolymers: inorganic polymeric new materials. *Journal of Thermal Analysis and calorimetry,* Volume 37(8), pp. 1633-1656.

Geiseler, J., 1996. Use of steelworks slag in Europe. *Waste management,* Volume 16(1-3), pp. 59-63.

He, F., Fang, Y., Xie, J. & Xie, J., 2012. Fabrication and characterization of glass–ceramics materials developed from steel slag waste. *Materials & Design,* Volume 42, pp. 198-203.

Ho, C., Huang, W. & Wang, H., 2017. Study of the volume stability of slag cement mortar applied to desulfurization slag during high temperature operation. *Construction and Building Materials,* Volume 144, pp. 147-157.

Ho, C., Huang, W. & Wang, H., 2017. Study of the volume stability of slag cement mortar applied to desulfurization slag during high temperature operation. *Construction and Building Materials,* Volume 14, pp. 147-157.

Huang, L., Wang, H. & Wei, C., 2016. Engineering properties of controlled low strength desulfurization slags (CLSDS). *Construction and Building Materials,,* Volume 115, pp. 6-12.

Hwang, C. & Lin, C., 1986. Strength development of blended blast- furnace slag- cement mortars. *Journal of the Chinese Institute of Engineers,* Volume 9(3),, pp. 233-239.

Inforce, 2019. *Inforce.* [Online] Available at: https://inforce.co.nz/inforce-products/fibres/cellulose-fibres-for-concrete/

Jang, J., Kim, G., Kim, H. & Lee, H., 2016. Review on recent advances in CO2 utilization and sequestration technologies in cement-based materials. *Construction and Building Materials,* Volume 127, pp. 762-773.

Kawatra, S. & Ripke, S., 2002. Pelletizing steel mill desulfurization slag. *International journal of mineral processing,,* Volume 65(3-4), pp. 165-175.

Kiisa, M., Lellep, K. & Trossek, M., 2016. THE EFFECT OF BASALT FIBRE ON THE PROPERTIES OF NORMAL-WEIGHT CONCRETE. *Professional Studies: Theory & Practice/Profesines Studijos: Teorija ir Praktika,* Volume (16).

Ko, M., Chen, Y. & Jiang, J., 2015. Accelerated carbonation of basic oxygen furnace slag and the effects on its mechanical properties. *Construction and Building Materials,* Volume 98, pp. 286-293.

Kuo, W., 2015. Properties of compressed concrete paving units made produced using desulfurization slag. *Environmental Progress & Sustainable Energy,* Volume 34(5), pp. 1365-1371.

Kuo, W., Hou, T. & Pan, H., 2014. Desulfurization Slag/Granulated Blast Furnace Slag Binder and Mortar without Portland Cement..

Kuo, W. & Shu, C., 2014. Application of high-temperature rapid catalytic technology to forecast the volumetric stability behavior of containing steel slag mixtures. *Construction and Building Materials,* Volume 50, pp. 463-470.

Kuo, W.-T. & Tsung-Chin Hou, 2014. Engineering properties of alkali-activated binders by use of desulfurization slag and GGBFS. *Construction and Building Materials,* p. 229–234.

Kuo, W., Wang, H. & Shu, C., 2014. Engineering properties of cementless concrete produced from GGBFS and recycled desulfurization slag. *Construction and Building Materials,* Volume 63, pp. 189-196.

Kuo, W. & Weng, M., 2009. Utilization of desulfurization/granulated blast furnace slag as controlled low strength material without Portland cement. *J. Chung Cheng Inst. Technol,* Volume 38, pp. 157-166.

Lea, F., 1971. Some Special Cements and Cement Properties. *The Chemistry of Cement and Concrete, Chemical Publishing Company, NY, USA,* pp. 544-547..

Li, N. S. C., Wang, Q., Zhang, Z. & Ou, Z., 2017. Composition design and performance of alkali-activated cements. *Materials and Structures,* Volume 50(3) , p. 178.

Ma, N. & Houser, J., 2014. Recycling of steelmaking slag fines by weak magnetic separation coupled with selective particle size screening. *Journal of cleaner production,* Volume 82, pp. 221-231.

Maslehuddin , M. et al., 2003. Comparison of properties of steel slag and crushed limestone aggregate concretes. *Construction and building materials,* Volume 17(2), pp. 105-112.

Mastali, M., Abdollahnejad, Z. & Pacheco-Torgal, F., 2018. Carbon dioxide sequestration on fly ash/waste glassalkali-based mortars with recycled aggregates: compressive strength, hydration products, carbon footprint, and cost analysis. *Woodhead Publishing Series in Civil and Structural Engineering,* pp. 299-348.

Mastali, M. & Dalvand, A., 2017. Fresh and Hardened Properties of Self-Compacting Concrete Reinforced with Hybrid Recycled Steel–Polypropylene Fiber. *Journal of Materials in Civil Engineering,* Volume 29(6), p. 04017012.

Mastali, M., Dalvand, A. & Sattarifard, A., 2016. The impact resistance and mechanical properties of reinforced self-compacting concrete with recycled glass fibre reinforced polymers. *Journal of Cleaner Production,* Volume 124, pp. 312-324.

Mastali, M. et al., 2019. A comparison of the effects of pozzolanic binders on the hardened-state properties of high-strength cementitious composites reinforced with waste tire fibers. *Composites Part B: Engineering,* Volume 134-153, p. 162.

McLellan, B. et al., 2011. Costs and carbon emissions for geopolymer pastes in comparison to ordinary portland cement. *Journal of cleaner production,* Volume 19(9-10) , pp. 1080-1090.

Motz, H. & Geiseler, J., 2001. Products of steel slags an opportunity to save natural resources. *Waste management,* Volume 21(3), pp. 285-293.

Nath, S., Maitra, S., Mukherjee, S. & Kumar, S., 2016. Microstructural and morphological evolution of fly ash based geopolymers. *Construction and Building Materials,* Volume 111, pp. 758-765.

Palankar, N., Shankar, A. & Mithun, B., 2016. Durability studies on eco-friendly concrete mixes incorporating steel slag as coarse aggregates. *Journal of cleaner production,* Volume 129 , pp. 437-448.

Pan, S., Tseng, D., Lee, C. & Lee, C., 2003. Influence of the fineness of sewage sludge ash on the mortar properties. *Cement and Concrete Research,* Volume 33(11), pp. 1749-1754.

Poulikakos, L. et al., 2017. Harvesting the unexplored potential of European waste materials for road construction. *Resources, Conservation and Recycling ,* Volume 116, pp. 32-44.

Proctor, D. et al., 2000. Physical and chemical characteristics of blast furnace, basic oxygen furnace, and electric arc furnace steel industry slags. *Environmental science & technology,* Volume 34(8), pp. 1576-1582.

Provis, J., 2014. Alkali Activated Materials. *State-of-the-Art Report, RILEM TC 224-AAM,* pp. 1-9.

Provis, J., 2014. Geopolymers and other alkali activated materials: why, how, and what?. *Materials and Structures,* Volume 47(1-2), pp. 11-25.

Rietveld, H., 1969. A profile refinement method for nuclear and magnetic structures. *Journal of applied Crystallography,* Volume 2(2), pp. 65-71.

Rostami, V., Shao, Y. & Boyd, A. J., 2011. Durability of concrete pipes subjected to combined steam and carbonation curing. *Construction and Building Materials,* Volume 25(8), pp. 3345-3355.

S.C Pal, A. M. S. P., 2003. Investigation of hydraulic activity of ground granulated blast furnace slag in concrete. *Cement and Concrete Research,* 33(9), pp. 1481-1486.

Santos, R. L. D. S. A. G. M. et al., 2012. Stabilization of basic oxygen furnace slag by hot-stage carbonation treatment. *Chemical Engineering Journal,* Volume 203, pp. 239-250.

Shaikh, F. & Supit, S., 2014. Mechanical and durability properties of high volume fly ash (HVFA) concrete containing calcium carbonate (CaCO3) nanoparticles. *Construction and building materials,* Volume 70, pp. 309-321.

Shen, D., Wu, C. & Du, J., 2009. Laboratory investigation of basic oxygen furnace slag for substitution of aggregate in porous asphalt mixture. *Construction and Building Materials,* Volume 23(1), pp. 453-461.

Shi, C., 2002. Characteristics and cementitious properties of ladle slag fines from steel production. *Cement and Concrete Research,* Volume 32(3) , pp. 459-462.

Shi, C. & Qian, J., 2000. High performance cementing materials from industrial slags—a review. *Resources, Conservation and Recycling,* Volume 29(3), pp. 195-207.

Shi, C., Roy, D. & Krivenko, P., 2003. *Alkali-activated cements and concretes.* s.l.:CRC press.

Shi, Y., Chen, H., Wang, J. & Feng, Q., 2015. Preliminary investigation on the pozzolanic activity of superfine steel slag. *Construction and Building Materials,* Volume 82, pp. 227-234.

Škvára, F. et al., 2009. Aluminosilicate polymers–influence of elevated temperatures, efflorescence.. *Ceramics–Silikáty,* Volume 53(4), pp. 276-82.

Tossavainen, M. et al., 2007. Characteristics of steel slag under different cooling conditions. *Waste management,* Volume 27(10), pp. 1335-1344.

Tsakiridis, P., Papadimitriou, G., Tsivilis, S. & Koroneos, C., 2008. Utilization of steel slag for Portland cement clinker production. *Journal of Hazardous Materials,* Volume 152(2), pp. 805-811.

Wang, G., 2010. Determination of the expansion force of coarse steel slag aggregate. *Construction and Building Materials,* Volume 24(10), pp. 1961-1966.

Wang, G., Wang, Y. & Gao, Z., 2010. Use of steel slag as a granular material: volume expansion prediction and usability criteria. *Journal of Hazardous Materials,* Volume 184(1-3), pp. 555-560.

Wang, Q., Yan, P. & Feng, J., 2011. A discussion on improving hydration activity of steel slag by altering its mineral compositions. *Journal of hazardous materials ,* Volume 186(2-3) , pp. 1070-1075.

Weil, M., Dombrowski, K. & Buchwald, A., 2009. Life-cycle analysis of geopolymers. *Geopolymers ,* pp. 194-210.

Wu, S., Xue, Y., Ye, Q. & Chen, Y., 2007. Utilization of steel slag as aggregates for stone mastic asphalt (SMA) mixtures. *Building and Environment,* Volume 42(7), pp. 2580-2585.

Xue, P. et al., 2016. Research on the sintering process and characteristics of belite sulphoaluminate cement produced by BOF slag. *Construction and Building Materials,* Volume 122, pp. 567-576.

Yang, K., Song, J. & Song, K., 2013. Assessment of CO2 reduction of alkali-activated concrete. *Journal of Cleaner Production,* Volume 39, pp. 265-272.

Yan, L., Kasal, B. & Huang, L., 2016. A review of recent research on the use of cellulosic fibres, their fibre fabric reinforced cementitious, geo-polymer and polymer composites in civil engineering. *Composites Part B: Engineering,* Volume 92, pp. 94-132.

You-zhi, C., Xin-cheng, P., Chang-hui, Y. & Qing-jun, D., 2002. Alkali aggregate reaction in alkali slag cement mortars. *Journal of Wuhan University of Technology-Mater. Sci.,* Volume 17(3), pp. 60-62.

Zhang, Z. H. et al., 2009. Preparation and mechanical properties of polypropylene fiber reinforced calcined kaolin-fly ash based geopolymer. *Journal of Central South University of Technology,* Volume 16(1), pp. 49-52.

Zhang, Z., Provis, J., Reid, A. & Wang, H., 2014. Fly ash-based geopolymers: the relationship between composition, pore structure and efflorescence. *Cement and concrete research,* Volume 64, pp. 30-41.